SKB

TECHNICAL REPORT 97-26

Thermoelastic stress due to a rectangular heat source in a semi-infinite medium

Application for the KBS-3 repository

Thomas Probert, Johan Claesson

Depts. of Mathematical Physics and Building Physics,
Lund University, Sweden

April 1997

SVENSK KÄRNBRÄNSLEHANTERING AB
SWEDISH NUCLEAR FUEL AND WASTE MANAGEMENT CO
P.O.BOX 5864 S-102 40 STOCKHOLM SWEDEN
PHONE +46 8 459 84 00
FAX +46 8 661 57 19

THERMOELASTIC STRESS DUE TO A RECTANGULAR HEAT SOURCE IN A SEMI-INIFINITE MEDIUM

APPLICATION FOR THE KBS-3 REPOSITORY

Thomas Probert, Johan Claesson

Depts. of Mathematical Physics and Building Physics, Lund University, Sweden

April 1997

THERMOELASTIC STRESS DUE TO A RECTANGULAR HEAT SOURCE IN A SEMI-INFINITE MEDIUM.

II. Application for the KBS-3 repository.

Thomas Probert

Johan Claesson

April 1997

Depts. of Mathematical Physics and Building Physics
Lund University, Sweden

Keywords: Thermoelastic stress, rectangular heat source, semi-infinite space, three-dimensional, time-dependent exact analytical solution, results for KBS-3 data.

Abstract

In the KBS-3 concept, canisters containing nuclear waste are deposited over a large rectangular area deep below the ground surface. The thermoelastic response due to such a time-dependent rectangular heat source in a semi-infinite medium is studied.

An analytical solution for this problem for any heat source has been presented in a preceding paper. The complete solution is summarized in this paper.

In this study the analytical solution is applied to the KBS-3 case. The temporal development of the stress field is calculated at points, along lines and in planes for KBS-3 data. The temperature field and in particular the stresses are illustrated in 56 figures for times up to 1500 years.

Some stress components exhibit local maxima and minima near edges or corners of the repository. The largest tensile stress occurs at the ground surface directly above the repository centre. This stress is equal to 1.7 and 5.8 MPa after 50 and 500 years, respectively. The largest horizontal and vertical compressive stresses at the centre of the repository are 18 MPa for $t = 67$ years and 3.7 MPa for $t = 680$ years, respectively.

The general picture of the tensile and compressive stresses in a *vertical* cross-section of the ground, through the repository centre, is the following. The horizontal stresses are compressive in the repository area. Above and below the compressive region the horizontal stresses are tensile. The distance to the tensile stresses above the repository is roughly 50, 100 and 300 m for $t = 5$, 50 and 500 years, respectively, while the distance to the tensile stresses below the repository is somewhat larger. The vertical stresses are compressive above, below and in the repository area. The vertical stresses are tensile outside this region. The horizontal distance to the tensile region is 2 and 30 m for $t = 50$ and 500 years, respectively.

The general picture of the tensile and compressive stresses in a *horizontal* cross-section of the ground, through the repository centre, is the following. The vertical stresses are compressive inside the repository area and tensile outside in bands parallel to the repository edges. The distance to these bands is roughly 2 and 30 m for $t = 50$ and 500 years, respectively. The horizontal stresses are compressive in the repository area and tensile outside. The distance to these tensile regions from an edge of the repository is roughly 40, 90 and 220 m for $t = 5$, 50 and 500 years, respectively, and somewhat shorter at the corners of the repository.

A parameter sensitivity analysis is presented. The stress field at the repository centre is rather insensitive to 10% variations of the repository length, width and depth as well as the rock's volumetric heat capacity, heat conductivity and Poisson's number. This is also true for stresses at the ground surface with the exception of the depth parameter. The change in the stresses is at the most $\pm 6\%$ at the repository centre, and $\pm 9\%$ at the ground surface.

The solution may be generalized to a repository that consists of several rectangular areas of different sizes and at different depths. The rectangular areas may be loaded at different times. An example is presented where two repositories are stacked, one on top of the other.

The analytical solution for the stresses is compared with two other semi-analytical models. The agreement is good.

Sammanfattning

I KBS-3 konceptet deponeras kapslar innehållande radioaktivt avfall över ett stort rektangulärt område djupt under markytan. Den termoelastiska responsen på en tidsberoende rektangulär värmekälla i ett halvoändligt medium analyseras.

En analytisk lösning till detta problem för en godtycklig värmekälla har presenterats i en föregående skrift. Lösningen sammanfattas i denna skrift.

I denna skrift tillämpas den analytiska lösningen på KBS-3 fallet. Tidsutvecklingen av spänningsfältet beräknas för data enligt KBS-3 i punkter, längs linjer och i plan. Temperaturfältet och framför allt spänningsfältet visas i 56 figurer för tider upp till 1500 år.

Vissa spänningskomponenter uppvisar lokala maxima och minima i närheten av förvarets hörn och kanter. De största dragspänningarna finns vid markytan rakt ovanför förvarets mittpunkt. Denna dragpåkänning är 1.7 MPa efter 50 år och 5.8 MPa efter 500 år. De största horisontella och vertikala tryckspänningarna i förvarets mittpunkt är 18 MPa för $t = 67$ år respektive 3.7 MPa för $t = 682$ år.

Den allmänna bilden av tryck- och dragpåkänningarna i en *vertikal* genomskärning av marken genom förvarets mittpunkt är följande. De horisontella spänningarna är kompressiva kring förvaret. Ovanför och nedanför dessa kompressiva områden finns områden med horisontella dragspänningar. Avståndet till dragspänningsområdet ovanför förvaret är ungefär 50, 100 och 300 m för $t = 5$, 50 respektive 500 år, och något större till området nedanför förvaret. De vertikala spänningarna är kompressiva ovanför, nedanför och i förvaret. Utanför detta område är de vertikala spänningarna dragpåkänningar. Det horisontala avståndet till dragspänningarna är 2 och 30 m för $t = 50$ respektive 500 år.

Den allmänna bilden av tryck- och dragpåkänningarna i en *horisontal* genomskärning av marken genom förvarets mittpunkt är följande. De vertikala spänningarna är kompressiva inom förvarsområdet. Vertikala dragspänningar finns i band parallella med förvarets sidor. Avståndet till dessa band är 2 och 30 m för $t = 50$ respektive 500 år. De horisontella spänningarna är kompressiva i förvarsområdet och ger upphov till dragpåkänningar utanför området. Avståndet till områden med dragspänningar är 40, 90 och 220 m för $t = 5$, 50 respektive 500 år, och något mindre vid hörnen.

En parameterkänslighetsanalys utförs. Spänningsfältet i förvarets mittpunkt är tämligen okänsligt för 10-procentiga variationer i förvarets längd, bredd och djup samt bergets volymspecifika värmekapacitet, värmeledningsförmåga och Poissons tal. Detta gäller också för spänningar vid markytan med undantag av förvarets djup. Ändringen i spänningarna är högst $\pm 6\%$ i förvarets mittpunkt och $\pm 9\%$ vid markytan.

Lösningen kan generaliseras till ett förvar som består av ett antal rektangulära ytor av olika storlekar och på olika djup. De rektangulära ytorna kan laddas vid olika tidpunkter. Ett exempel presenteras där två förvar placeras ovanför varandra.

Den analytiska lösningen för spänningarna jämförs med två semianalytiska modeller. Överensstämmelsen är god.

Contents

1 Introduction

In the KBS-3 concept, nuclear waste from the Swedish nuclear power plants is put in some six thousand canisters, which are buried in solid rock at a depth H of 500 m below the ground surface. See Figure 1, left.

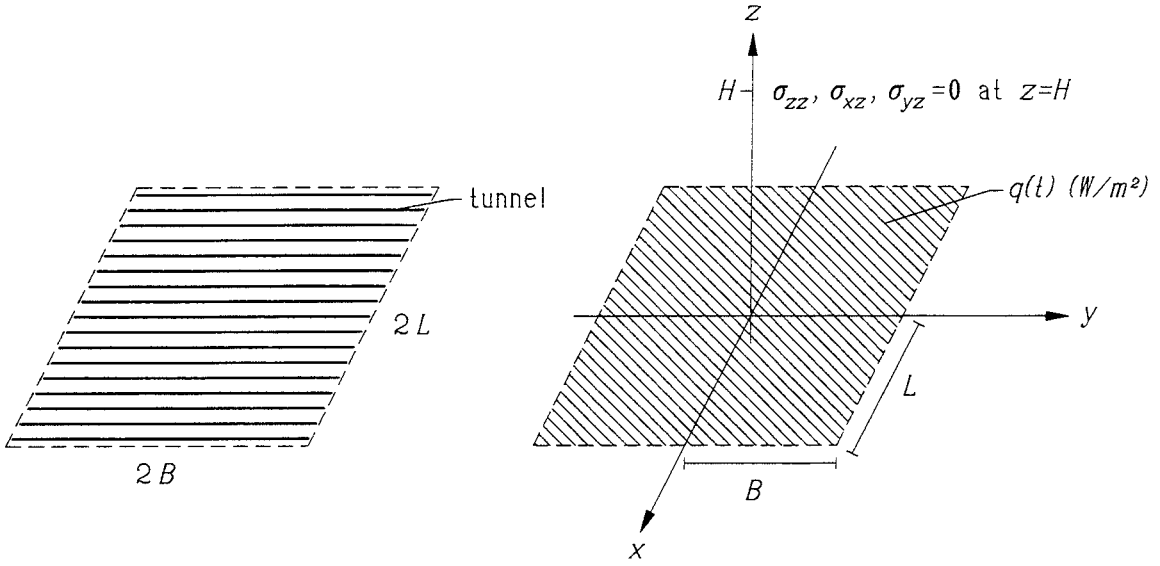

Figure 1. Left: Nuclear waste repository with heat-emitting canisters placed along tunnels within a rectangular area. Right: Thermoelastic problem with a time-dependent rectangular heat source plane. The stress is zero at the ground surface ($z = H$).

The canisters are placed in boreholes below parallel tunnels at a spacing D of about 6 m. The distance D' between the tunnels is about 25 m. The nuclear waste repository consists of canisters in a large, rectangular grid. The total area of the rectangle with the side lengths 2L and 2B is almost 1 km^2 ($6{\cdot}25 \cdot 6000$ m^2). Each canister lies at the center of a small rectangle with the side lengths D and D'.

The canisters emit heat due to radioactive decay in the nuclear waste. The heat sources from all canisters create a complex three-dimensional, time-dependent temperature field in the ground in and around the repository. This thermal problem is studied in (Claesson J, Probert T, Jan. 1996). The local problem around a particular canister is not considered here. On a larger scale (above D and D'), there is a rectangular heat source plane:

$$q(t) \quad \mathrm{W/m^2} \quad \text{at} \quad -L < x < L, \; -B < y < B \; z = 0 \tag{1}$$

The heat emission per canister is $DD'q(t)$ (W). The heat emission decreases with time in a known way. We will use a sum of exponentials with different decay times to represent the function $q(t)$.

The emitted heat warms the rock and induces a thermoelastic stress field. The rock mass serves as a protective barrier for the nuclear waste. In the worst-case scenario, groundwater may transport nuclear waste all the way from damaged canisters to the biosphere. Groundwater flow requires an open fracture and crack system. The stress and strain fields are therefore of main interest, since they influence crack closure, opening, formation and widths.

The purpose of this study is to analyse the thermoelastic process in the rock caused by the rectangular heat source. The process is of interest for different time-scales from the first years

to thousands of years. The behavior in and around the repository region, but also far away from the canisters, is of interest.

A particular aim for the analytical approach is to gain a physical understanding and the possibility to quantify particular processes and their interactions.

An exact analytical solution for the time-dependent, three-dimensional process is derived in (Claesson J, Probert T, May 1996). The solution, which is not valid in the immediate vicinity of single canisters with their local complications, is surprisingly simple, considering the complexity of the coupled process. The corresponding problem of the thermoelastic response to a single, finite line heat source is studied in (Claesson J, Hellström G, 1995). The temperature field, including the local process around the canisters, is studied in (Claesson J, Probert T, Jan. 1996).

In this study the analytical solution of the thermoelastic stress derived in (Claesson J, Probert T, May 1996) is applied to the KBS-3 repository. At first, a summary of the solution formulas are given. The stress field is calculated at points, along lines and in planes for different times using the particular data of the KBS-3 repository. The analytical solution for the temperature field derived in (Claesson J, Probert T, Jan. 1996) is applied to the KBS-3 repository in (Probert T, Claesson J, Apr. 1997). In Appendix 3 the results obtained in this study are compared with results from two other models.

2 The complete solution

2.1 Assumptions and approximations

The displacement $\mathbf{u} = (u, v, w)$ satisfies Navier's equation in a semi-infinite, linearly elastic, isotropic, homogeneous medium:

$$\nabla^2(\mathbf{u}) + \frac{1}{1-2\nu}\nabla(e) = \frac{2\alpha(1+\nu)}{1-2\nu}\nabla T \qquad e = \nabla \cdot \mathbf{u}$$

$$-\infty < x < \infty \qquad -\infty < y < \infty \qquad -\infty < z < H \tag{2}$$

The temperature field $T(x, y, z, t)$ which is the excess temperature above undisturbed conditions is caused by the time-dependent heat source $q(t)$ (W/m^2) over a rectangular area: $-L < x < L$, $-B < y < B$, $z = 0$ (See Figure 1). The heat is emitted from the start $t = 0$. In particular, we will consider the case where the heat source $q(t)$ consists of a sum of J exponentials:

$$q(t) = \sum_{j=1}^{J} q_j \cdot \mathrm{e}^{-t/t_j} \tag{3}$$

The strengths q_j and the decay time constants t_j are any positive numbers.

The solution $(u, \varepsilon_{xx}, \sigma_{xx} \ldots)$ shall tend to zero at infinity ($\sqrt{x^2+y^2} \to \infty$ or $z \to -\infty$). The three stress components σ_{xz}, σ_{yz}, and σ_{zz} are zero at the ground surface $z = H$. We have the boundary conditions:

$$\sigma_{zz}(x, y, H, t) = 0 \quad \sigma_{xz}(x, y, H, t) = 0 \quad \sigma_{zy}(x, y, H, t) = 0 \tag{4}$$

The excess temperature T is zero at the ground surface $z = H$.

The above problem is solved in six steps described in Section 24 of (Claesson J, Probert T, May 1996). One main assumption is made in order to simplify the solving process. The assumption is that the far-field approximation of the so-called quadrantal solution (index qi, see (Claesson J, Probert T, May 1996), p. 4) can be used at the ground surface $z = H$. This is the case with good accuracy when t satisfies:

$$t < \frac{H^2}{16a} \tag{5}$$

In the KBS-3 example, t must be less than 300 years ($a = 1.62 \cdot 10^{-6}\mathrm{m}^2/\mathrm{s}$, $H = 500$ m). After about 300 years the solution at the ground surface ($z = H$) is disturbed. The disturbance will increase at the ground surface and will move deeper into the medium. The solution at the repository level ($z = 0$) is valid if:

$$t < \frac{H^2}{4a} \tag{6}$$

It will take four times longer for the disturbance to reach the repository level (roughly 1200 years) than the ground surface. The solution is incorrect for large times ($\simeq$10,000).

2.2 Solution formula

The solution formula for a heat source $q(t)$ over a rectangular area at a depth H under the ground surface $z = H$ involves a sum of four so called quadrantal terms corresponding to the four corners of the rectangle and an integration in time. Let f denote any displacement, strain or stress component. We have:

$$f(x,y,z,t) = \sum_{n_x=\pm 1} \sum_{n_y=\pm 1} \frac{n_x n_y}{4} \int_0^t \frac{q(t')}{e_0} f^{qs}(x + n_x L, y + n_y B, z, t - t')\mathrm{d}t' \tag{7}$$

The function f^{qs} can be separated into a time-dependent and a time-independent part, f^{qi} and f^{mb} respectively, which simplifies the time integration in Eq. (7).

$$f^{qs}(x,y,z,t) = f^{qi}(x,y,z,t) + f^{mb}(x,y,z) \tag{8}$$

The indices *qs*, *qi*, and *mb* stand for *quadrantal* solution in a *semi-infinite* region, *quadrantal* solution in an *infinite* region, and *mirror* and *boundary* solution, respectively (See (Claesson J, Probert T, May 1996), pp. 9, 22-23). The basic solution is the so-called quadrantal solution which is the solution for a heat source $+e_0$ at time $t = 0$ in the first and third quadrant ($x > 0$, $y > 0$ and $x < 0$, $y < 0$) of the plane $z = 0$, and the heat release $-e_0$ in the other two quadrants. For the sum (3) of exponentials we get:

$$f(x,y,z,t) = \sum_{j=1}^{J} \sum_{n_x=\pm 1} \sum_{n_y=\pm 1} \frac{n_x n_y}{4} \int_0^t \frac{q_j \cdot \mathrm{e}^{-t'/t_j}}{e_0} f^{qs}(x + n_x L, y + n_y B, z, t - t')\mathrm{d}t' \tag{9}$$

The three displacement components are obtained for:

$$f = u,\ v \text{ or } w \tag{10}$$

The time-dependent and time-independent components of u^{qs}, v^{qs} and w^{qs} are given by Eqs. (23) and Eqs. (24), respectively. The six components of the strain field are obtained for:

$$f = \varepsilon_{xx},\ \varepsilon_{yy},\ \varepsilon_{zz},\ \varepsilon_{xy},\ \varepsilon_{xz} \text{ or } \varepsilon_{yz} \tag{11}$$

The time-dependent and time-independent components of ε_{xx}^{qs}, ε_{yy}^{qs}, etc. are given by Eq. (25) and Eq. (26), respectively. The six components of the stress field are obtained for:

$$f = \sigma_{xx},\ \sigma_{yy},\ \sigma_{zz},\ \sigma_{xy},\ \sigma_{xz} \text{ or } \sigma_{yz} \tag{12}$$

The time-dependent and time-independent components of σ_{xx}^{qs}, σ_{yy}^{qs}, etc. are given by Eq. (27) and Eq. (28), respectively.

2.3 Parameters and auxiliary functions

The geometry of the repository is described by the three length parameters H, L and B. The length H is the depth of the repository plane under the ground surface (The repository plane is situated at $z = 0$ and the ground surface at $z = H$). The size of the rectangular repository area is given by the lengths $2L$ and $2B$ parallel to the x and y axes, respectively.

The mechanical properties of the rock mass are described by the density ρ (kg/m^3), Young's modulus E (Pa) and Poisson's ratio ν (-). The density of the rock ρ also affects the heat transport by way of the thermal diffusivity $a = \lambda/(\rho c)$ (m^2/s).

The thermal properties of the rock mass are given by the specific heat capacity c (J/(kgK)), the coefficient of linear thermal expansion α (1/K), the heat conductivity λ (W/(m·K) and the thermal diffusivity $a = \lambda/(\rho c)$ (m^2/s). The volumetric heat capacity, C (J/m^3), of the rock mass is equal to ρc where ρ is the density and c is the specific heat capacity of the rock mass.

The properties of the heat source are given by J, t_j, q_j and e_0. The integer J is the number of exponentials. The strength of exponential number j is q_j (W/m^2), and its exponential decay-time is t_j (s) which corresponds to a half-life $t_{\frac{1}{2}} = t_j \ln 2$ (s). The constant e_0 (J/m^2) is the instantaneous heat release per unit area at $t = 0$. Since we no longer consider an instantaneous heat release, but instead look at a continuous heat release, this constant is redundant and is chosen equal to 1.

The components of the stress, strain and displacement fields involve two constants u_0 (m) and p_0 (Pa· m):

$$u_0 = \frac{1+\nu}{1-\nu} \cdot \frac{e_0 \alpha}{\pi \rho c} \tag{13}$$

$$p_0 = \frac{E}{1+\nu} \cdot u_0 = \frac{E}{1-\nu} \cdot \frac{e_0 \alpha}{\pi \rho c} \tag{14}$$

The space variables used are x, y, and z (Figure 1, right) along with the two radial lengths (m):

$$r = \sqrt{x^2 + y^2 + z^2} \tag{15}$$

$$r_m = \sqrt{x^2 + y^2 + (2H - z)^2} \tag{16}$$

The radial distance from the point (0,0,0) is r, and r_m is the radial distance from the point (0,0,2H). The time-dependent components of the stress and strain fields obtain their time-dependency from the two functions T_{qi} (K) and C (1/m^2):

$$T_{qi}(x,y,z,t) = \frac{e_0}{\rho c} \cdot \operatorname{erf}\left(\frac{x}{\sqrt{4at}}\right) \cdot \operatorname{erf}\left(\frac{y}{\sqrt{4at}}\right) \cdot \frac{1}{\sqrt{4\pi at}} \cdot e^{-z^2/(4at)} \tag{17}$$

$$C(p,r,t) = \frac{1}{r} \cdot \frac{p}{r^2 - p^2} \cdot \left[\operatorname{erf}\left(\frac{r}{\sqrt{4at}}\right) - r \cdot \mathrm{e}^{-(r^2-p^2)/(4at)} \cdot \frac{\operatorname{erf}(p/\sqrt{4at})}{p}\right] \quad p = x,\ y \tag{18}$$

The error function erf(x) that appears in the time-dependent functions T_{qi} and C is defined as:

$$\operatorname{erf}(x) = \frac{2}{\sqrt{\pi}} \int_0^x \mathrm{e}^{-s^2} ds \tag{19}$$

The behaviour of the strain and stress fields of the basic quadrantal solution can be studied by examining the functions $T_{qi}(x,y,z,t)$ and $C(p,r,t)$ in their dimensionless forms where the number of variables is reduced (See Appendix 1).

The following three time-independent functions are used in the formulas for the time-independent components of the stress and strain fields.

$$D(p, r_m) = r_m^2 - p^2 \quad p = x,\ y \quad (\mathrm{m}^2) \tag{20}$$

$$B(p, z, r_m) = 2(H - z)(2H - z)\left(\frac{1}{r_m^2} + \frac{2}{D(p, r_m)}\right) \quad p = x,\ y \quad (-) \tag{21}$$

$$G(p, z, r_m; \xi) = \frac{1}{r_m}\frac{p}{D(p, r_m)}(\xi - B(p, z, r_m)) \quad p = x,\ y \quad (1/\mathrm{m}^2) \tag{22}$$

Most of the parameters and functions introduced here are the same as those used in (Claesson J, Probert T, May 1996). The functions D_x, D_y, B_x and B_y defined in (Claesson J, Probert T, May 1996), Eqs. (146-148) have, however, been altered so that D_x, $D_y \rightarrow D(p, r_m)$, $p = x,\ y$ and B_x, $B_y \rightarrow B(p, z, r_m)$, $p = x,\ y$. The functions C and G are new definitions and they were not used in (Claesson J, Probert T, May 1996).

2.4 Temperature field

The temperature field caused by the quadrantal heat source (See (Claesson J, Probert T, Jan. 1996), pp. 4-5) is given by Eq. (17). The temperature field of the rectangular heat source of Eq. (1) is given by a superposition of the type (7) with f^{qs} replaced by T_{qi}. The derivation of the rectangular heat source temperature field is described in detail in (Claesson J, Probert T, Jan. 1996). The temperature field is illustrated in Section 6.

2.5 Displacement components

The time-dependent parts of the displacements are given by:

$$u^{qi}(x, y, z, t) = -u_0 \int_0^{1/\sqrt{4at}} \frac{\mathrm{erf}(ys)}{s} \cdot \mathrm{e}^{-(r^2 - y^2)s^2} ds$$

$$v^{qi}(x, y, z, t) = u^{qi}(y, x, z, t)$$

$$w^{qi}(x, y, z, t) = u_0\sqrt{\pi} z \int_0^{1/\sqrt{4at}} \mathrm{erf}(xs) \cdot \mathrm{erf}(ys) \cdot \mathrm{e}^{-z^2 s^2} ds \tag{23}$$

The calculation of the time-dependent displacement components according to Eqs. (7) or (9) and (23) involves a double integral which may be reduced to a single integral by integration by parts. The partial integration has been performed on the displacement components in Appendix 2.

The time-independent parts of the displacements are given by:

$$u^{mb}(x, y, z) = -u_0 \cdot \left(\frac{3}{2} - 2\nu\right) \ln\left(\frac{r_m + x}{r_m - x}\right) + \frac{2(H - z)}{r_m} \cdot \frac{x(2H - z)}{r_m^2 - x^2}$$

$$v^{mb}(x, y, z) = u^{mb}(y, x, z)$$

$$w^{mb}(x, y, z) = u_0\left[(3 - 4\nu)\arctan\left(\frac{xy}{(2H - z)r_m}\right) + \frac{2(H - z)}{r_m}\left(\frac{xy}{r_m^2 - x^2} + \frac{xy}{r_m^2 - y^2}\right)\right] \tag{24}$$

2.6 Strain components

The time-dependent parts of the strains are given by:

$$\varepsilon_{xx}^{qi}(x, y, z, t) = u_0 \cdot x \cdot C(y, r, t)$$

$$\varepsilon_{yy}^{qi}(x, y, z, t) = u_0 \cdot y \cdot C(x, r, t)$$

$$\varepsilon_{zz}^{qi}(x,y,z,t) = \frac{1+\nu}{1-\nu}\alpha \cdot T_{qi}(x,y,z,t) - u_0\left[x \cdot C(y,r,t) + y \cdot C(x,r,t)\right]$$

$$\varepsilon_{xy}^{qi}(x,y,z,t) = -\frac{u_0}{r} \cdot \mathrm{erf}\left(\frac{r}{\sqrt{4at}}\right)$$

$$\varepsilon_{xz}^{qi}(x,y,z,t) = u_0 \cdot z \cdot C(y,r,t)$$

$$\varepsilon_{yz}^{qi}(x,y,z,t) = u_0 \cdot z \cdot C(x,r,t) \tag{25}$$

The time-independent parts of the strains are given by:

$$\varepsilon_{xx}^{mb}(x,y,z) = u_0 \cdot x \cdot G(y,z,r_m;3-4\nu)$$

$$\varepsilon_{yy}^{mb}(x,y,z) = u_0 \cdot y \cdot G(x,z,r_m;3-4\nu)$$

$$\varepsilon_{zz}^{mb}(x,y,z) = -u_0 \cdot \left[x \cdot G(y,z,r_m;4\nu-1) + y \cdot G(x,z,r_m;4\nu-1)\right]$$

$$\varepsilon_{xy}^{mb}(x,y,z) = \frac{u_0}{r_m}\left[\frac{2(H-z)(2H-z)}{r_m^2} - 3 + 4\nu\right]$$

$$\varepsilon_{xz}^{mb}(x,y,z) = -u_0\left[\frac{1}{r_m}\frac{y(4H-3z)}{D(x,r_m)} - (2H-z)\cdot G(y,z,r_m;0)\right]$$

$$\varepsilon_{yz}^{mb}(x,y,z) = \varepsilon_{xz}^{mb}(y,x,z) \tag{26}$$

2.7 Stress components

The time-dependent parts of the stresses are given by:

$$\sigma_{xx}^{qi}(x,y,z,t) = \frac{p_0}{u_0} \cdot \varepsilon_{xx}^{qi}(x,y,z,t) - \frac{E\alpha}{1-\nu} \cdot T_{qi}(x,y,z,t)$$

$$\sigma_{yy}^{qi}(x,y,z,t) = \frac{p_0}{u_0} \cdot \varepsilon_{yy}^{qi}(x,y,z,t) - \frac{E\alpha}{1-\nu} \cdot T_{qi}(x,y,z,t)$$

$$\sigma_{zz}^{qi}(x,y,z,t) = \frac{p_0}{u_0}\left[\varepsilon_{zz}^{qi}(x,y,z,t) - \frac{1+\nu}{1-\nu}\alpha \cdot T_{qi}(x,y,z,t)\right]$$

$$\sigma_{xy}^{qi}(x,y,z,t) = \frac{p_0}{u_0} \cdot \varepsilon_{xy}^{qi}(x,y,z,t)$$

$$\sigma_{xz}^{qi}(x,y,z,t) = \frac{p_0}{u_0} \cdot \varepsilon_{xz}^{qi}(x,y,z,t)$$

$$\sigma_{yz}^{qi}(x,y,z,t) = \frac{p_0}{u_0} \cdot \varepsilon_{yz}^{qi}(x,y,z,t) \tag{27}$$

The time-independent parts of the stresses are given by:

$$\sigma_{xx}^{mb}(x,y,z) = p_0\left[x \cdot G(y,z,r_m;3) + 4\nu\frac{1}{r_m}\frac{xy}{D(x,r_m)}\right]$$

$$\sigma_{yy}^{mb}(x,y,z) = p_0\left[y \cdot G(x,z,r_m;3) + 4\nu\frac{1}{r_m}\frac{xy}{D(y,r_m)}\right]$$

$$\sigma_{zz}^{mb}(x,y,z) = -p_0\left[x \cdot G(y,z,r_m;-1) + y \cdot G(x,z,r_m;-1)\right]$$

$$\sigma_{xy}^{mb}(x,y,z) = \frac{p_0}{u_0} \cdot \varepsilon_{xy}^{mb}(x,y,z)$$

$$\sigma_{xz}^{mb}(x,y,z) = \frac{p_0}{u_0} \cdot \varepsilon_{xz}^{mb}(x,y,z)$$

$$\sigma_{yz}^{mb}(x,y,z) = \frac{p_0}{u_0} \cdot \varepsilon_{yz}^{mb}(x,y,z) \tag{28}$$

3 Numerical model

The above solution has been implemented on PC for rapid computer solution. This manual for the computer code is in Appendix 4. Briefly, the model is implemented in MATLAB version 4.2c.1 and run on a Intel Pentium 90 MHz PC.

The calculation of the stress field at a point takes from 1.5 to 2 seconds depending on the size of the arguments of the Error functions. The time integral is evaluated numerically.

All the figures showing stresses have been generated by MATLAB. The resolution and execution times for stresses illustrated in the figures of Sections 5, 7, 8, 9 and 10 are the following. The stress field at a given point for 300 times or the stress field at 300 points along a line for a given time takes 7 to 10 minutes to calculate. The stress field for a given time in a plane consisting of 100×100 points takes 4 to 6 hours.

4 Input data

The input data can be divided into four parts concerning the geometry of the heat-source, properties of the heat source, mechanical properties, and thermal properties. The following data are used in the reference case:

$$L = 500 \text{ m} \quad B = 500 \text{ m} \quad H = 500 \text{ m}$$

$$J = 2 \quad q_1 = 5 \text{ W/m}^2 \quad q_2 = 5/3 \text{ W/m}^2 \quad t_1 = 46 \text{ y} \quad t_2 = 780 \text{ y}$$

$$\rho = 2700 \text{ kg/m}^3 \quad E = 50 \cdot 10^9 \text{Pa} \quad \nu = 0.25$$

$$c = 800 \text{ J/(kg} \cdot \text{K)} \quad \lambda = 3.5 \text{ W/(m} \cdot \text{K)} \quad \alpha = 8.3 \cdot 10^{-6} \text{ 1/K} \tag{29}$$

The heat release from each canister is given by two exponentials:

$$Q_0(t) = Q_1 \cdot \mathrm{e}^{-t/t_1} + Q_2 \cdot \mathrm{e}^{-t/t_2} \qquad \text{(W)} \qquad Q_0(0) = 1000 \text{ W} \tag{30}$$

The heat release per unit area of the heat source is:

$$q(t) = q_1 \cdot \mathrm{e}^{-t/t_1} + q_2 \cdot \mathrm{e}^{-t/t_2} \qquad (\text{W/m}^2) \qquad q_i = Q_i/(DD'),\ i = 1,2 \tag{31}$$

The total initial effect emitted from a canister is $Q_0(0)$ =1000 W. This effect is divided between the two decay components at a ratio 3:1 (750 W/250 W). The initial amplitude of the heat emission rate with the decay time t_1 = 46 years is Q_1 =750 W (3/4 of 1000 W) for each canister. The area around a canister is $DD' = 6 \cdot 25$ m^2. The effect per unit area q_1 is then 750/150 = 5 W/m^2. The second effect Q_2 with the longer decay time t_2 =780 years has initially one fourth of the total initial effect $Q_0(0)$ or a third of Q_1. In this case Q_2 = 250 W. The expression (30) for the heat release is valid for the first 1000 years. It has been obtained by curve fitting using the least squares approximation. The effect is underestimated for times longer than 1000 years since there are small components with longer decay times in the true expression.

The stresses due to the weight of the overlaying rock at the depth z ($z \leq H$) is equal to $\rho g(z-H)$, which amounts to -13 MPa at the repository level ($z = 0$) if $H = 500$. The horizontal stresses are larger than the vertical stress (See (Israelsson J, 1995), p. 10). These two naturally occurring stresses should be added to the thermoelastic stresses. It should be stressed that the stresses calculated in this paper are the excess stresses above the undisturbed, natural stresses mentioned above.

According to the sign convention used in this paper, positive stresses are tensile stresses and negative stresses are compressive stresses.

All results presented in this study concern the above reference case. In the sensitivity analysis of Section 12, the parameters are varied to determine the effect of the parameters on the stresses.

5 Representation of the solution

The components of the stress field are functions of space and time, for instance $\sigma_{xx} = \sigma_{xx}(x, y, z, t)$. The function of four variables may be illustrated by restricting the space coordinates to points, lines or planes.

We may consider the development in time at any particular *point*. As an example, let us look at the centre point P_1: (0,0,0). Figure 2, left, shows the stress component $\sigma_{xx}(0, 0, 0, t)$ for $0 \leq t \leq 1500$ years. Figure 2, right, is a blow-up of the stress component $\sigma_{xx}(0, 0, 0, t)$ during the first 100 years. The stress σ_{xx} in Figure 2 is negative which means compression. The compressive stress increases steeply to -17.92 MPa after 66.6 years because of the heat release. Then the stress decreases due to the exponentially decreasing nature of the heat release.

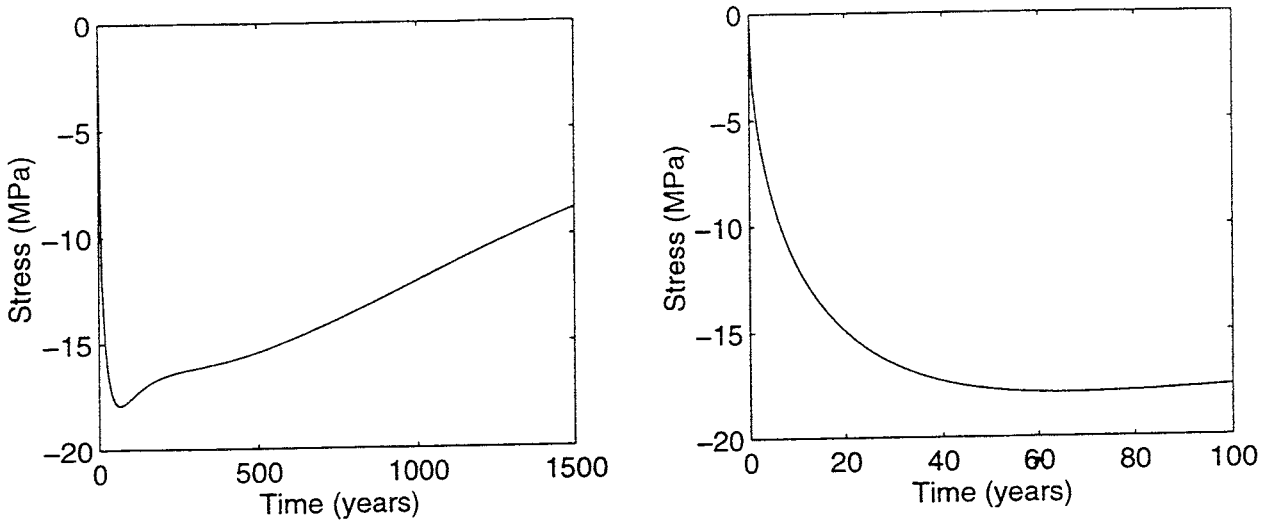

Figure 2. The stress $\sigma_{xx}(0, 0, 0, t)$ at the point (0,0,0) as a function of time for $0 \leq t \leq 1500$ years (left) and for $0 \leq t \leq 100$ years (right).

We may also consider points along a *line*. For example Figure 3 shows $\sigma_{xx}(0, 0, z, t)$ along a segment of the z-axis $-500 \leq z \leq 500$ (Line L_1 in Figure 15) for three different times $t = 5$, 50 and 500 years (one curve for each time). The point P_1: (0,0,0) is at the centre of the line L_1. The largest compressive stress along the z-axis occurs at the repository level $z = 0$. The actual maximum occurs after 66.6 years as can be seen in Figure 2, and the curve for that time would

be slightly higher than the curve $t = 50$ shown in Figure 3. Tensile stresses occur on both sides at a certain distance from the repository level $z = 0$. The tensile stresses are small at first but more pronounced later on. This is especially noticeable at the ground surface ($z = 500$) where the stress is 0.24, 1.73 and 5.81 MPa for the times 5, 50 and 500 years as shown in Figure 3.

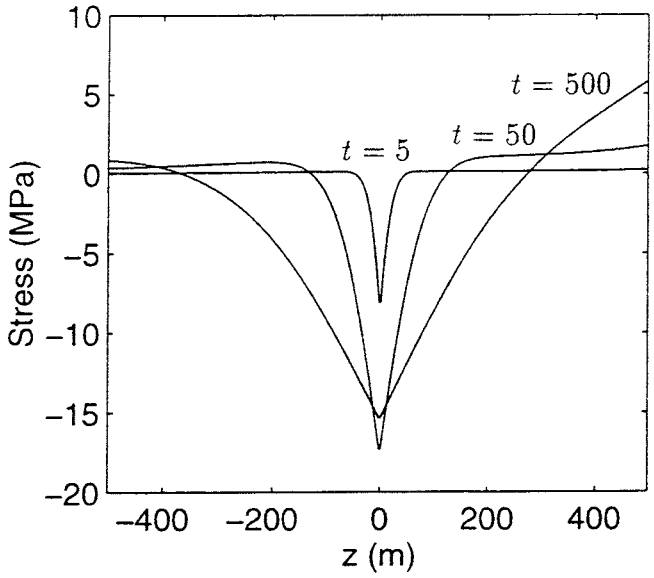

Figure 3. The stress $\sigma_{xx}(0, 0, z, t)$ along the z-axis, $-500 \leq z \leq 500$, for different times (5, 50 and 500 years). Each curve represents a different time.

Finally, we may consider points in a *plane*. Figure 4 shows the stress $\sigma_{xx}(x, 0, z, 500)$ in the xz-plane (plane S_1) after 500 years. The ground surface ($z = 500$) can be seen at the top of Figure 4, and the repository level is at $z = 0$. Half of the repository lies along $z = 0$, $0 \leq x \leq 500$. Level curves of the stress component are shown in Figure 4. The stresses are compressive around the repository from $x = 0$ to 1000 and z between -360 and 280. The level curves are marked in MPa. The largest compressive stress of over −15 MPa occurs at the centre of the repository ($x = z = 0$). This large stress can also be seen at the point P_1 in Figure 2 and along the line L_1 in Figure 3 for $t = 50$ years. Compressive stresses are also found at the ground surface $z = 500$ for x =700 to 1000. Tensile stresses are present above and below the repository level. The stresses above the centre of the repository are tensile for $z \geq 280$. The tensile stresses grow with increasing z until 6 MPa is reached at the ground surface. The stresses below the repository are tensile for $z \leq -360$ but the largest value is below 1 MPa. The large tensile stress at the ground surface can also be seen along the line L_1 in Figure 3 for $t = 500$. The whole line L_1 for $t = 500$, which is shown in Figure 3, is also present along the left side of Figure 4 ($x = 0$, $z = -500$ to 500).

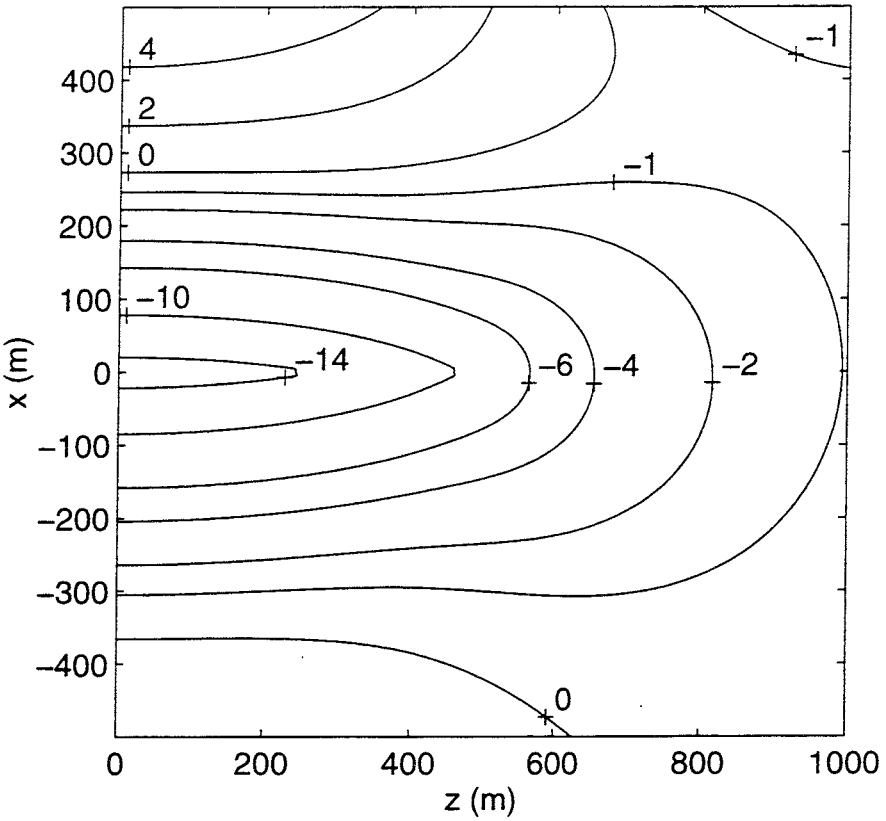

Figure 4. The stress $\sigma_{xx}(x, 0, z, 500)$ shown in a vertical cross-section of the repository after 500 years (xz-plane, $y = 0$). This figure is also shown in colour (Figure A5.1 in Appendix 5).

If the temporal development of a stress in a plane is to be studied, then a series of figures depicting the cross-section are needed – one figure for each time.

6 Temperature field

The temporal development of the temperature field derived in (Claesson J, Probert T, Jan. 1996) is illustrated in this section. The quadrantal heat source with the corresponding quadrantal temperature field is a fundamental part of the solution. The temperature field induced by a quadratic heat source situated at $-500 \leq x, y \leq 500$, $z = 0$ is constructed by summing four quadrantal heat sources (one for each corner of the quadratic heat source) followed by an integration in time. The rectangular heat source consists of two exponentials, Eq. (31).

In Figure 5 the temporal development of the temperature field is shown at the centre point P_1 for $0 \leq t \leq 1500$ years (left), and for $0 \leq t \leq 500$ years (right). It should be noted that the temperature is the excess temperature above the undisturbed temperature. The temperature increases rapidly during the first ten years. The maximum temperature 34.8°C occurs after 82.6 years. There is a second maximum of 34.5°C at $t = 396.0$ years, and an intermediate minimum of 34.1°C at $t = 198.1$ years. The temperature is between 34°C and 35°C for over 500 years from $t = 52$ to 558 years.

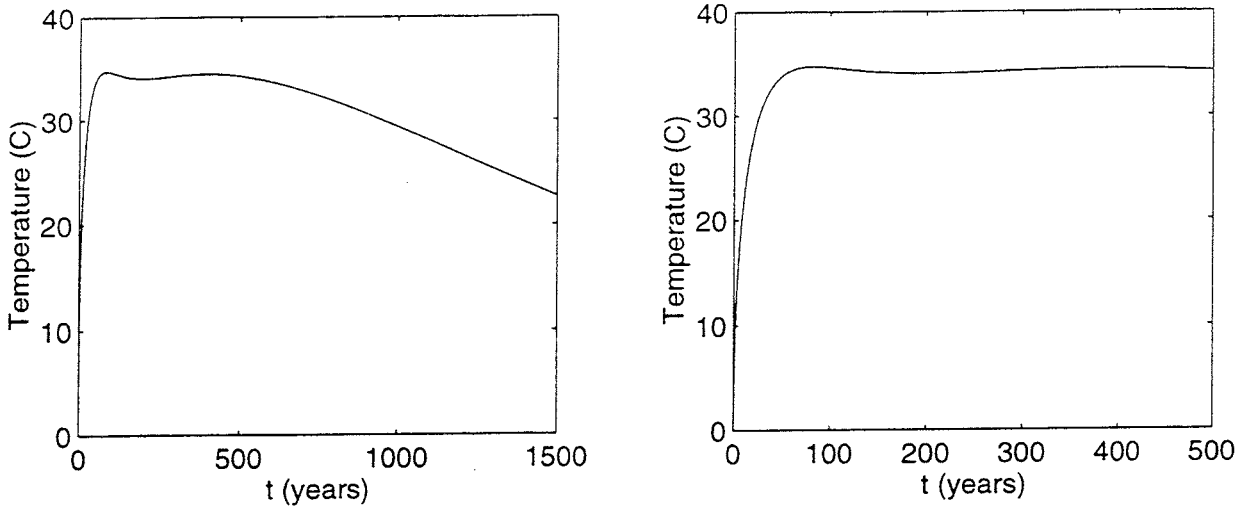

Figure 5. The temperature at the centre of the repository (point P_1) for $0 \leq t \leq 1500$ (left) and for $0 \leq t \leq 500$ (right).

The temperature field along the z-axis (the line L_1 in Figure 15) is shown in Figure 6 for four different times, $t = 5$, 50, 500 and 1000 years. The maximum temperature is reached between the $t = 50$ and $t = 500$ year curves.

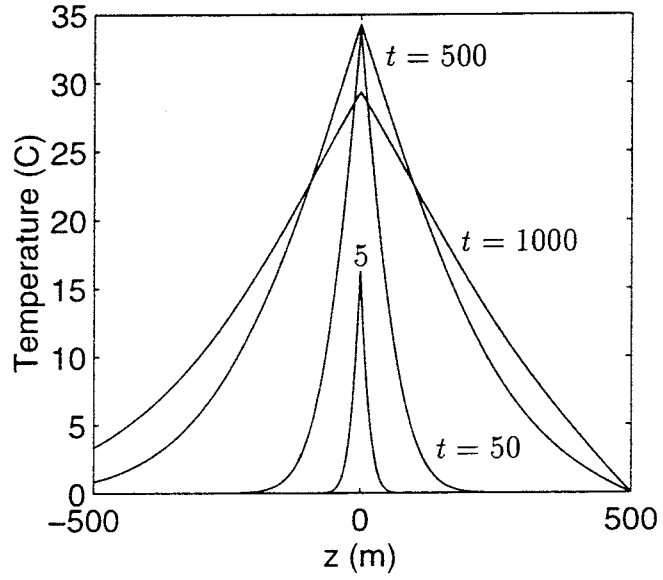

Figure 6. The temperature along the line L_1 for four times t =5, 50, 500 and 1000 years.

The temperature along the x-axis (the line L_2 in Figure 15) is shown in Figure 7 for four different times, $t = 5$, 50, 500 and 1000 years.

The temperature in the plane $y = 0$ (the plane S_1 in Figure 25) is shown in Figure 8 for t =50 years. The highest temperature is just under 34°C (not shown). The level curves of the temperature field are shown for the values 30, 15, 15, 1, 0.1, 0.01 and 0.0001°C. The level curves

encircle the repository at $0 \leq x \leq 500$, $z = 0$.

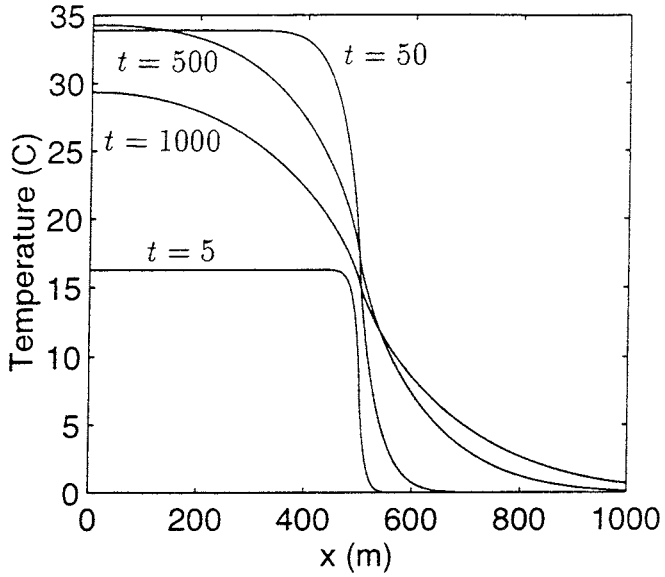

Figure 7. The temperature along the line L_2 for four times t =5, 50, 500 and 1000 years.

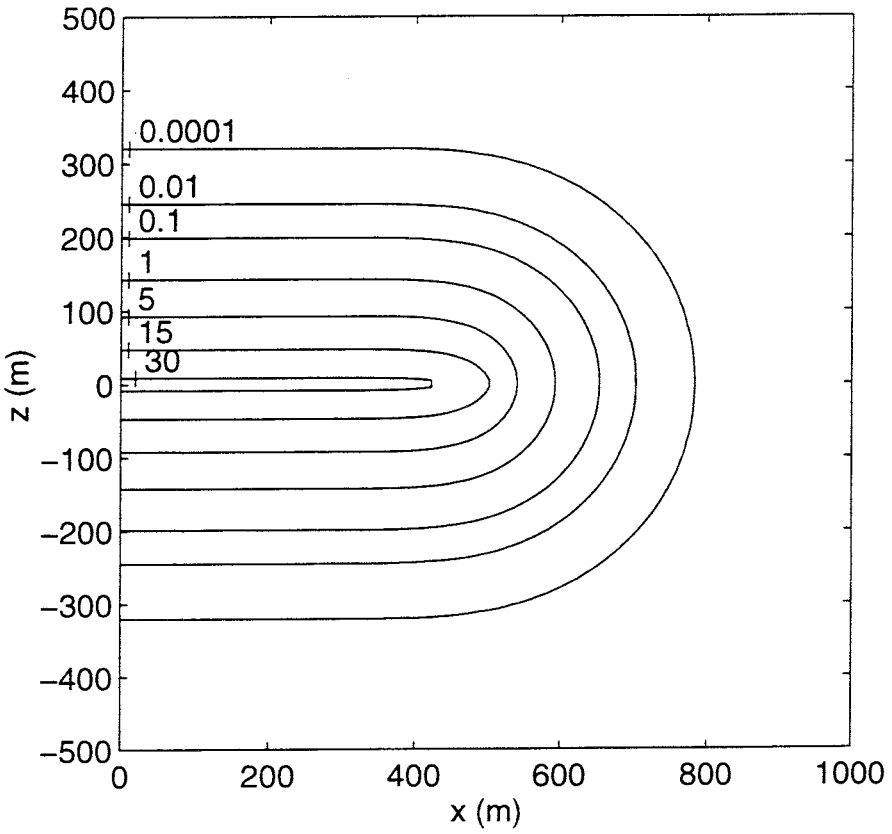

Figure 8. The temperature field in the plane $y = 0$ for $t = 50$ years.

The temperature field in the plane $z = 0$ (the plane S_2 in Figure 25) is shown in Figure 9 for t =50 years. The level curves of the temperature field are shown for the values 33, 25, 5, 1, 0.1, 0.01 and 0.0001°C. The level curves encircle the repository at $0 \leq x, y \leq 500$.

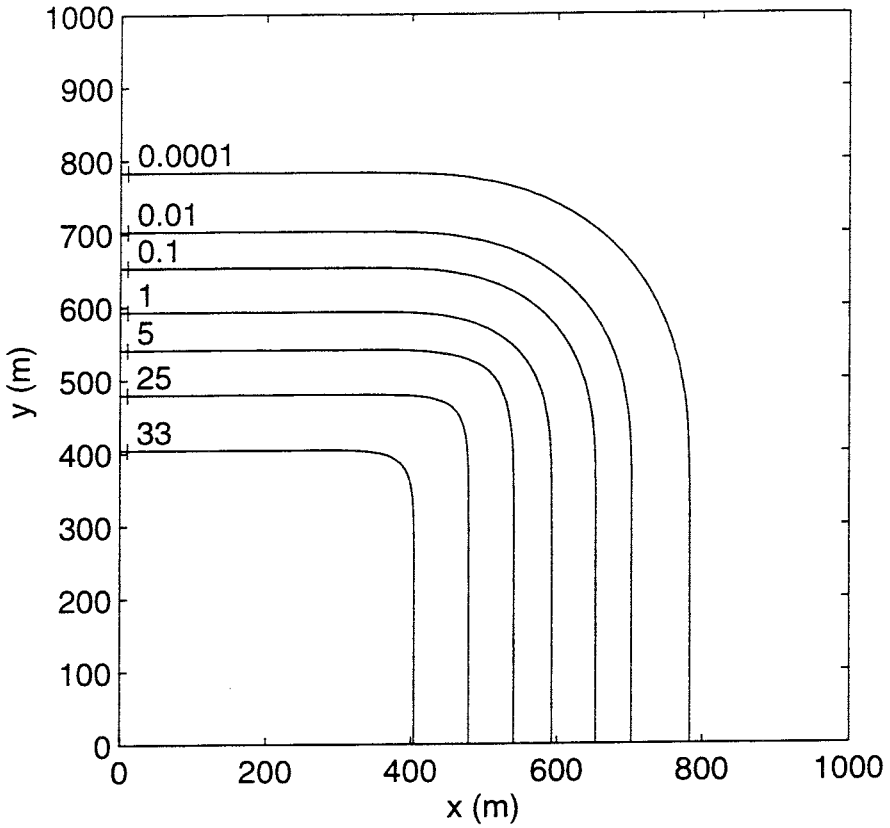

Figure 9. The temperature field in the plane $z = 0$ for $t = 50$ years.

7 Stresses at particular points

In this section we will look at the temporal development of stress components at certain points of interest. We will consider the points shown in Figure 10.

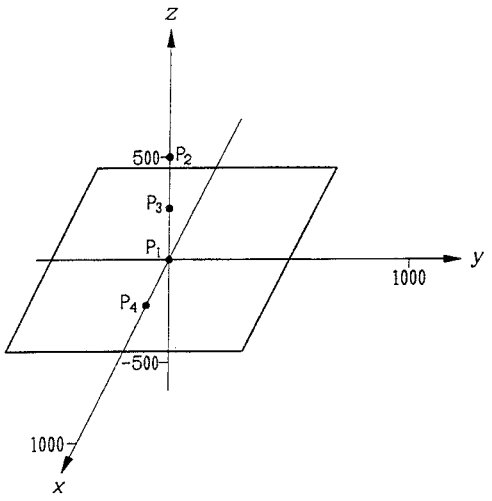

Figure 10. The points considered in this section.

The centre point P_1: (0,0,0) has symmetries that make $\sigma_{xy} = \sigma_{xz} = \sigma_{yz} = 0$ and $\sigma_{xx} = \sigma_{yy}$. We have:

$$P_1\text{: } (0,0,0) \qquad \sigma_{xx} = \sigma_{yy},\ \sigma_{xy} = \sigma_{xz} = \sigma_{yz} = 0$$

The two independent components σ_{xx} and σ_{zz} are shown in Figure 11 as functions of time.

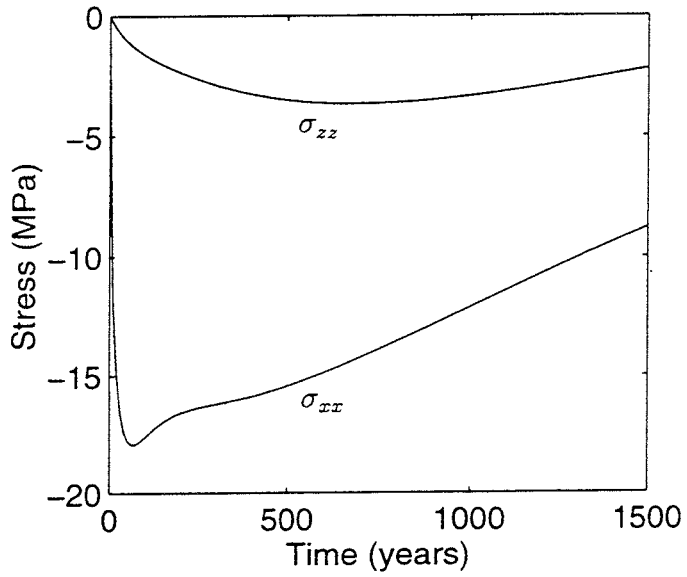

Figure 11. Stresses σ_{xx} and σ_{zz} at the centre point P_1.

The component σ_{xx} has been shown earlier in Figure 2. The two stresses are negative during the first 1500 years This results in compression at the centre of the repository. The horizontal stress σ_{xx} reaches its minimum value -17.92 MPa after 66.6 years, and the vertical stress σ_{zz} reaches its minimum value -3.66 MPa after approximately 682 years. The latter minimum is very flat and the former quite acute (See Table 1).

t (yrs.)	$\sigma_{xx}(0,0,0,t)$ (MPa)	$\sigma_{zz}(0,0,0,t)$ (MPa)
0	0.00	0.00
1	-4.18	-0.03
5	-8.86	-0.14
10	-11.81	-0.28
20	-14.94	-0.52
40	-17.33	-0.90
60	-17.90	-1.20
80	-17.85	-1.43
100	-17.61	-1.63
200	-16.59	-2.36
300	-16.21	-2.89
400	-15.89	-3.27
500	-15.45	-3.51
600	-14.90	-3.64
660	-14.53	-3.662
680	-14.40	-3.664
700	-14.26	-3.663
1000	-12.14	-3.35
1500	-8.77	-2.21

Table 1. Values of the two stresses σ_{xx} and σ_{zz} at point P_1 for selected times between 0 and 1500 years.

The symmetries of the point P_2: (0,0,500), at the ground surface directly above the centre of the repository, are the same as those of point P_1 and of every point situated on the z-axis. We have:

P_2: (0,0,500) $\qquad \sigma_{xx} = \sigma_{yy}, \sigma_{xy} = \sigma_{xz} = \sigma_{yz} = 0$

The temporal development at the point P_2 is shown in Figure 12.

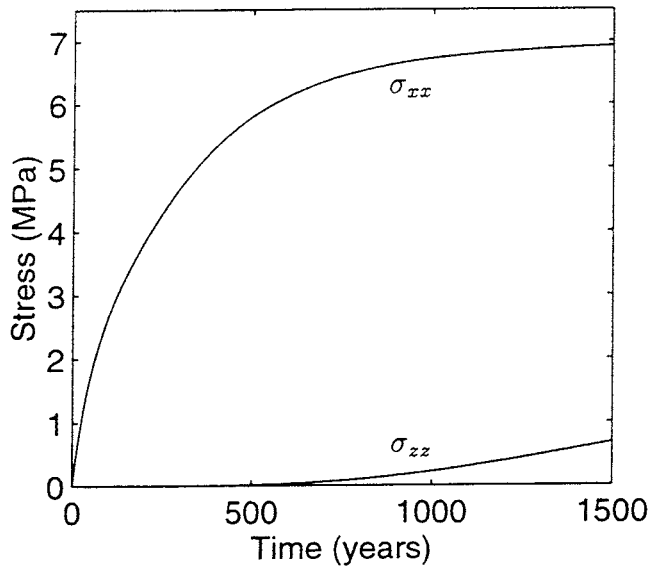

Figure 12. Stresses σ_{xx} and σ_{zz} at the point P_2.

The component σ_{zz} is zero for the first 500 years due to the construction of the solution. After this time, there is a small, gradual increase of this component, and a small violation of the boundary condition (4). We have stated that our solution is valid for at least 300 years at the ground surface. Here we see that the solution is valid for over 500 years. Values of the stress $\sigma_{zz}(0,0,500,t)$ are given in Table 2 for some times. The horizontal component σ_{xx} is also positive. This means that purely tensile stresses exist at the ground surface. The tensile stresses that occur at the ground surface are large, and they tend to grow with time, as can be seen in Figure 12 and in Table 3. The stress σ_{xx} at the ground surface for $t = 1500$ years is the largest tensile stress encountered in this study (See Table 3).

t (yrs.)	σ_{zz}(0,0,500,t) (MPa)
0	0.00000
100	−0.00003
200	−0.00012
300	−0.00005
400	0.0019
500	0.0095
600	0.027
700	0.056
800	0.099
900	0.15
1000	0.22
1100	0.30
1200	0.39
1300	0.48
1400	0.58
1500	0.68

Table 2. Values of the vertical stress σ_{zz} at point P_2 for the first 1500 years showing how the boundary condition σ_{zz}(0,0,500,t)= 0 is disturbed.

t (yrs.)	σ_{xx}(0,0,500,t) (MPa)
0	0.00
1	0.05
5	0.24
10	0.46
50	1.73
100	2.68
300	4.72
500	5.81
1000	6.72
1500	6.92

Table 3. Values of the horizontal stress $\sigma_{xx} = \sigma_{yy}$ at point P_2 for the first 1500 years. Large tensile stresses occur at the ground surface. The overall maximum tensile stress occurs here.

The point half-way between P_1 and P_2 is P_3: (0,0,250) (See Figure 10). This point is also on the z-axis so it has the same symmetries as P_1 and P_2. We have:

P_3: (0,0,250) $\qquad \sigma_{xx} = \sigma_{yy}, \sigma_{xy} = \sigma_{xz} = \sigma_{yz} = 0$

Figure 13 shows that σ_{xx} is positive (tensile) for the first 350 years and negative (compressive) during the next 1150 years. Figure 13 also shows that σ_{zz} is negative (compressive) for the first 1500 years after deposition. Both tension and compression exist at P_3. The horizontal stress σ_{xx} reaches its largest tensile value 1.58 MPa after 113 years and its largest compressive value −2.00 after 1102 years. The component σ_{zz} has a minimum of −1.60 MPa after 616 years.

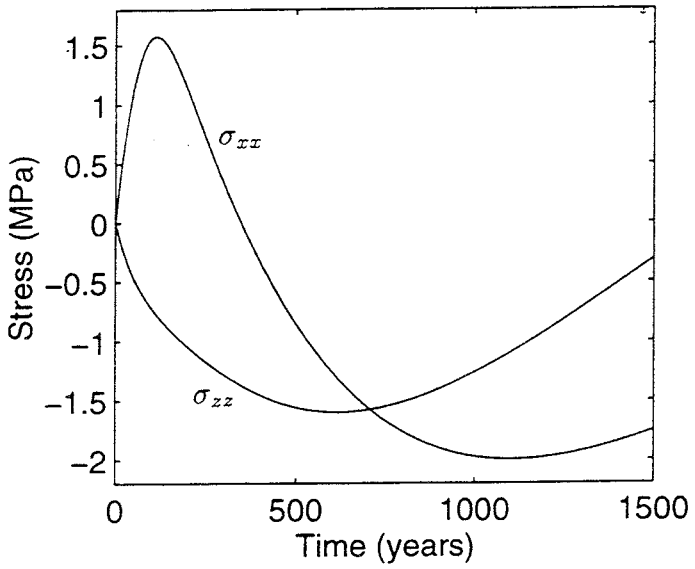

Figure 13. Stresses σ_{xx} and σ_{zz} at the point P_3.

A point that is in the repository plane but not on the z-axis is P_4: (250,0,0) (See Figure 10). This point lies on the x-axis so $y = 0$. The plane $y = 0$ is a symmetry plane which accounts for $\sigma_{xy} = \sigma_{yz} = 0$. We have:

P_4: (250,0,0) $\qquad \sigma_{xy} = \sigma_{yz} = 0$

The four nonzero components of the stress field at P_4 are shown in Figure 14. The four components are negative and three of them have minima. The horizontal stresses have their minima at $t = 62$ years for $\sigma_{xx} = -17.4$ MPa and at $t = 67$ years for $\sigma_{yy} = -18.0$ MPa. The vertical stress σ_{zz} reaches its minimum of -3.7 MPa for $t = 543$ years.

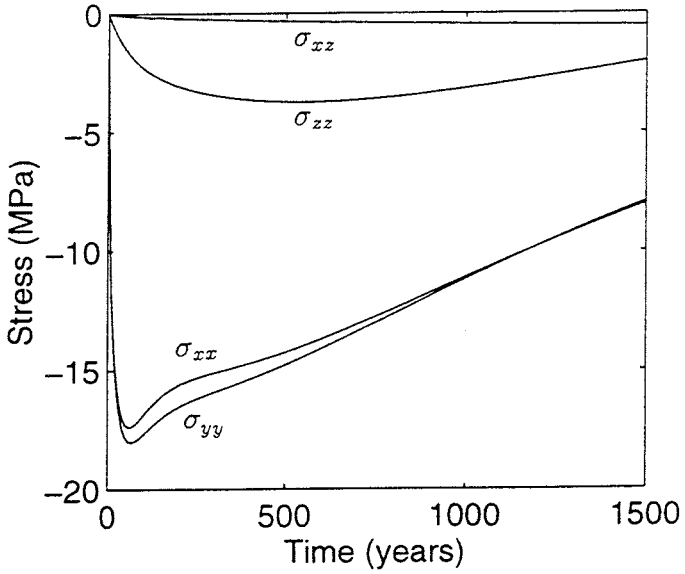

Figure 14. Stresses σ_{xx}, σ_{yy}, σ_{zz} and σ_{xz} at the point P_4.

8 Stresses along particular lines

In this section we will look at the temporal development of stress components along certain lines. We will consider the lines shown in Figure 15.

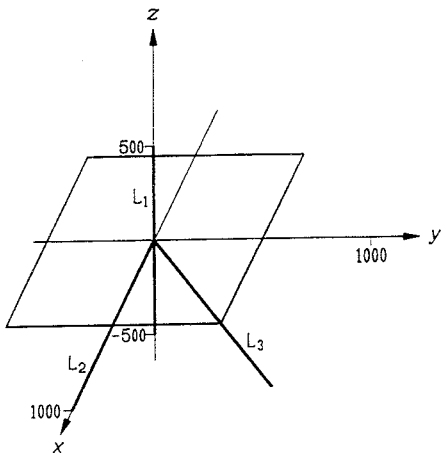

Figure 15. The lines considered in this section.

The line L_1 in Figure 15 is the z-axis from $z = -500$ to $z = 500$. It covers the stresses at the ground surface ($z = 500$) and at the centre of the repository (0,0,0). The symmetries that applied to P_1, P_2 and P_3 are valid. We have:

L_1: (0,0,z) $\quad -500 \leq z \leq 500 \quad \sigma_{xx} = \sigma_{yy}, \sigma_{xy} = \sigma_{xz} = \sigma_{yz} = 0$

The stress components σ_{xx} and σ_{zz} along L_1 are shown for different times in Figures 16 and 17. Curves are shown for the times 5, 50, 300, 500 and 1000 years.

The horizontal stress σ_{xx}, parallel to the repository plane, is in the beginning, very localized around the repository, though its influence can be noticed at the ground surface as early as after 5 years (See Figure 16). The largest compressive stresses along L_1 are found at the repository level, at point P_1. (See Figure 16 and Table 1). There is a local maximum below the repository ($z < 0$) that moves away from repository (decreasing z) with time. The largest value of this local maximum is 1.01 MPa at $z = -376$ metres for $t = 204$ years. Other values and locations of this local maximum are 0.73 MPa at $z = -210$ m for $t = 50$ years, 0.99 MPa at $z = -442$ m for $t = 300$ years and 0.95 MPa at $z = -500$ m for $t = 400$ years. In a region directly above and below the repository the stresses are compressive. Tensile stresses appear after 5 years at 50 metres above and below the repository. The region of compression increases outwards from the repository with time so that after 50 and 300 years the tensile stresses appear 100 and 200 metres, respectively, above and below the repository level. The largest stresses occur at the centre of the repository between 50 and 300 years (approximately -17 MPa). At the ground surface large tensile stresses occur, and they tend to grow with time (approximately 6 MPa after 1000 years. See Table 3). The solution is not strictly valid for these large times but for times around 500 years, for which the solution is valid, large tensile stresses are found at the ground surface $z = 500$.

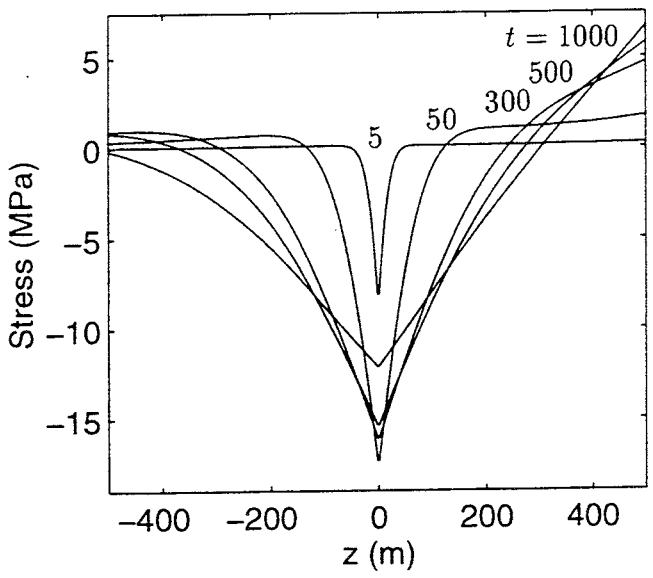

Figure 16. Stress σ_{xx} along the line L_1.

The stress σ_{zz}, normal to the repository plane, is with good accuracy zero at the ground surface for over 500 years which confirms that the solution is valid there during at least the first 300 years. This limit can be extended to 500 years or more as Figure 17 shows. This component has a very smooth appearance. There is a local minimum just below the repository level $z = 0$. This minimum moves downwards with time. The smallest value of this minimum is -3.77 MPa at $z = 668$ m for $t = 705$ years. Other values and locations of this minimum are 0.11 MPa at $z = -47$ m for $t = 50$ years, 0.36 MPa at $z = -56$ m for $t = 500$ years and 0.35 MPa at $z = -88$ m for $t = 1000$ years. After 1000 years the zero condition at the ground surface is no longer

fulfilled. The stress is compressive all along the z-axis until after 500 years when the stress at the ground surface changes sign and becomes tensile. Gradually, the tensile stress at the ground surface penetrates into the semi-infinite medium. The distance penetrated after 1000 years is 100 metres, and after 1500 years over 300 metres. The curve for $t = 1500$ years is not shown in Figure 17.

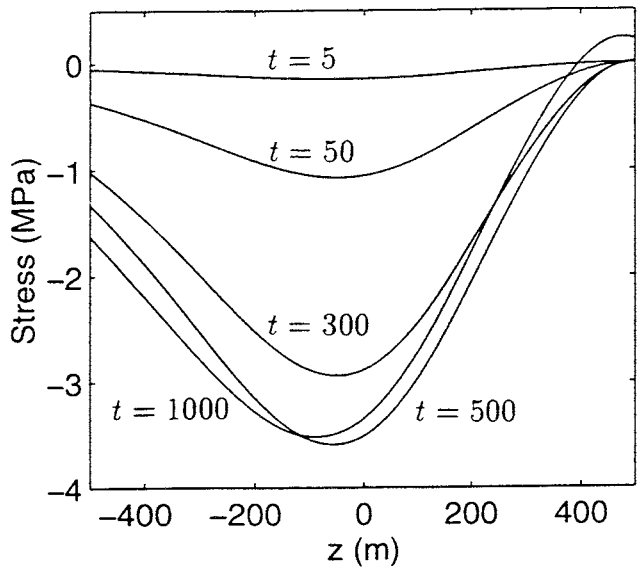

Figure 17. The vertical stress σ_{zz} along the line L_1.

The line L_2 in Figure 15 along the x-axis, from the repository centre (0,0,0) to $x = 1000$, is also of interest in the assessment of the stresses. Along the line L_2 the stresses σ_{xy} and σ_{yz} are zero because L_2 lies on the symmetry plane $y = 0$. We have:

$$L_2\text{: } (x,0,0) \qquad 0 \leq x \leq 1000 \qquad \sigma_{xy} = \sigma_{yz} = 0$$

The four remaining nonzero components along L_2 are shown in Figures 18-21.

The horizontal stresses σ_{xx} and σ_{yy} along the line L_2 are similar (See Figures 18 and 19). The two main differences are that σ_{yy} is tensile outside the repository ($x > 500$) and that σ_{yy} changes more rapidly than σ_{xx} when crossing the repository edge ($x = 500$) (Compare Figures 18 and 19). Both horizontal stress components are below −15 MPa in the repository area for times between 50 and 500 years. The stress σ_{yy} has an extreme point inside (minimum) and one outside (maximum) the repository. These extremes are very flat and hard to see. In Table 4 the position and value of the minimum of σ_{yy} along L_2 is shown for a few times. The minimum is located at the centre point P_1 for times larger than 330 years. The maximum compressive stress along L_2 occurs at $x = 303$ m for $t = 66.5$ years. The maximum compressive stress is −18.06 MPa and this is actually the overall largest compressive stress encountered in this study.

t (yrs.)	x (m)	$\sigma_{yy}(x,0,0,t)$ (MPa)
1	465	-4.18
5	432	-8.90
20	380	-15.04
40	340	-17.46
60	311	-18.04
66.5	303	-18.06
80	287	-17.99
100	265	-17.74
200	176	-16.64
300	80	-16.21
329	13	-16.12

Table 4. Values and position of the minimum of σ_{yy} along L_2 for times less than 330 years. The overall largest compressive stress occurs along L_2.

The value and position of the maximum of σ_{yy} along L_2 for the times 5, 50 and 500 years are 0.08 MPa at $x = 568$ m, 0.43 MPa at $x = 672$ m and 0.71 MPa at $x = 921$ m. The largest value of the maximum is 0.71 MPa at $x = 919$ for $t = 493$. Both extreme points (maximum and minimum) move away from the repository edge with time. This means that the minimum moves towards the centre of the repository and the maximum moves away from the repository.

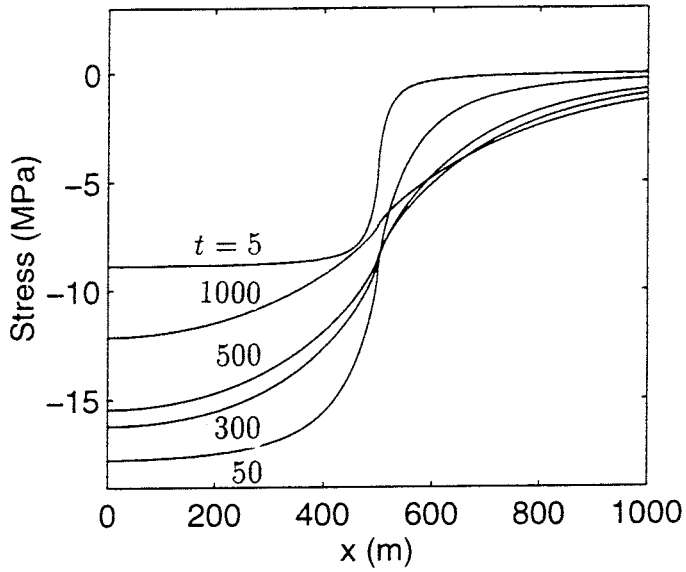

Figure 18. The horizontal stress component σ_{xx} along the line L_2.

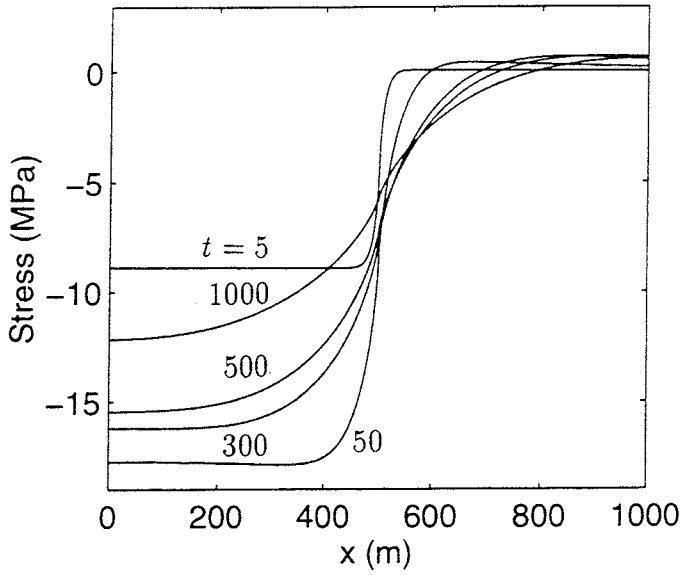

Figure 19. The horizontal stress component σ_{yy} along the line L_2.

The vertical stress σ_{zz} is shown in Figure 20. This stress is compressive in the repository area and tensile outside. The largest value of σ_{zz} is found just outside the repository area. The maximum is sharp for small times, but becomes rather flat for large times. Also, the maximum moves outwards from the repository with time. The largest value of the maximum is 2.36 MPa at $x = 574$ m for $t = 61$ years. The minimum, just inside the repository area, behaves in a similar manner, and moves inwards, to the center of the repository with time. The smallest value of the minimum is -3.74 MPa at $x = 227$ m for $t = 567$ years.

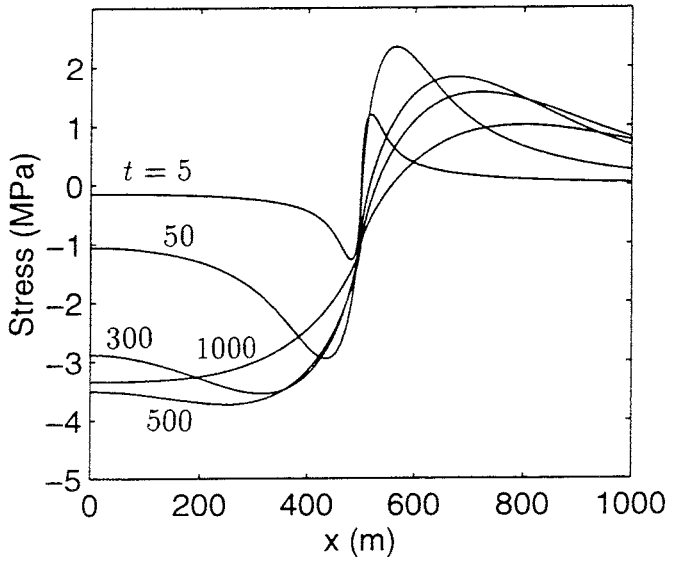

Figure 20. Stress σ_{zz} along the line L_2.

In Figure 21 the stress σ_{xz} is shown. This component is compressive and does not vary that much along the line L_2. It has a minimum just outside the repository at $x = 524$ m. The minimum is stationary (within the accuracy of less than 0.5 m) and its value decreases with time. After 500, 1000 and 1500 years the minimum value is -0.49, -0.68 and -0.78 MPa, respectively.

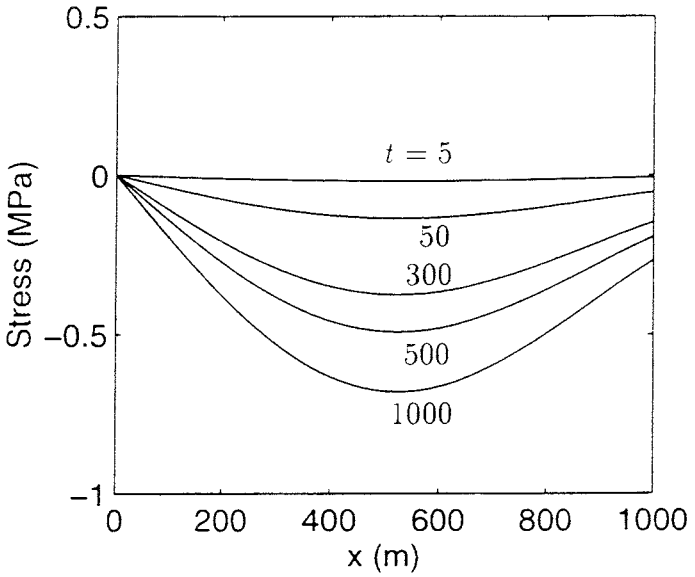

Figure 21. The stress component σ_{xz} along the line L_2.

The stresses along the diagonal $x = y$ of the repository, from the centre (0,0,0) to (707,707,0), are also examined. Along this line, called L_3 in Figure 15, the stresses σ_{xx} and σ_{xz} are equal to σ_{yy} and σ_{yz}, respectively, because $x = y$ is a plane of symmetry. We have:

$$L_3\text{: } (s/\sqrt{2},s/\sqrt{2},0) \qquad 0 \leq s \leq 1000 \qquad \sigma_{xx} = \sigma_{yy},\ \sigma_{xz} = \sigma_{yz}$$

Since we are following the diagonal $x = y$ (L_3) in the xy-plane we need a length variable along this line. This variable is called s and is defined by:

$$s = \sqrt{2}x,\ x = y \tag{32}$$

The stresses along L_2 and L_3 are similar. Stresses along the line L_3 behave in much the same manner as stresses along the line L_2 (Compare Figures 22-25 with Figures 18-21). The curves in Figures 18-22 seem to be 'stretched' in the x-direction by a factor $\sqrt{2}$.

The stress σ_{xx} shown in Figure 22 seems to be a mixture of σ_{xx} in Figure 18 and σ_{yy} in Figure 19. The horizontal stress is compressive all along L_3. There are, however, no local extremes near the corner of the repository, $s = \sqrt{2}x = 707$, inside or outside the repository.

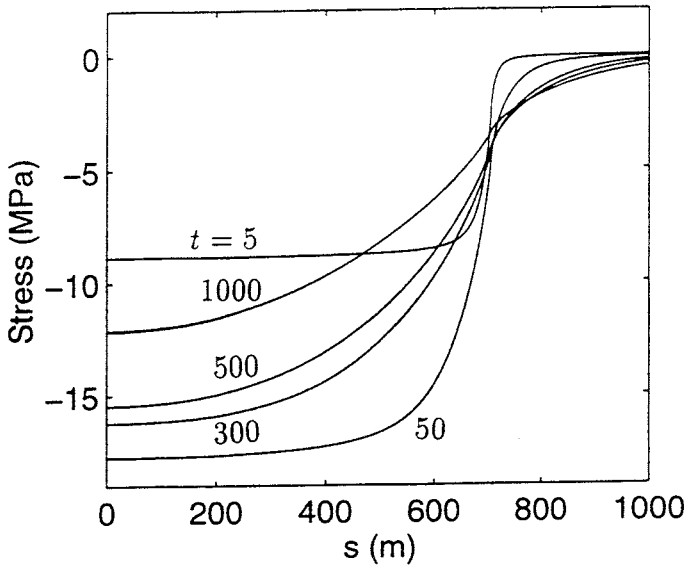

Figure 22. Horizontal stress $\sigma_{xx} = \sigma_{yy}$ along the line L_3.

In Figure 23, the vertical stress σ_{zz} along L_3 is shown. This stress resembles σ_{zz} along L_2 in Figure 20.

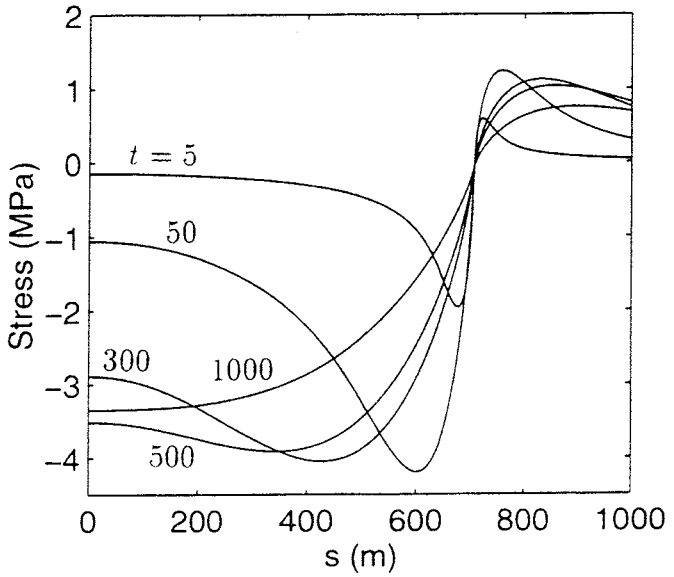

Figure 23. Vertical stress σ_{zz} along the line L_3.

The stress σ_{xy} along L_3 is shown in Figure 24. The shear stress reaches its largest value −2.6 MPa between 50 and 100 years at the repository corner. After reaching this maximum the compressive extreme point decreases in magnitude and moves gradually outwards from the repository. The stress σ_{xz} is not shown but it is nearly identical to the stress component shown in Figure 21.

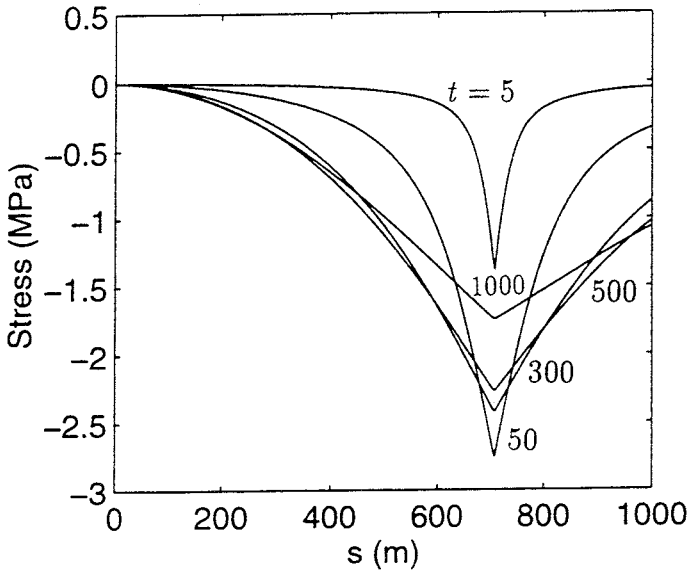

Figure 24. The stress component σ_{xy} along the line L_3.

9 Stresses for particular planes

In this section we will look at stresses for given planes. In particular, we will look at the temporal development of the stresses in the planes. The planes, which all cover an area 1000×1000 m^2, are shown in Figure 25.

The planes are:

$S_1 : y = 0 \qquad S_2 : z = 0 \qquad S_3 : x = y$

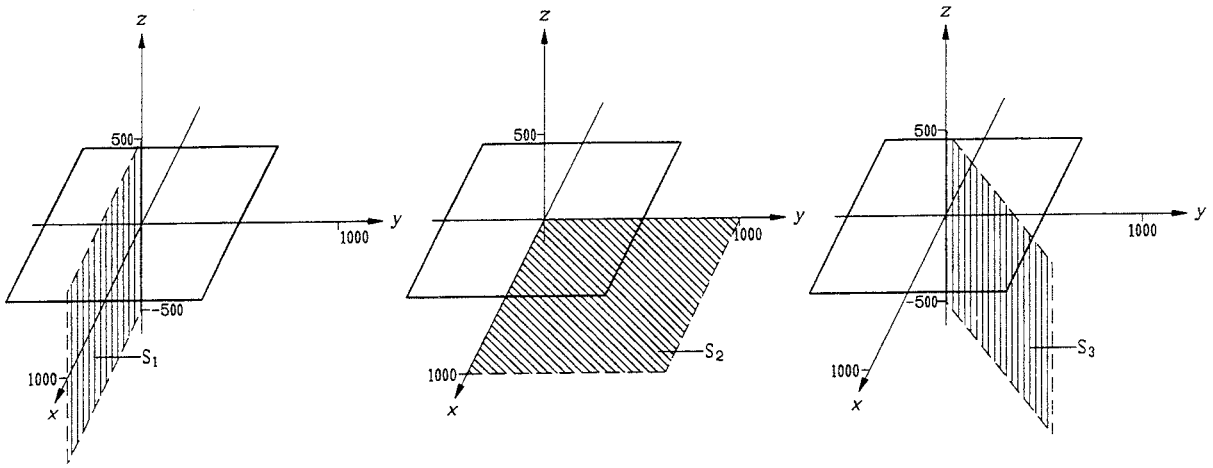

Figure 25. The planes S_1, S_2, and S_3 considered in this section.

For the plane S_1 we have:

S_1: $(x,0,z) \qquad 0 \leq x \leq 1000, \; -500 \leq z \leq 500 \qquad \sigma_{xy} = \sigma_{yz} = 0$

We calculate one of the stress components, say $\sigma_{xx}(x,0,z,t)$ for points in S_1 for a given time t. The level curves of $\sigma_{xx}(x,0,z,t)$ can then be plotted as is done in Figure 26 where $t = 50$ years. The unit MPa is used for the stresses in all the figures showing level curves.

Figure 26 shows the horizontal stress σ_{xx} in the vertical cross-section S_1. The stresses around the repository are compressive. The largest compressive stress reaches over −16 MPa along the repository ($0 \leq x \leq 300$, $z = 0$) in compliance with earlier results along the line L_2. A region where tensile stresses reign is found 140 metres above the repository level, and it stretches all the way up to the ground surface. The tensile stress is between 0 and 2 MPa. A similar region is found 140 metres below the repository level but the tensile stresses are smaller there (0-1 MPa). The unlabelled level curve in the upper right-hand corner of Figure 26 is the −0.3 MPa contour.

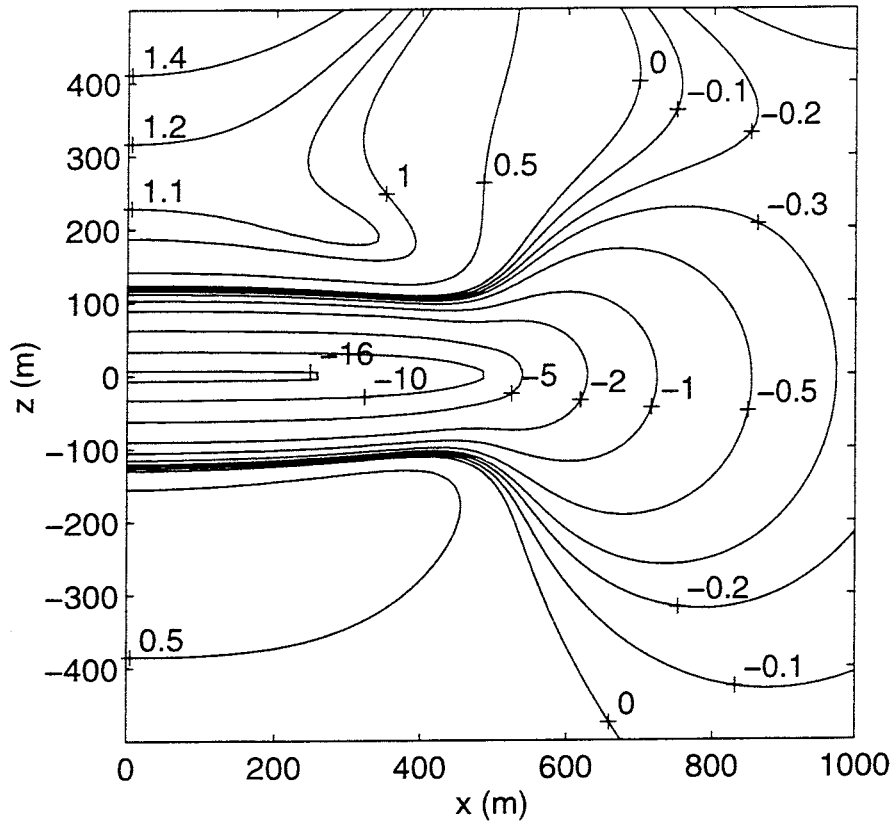

Figure 26. The horizontal stress σ_{xx} in the plane S_1 after 50 years. This figure is also shown in colour (Figure A5.2 in Appendix 5).

Figure 27 shows the same stresses as in Figure 26 but for $t = 300$ years. The temporal development is quite apparent. The compressive stresses around the repository level have decreased slightly and the level curves are more outspread. The tensile stresses above and below the repository level have grown in amplitude. The increase is less than 1 MPa below the repository level, but over 3 MPa above. At the ground surface the large tensile stresses (>4 MPa) noted earlier can be seen. The unlabelled level curve in the upper right-hand corner of Figure 27 is the -1 MPa contour.

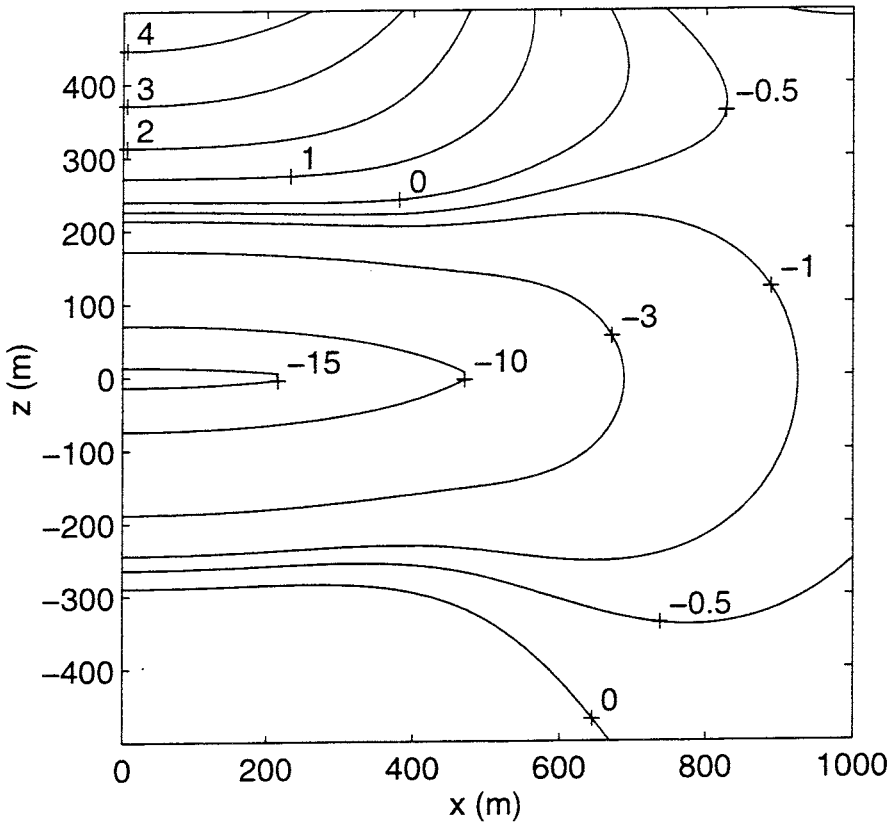

Figure 27. The stress σ_{xx} in the plane S_1 after 300 years.

After 1000 years the stresses at the ground surface have become larger (5 MPa) and the level curves have moved together as can be seen in Figure 28. The tensile stresses below the repository have almost died out and the compressive stresses around the repository have decreased in magnitude. The level curves are more dispersed than before. The unlabelled level curve in the upper left-hand corner of Figure 28 is the 6 MPa contour.

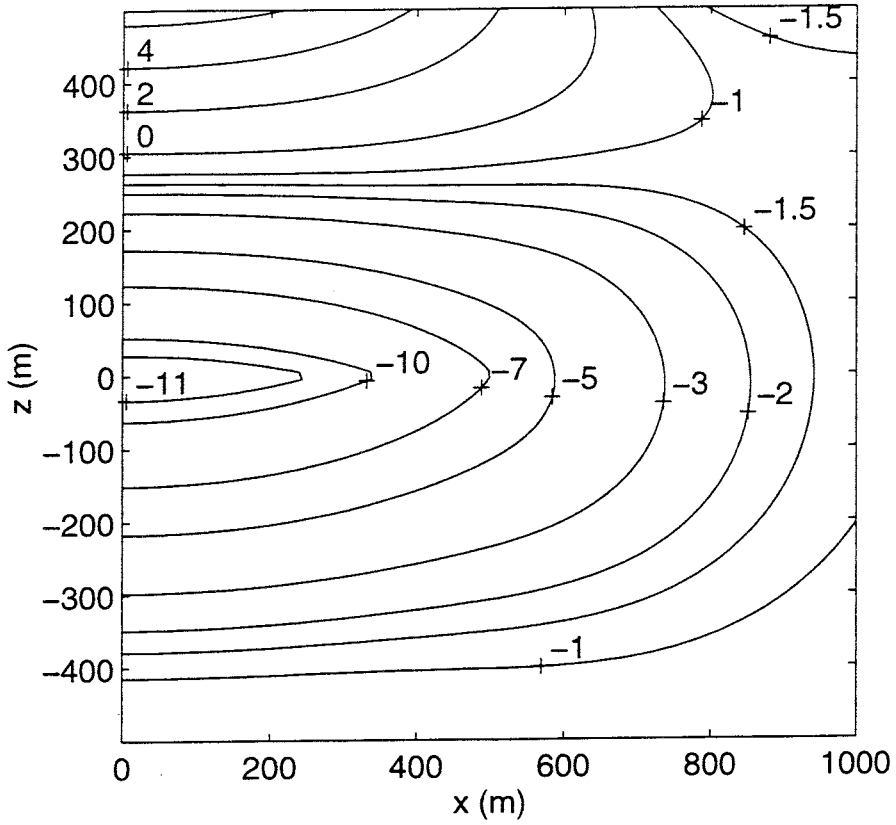

Figure 28. The stress σ_{xx} in the plane S_1 after 1000 years.

The stress σ_{yy}, shown in Figure 29 for $t = 1000$ years, is similar to σ_{xx}. The temporal development of the stress σ_{zz} is not as dramatic as that of σ_{xx}. The unlabelled level curve in the upper left-hand corner of Figure 29 is the 6 MPa contour.

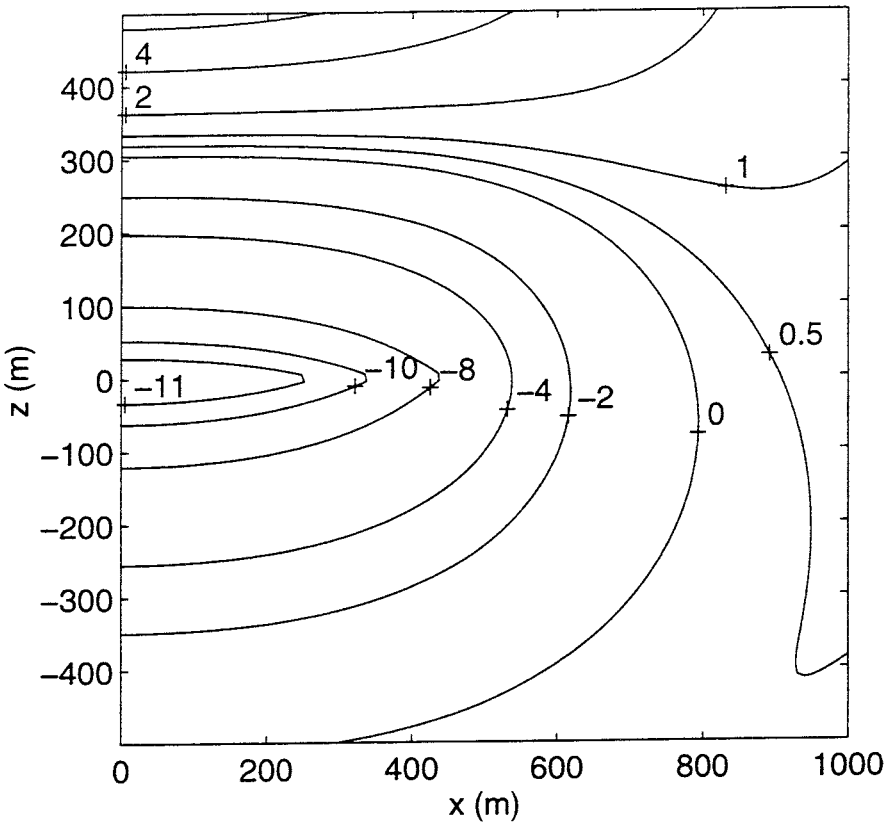

Figure 29. The horizontal stress σ_{yy} in the plane S_1 after 1000 years. This figure is also shown in colour (Figure A5.3 in Appendix 5).

Figure 30 shows the stress σ_{zz} after 100 years. The maximum tensile and compressive stresses occur around this time and they are located 100 metres to the right (tensile) and left (compressive) of the repository edge ($x = 500$, $z = 0$). Before this time the compressive stresses cover a smaller area and the maximum is smaller. The same applies to the tensile stresses. After 100 years the maxima decrease in magnitude and the level curves become more dispersed.

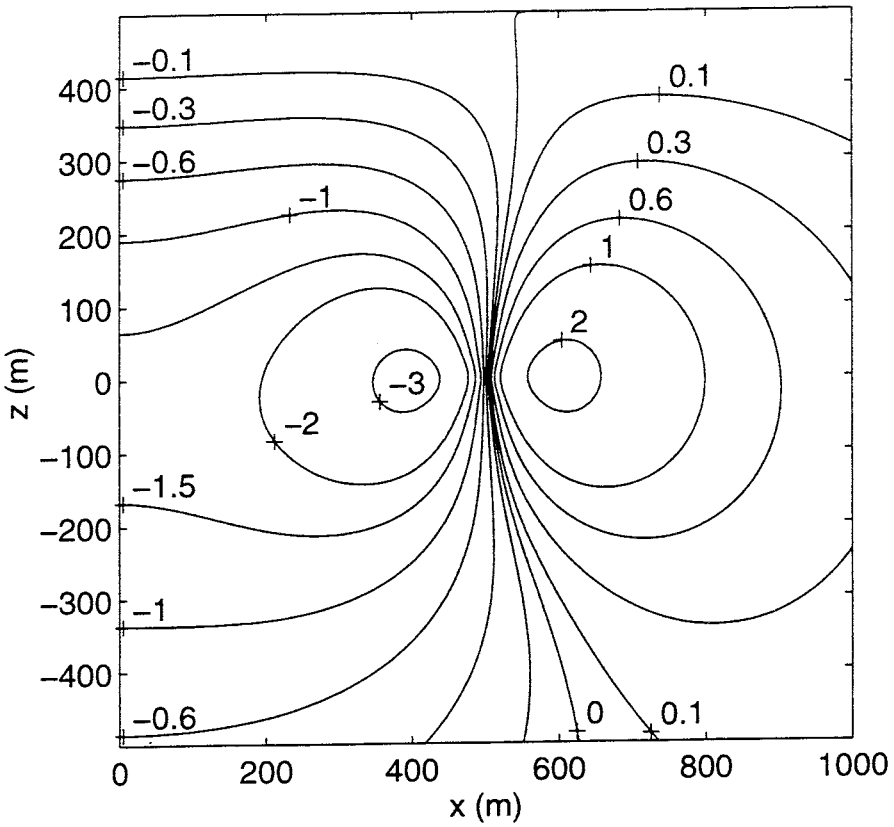

Figure 30. The vertical stress σ_{zz} in the plane S_1 after 100 years. This figure is also shown in colour (Figure A5.4 in Appendix 5).

The repository plane S_2 ($z = 0$, Figure 25) is also studied. The line L_3 ($x = y$) is a symmetry line to the stresses in S_2 which means that $\sigma_{yy}(x,y,0,t) = \sigma_{xx}(y,x,0,t)$ and $\sigma_{yz}(x,y,0,t) = \sigma_{xz}(y,x,0,t)$. We have:

S_2: $(x,y,0)$	$0 \leq x \leq 1000,\ 0 \leq y \leq 1000$	$\sigma_{yy}(x,y,0,t) = \sigma_{xx}(y,x,0,t)$ $\sigma_{yz}(x,y,0,t) = \sigma_{xz}(y,x,0,t)$

The stresses in the plane S_2 are shown in Figures 31-34.

In Figure 31 the horizontal stress σ_{xx} in the plane S_2 is shown after 50 years. The largest compressive stress is over −16 MPa, covering a large area of the repository. This can be compared with the stresses at point P_1 and along the lines L_1 and L_2 (See Figures 2, 3 and 18). The compressive stress changes rather abruptly, in the y-direction, from −16 to 0 MPa at the top edge of the repository ($y = 500$) in Figure 31. In the x-direction, at the right edge of the repository , the change is smoother. Tensile stresses are beginning to develop outside the repository, in the region y =600 to 800 and x =0 to 400. The horizontal stress σ_{yy} is not shown but it is identical to σ_{xx} mirrored in the line $x = y$ ($\sigma_{yy}(x,y,0,t) = \sigma_{xx}(y,x,0,t)$).

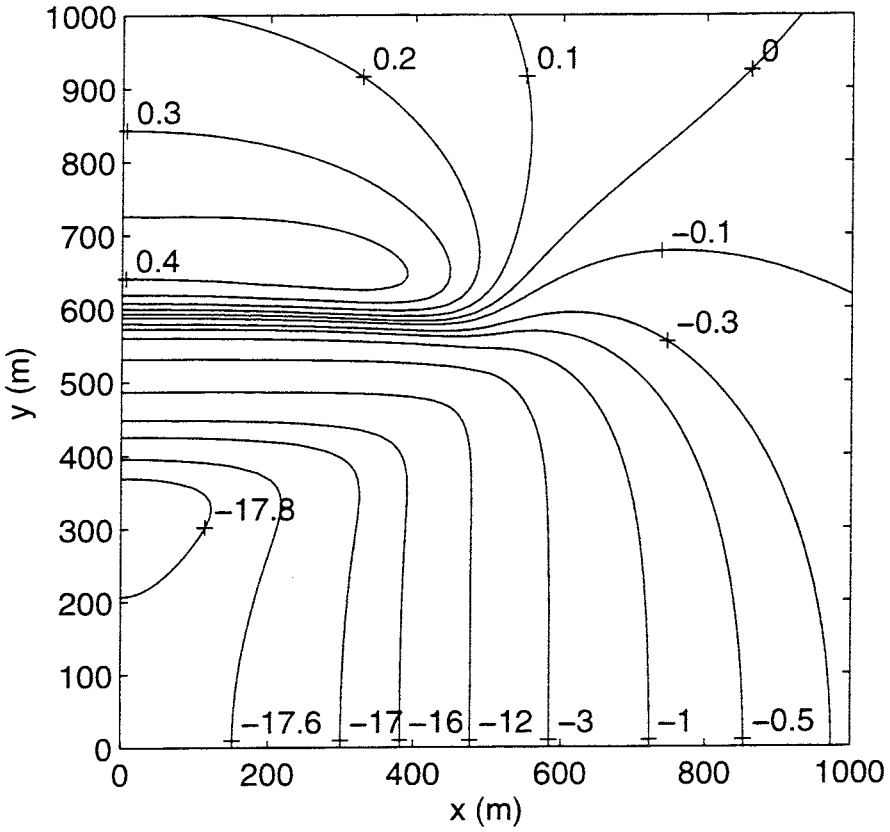

Figure 31. The stress σ_{xx} in the plane S_2 after 50 years. This figure is also shown in colour (Figure A5.5 in Appendix 5).

In Figures 32-34 the temporal development of the normal stress σ_{zz} in the plane S_2 is illustrated. Figure 32 shows the stress $\sigma_{zz}(x, y, 0, 50)$ in the plane S_2 after 50 years. The figure shows one quarter of the repository in the bottom, left corner of the figure ($0 \leq x,\ y \leq 500$). Level curves of the stress σ_{zz} are shown. The vertical stress σ_{zz} is normal to the plane S_2. The stress is compressive in and close to the repository area. A local minimum of –4 MPa at (440,440,0) can be seen near the repository corner. Another (local) compressive maximum of –2 MPa is located at the centre of the repository (0,0,0). Tensile stresses (0-2 MPA) exist outside the repository area, the largest of which (2 MPa) are located on islands parallel to the sides of the repository. This figure shows the intricate fine structure near the corner of the repository.

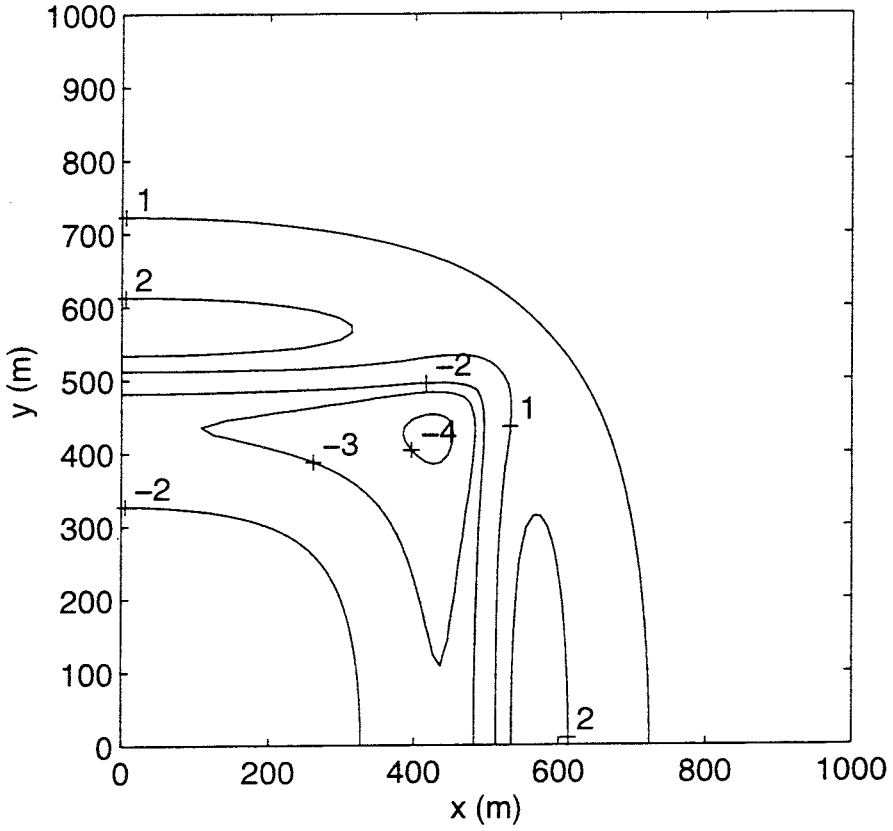

Figure 32. The vertical stress σ_{zz} in the horizontal plane S_2 after 50 years. This figure is also shown in colour (Figure A5.6 in Appendix 5).

The main trend of the temporal development of the normal stress σ_{zz} in the plane S_2, shown in Figures 32-34, is that after the maximum compressive and tensile stresses are reached (between 50 and 300 years) the stresses start to decrease and move away from the repository periphery. Compressive stresses are found inside and in the vicinity of the repository area, and the tensile stresses are found outside the compressive stresses, and they have a tendency to concentrate in islands parallel to the sides of the repository. The maximum compressive stress found just inside the repository, at the corner, has disappeared after 1000 years.

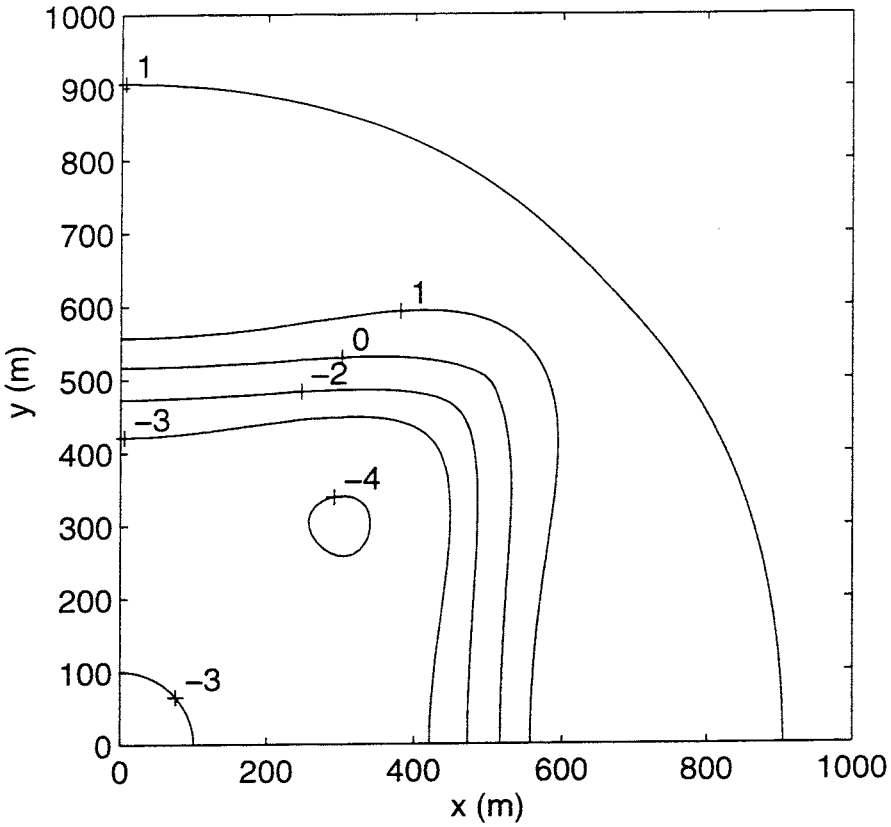

Figure 33. The vertical stress σ_{zz} in the plane S_2 after 300 years.

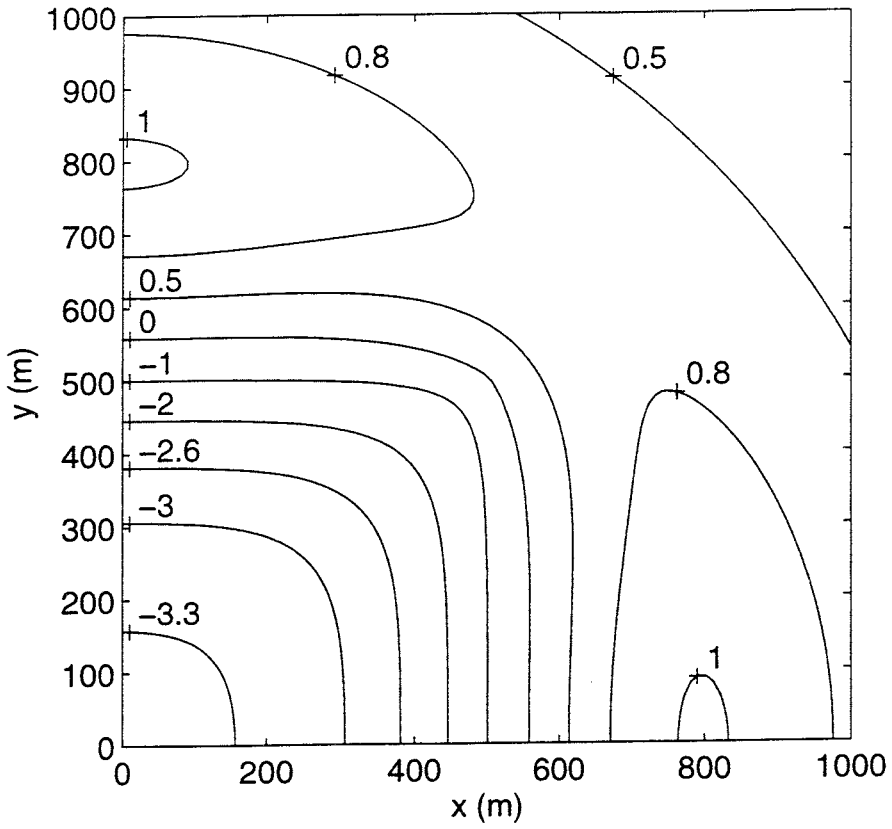

Figure 34. The vertical stress σ_{zz} in the plane S_2 after 1000 years. This figure is also shown in colour (Figure A5.7 in Appendix 5).

The remaining stresses σ_{xy}, σ_{xz} and σ_{yz} are not shown in the plane S_2. Some of them are however shown along the lines L_2 and L_3 which lie in the plane S_2. These stresses do not attain the large values of the horizontal and vertical stresses.

The stresses in the plane S_3 through L_1 and L_3 are also examined. The symmetries of the stresses along L_3 are also valid here. We have:

S_3: (x,x,z) $\quad 0 \leq x \leq 707, -500 \leq z \leq 500 \quad$ $\sigma_{yy} = \sigma_{xx}, \sigma_{yz} = \sigma_{xz}$

Some of the stresses in the plane S_3 are shown in Figures 35 and 36.

The stress σ_{xx} and σ_{zz} in the plane S_3, shown in Figures 35 and 36 respectively, resemble the same stresses in the plane S_1 shown earlier in Figures 27 and 30. The stresses in planes S_1 and S_3 are similar and behave in a similar way. The unlabelled level curve in the upper right-hand corner of Figure 35 is the 0 MPa contour.

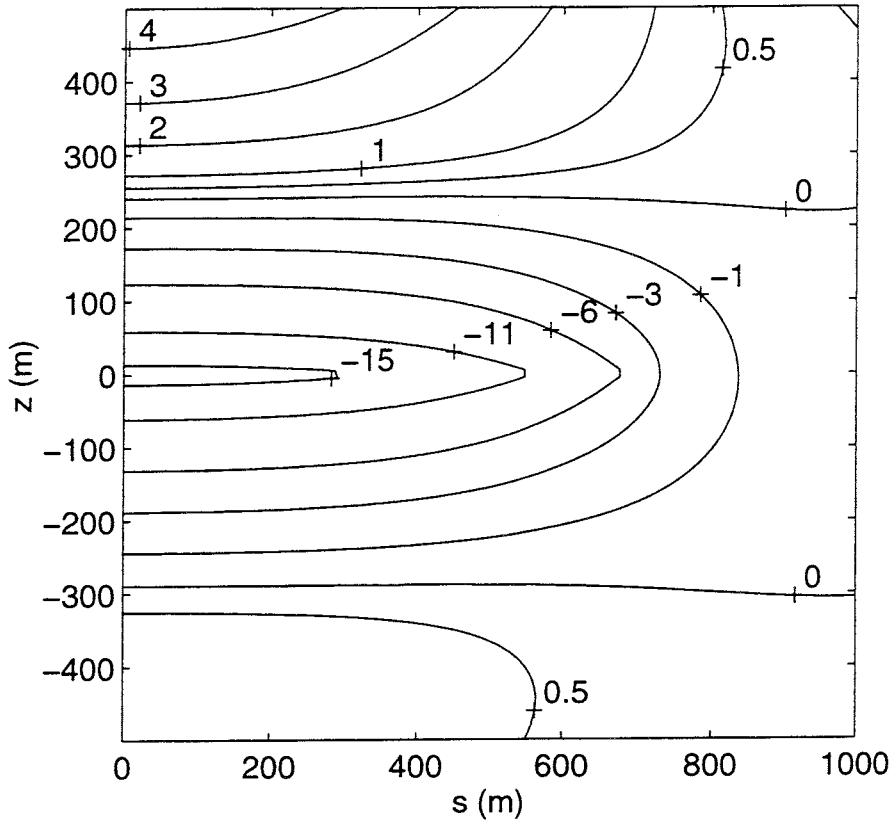

Figure 35. The stress σ_{xx} in the plane S_3 after 300 years.

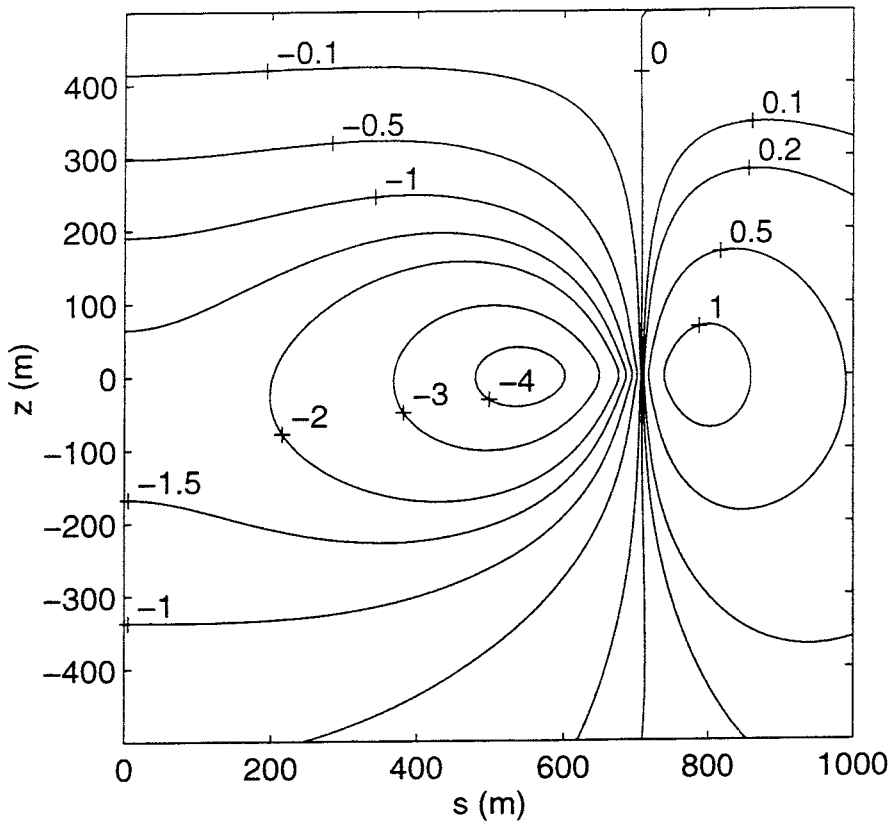

Figure 36. The stress σ_{zz} in the plane S_3 after 100 years. This figure is also shown in colour (Figure A5.8 in Appendix 5).

10 Principal stresses

The stress field that we have calculated consists of six components. Three of these are shear stresses. It is often simpler to consider the three principal stresses since the shear stresses vanish in the principal direction. This is especially the case if we choose to look at the principal stresses in symmetry planes where one of these is orthogonal to the plane.

The three planes S_1, S_2, and S_3 in Figure 25 are symmetry planes. In the planes $x = 0$ (yz-plane) and $y = 0$ (plane S_1) one of the principal axes is perpendicular to the plane, and thus, the other two principal stresses are parallel to the plane, which means that they can be represented by arrows there, indicating their orientation and magnitude. Furthermore, if L=B then one of the principal axes will be orthogonal to the planes $x - y = 0$ (plane S_3) and $x + y = 0$. The quadrantal solution (index qi) is symmetrical with respect to z The stresses at (x,y,z) are equal to the stresses at (x,y,$-z$). This means that one principal axis in the quadrantal solution is normal to the plane $z = 0$ (plane S_2). This will also be nearly true for the total solution, at least for small times, since the disturbance from the mirror solution (index m, see (Claesson J, Probert T, May 1996), Section 13) will not yet have reached the repository for these short times.

In this section we will look at orientation and magnitude of the principal stresses in the planes S_1, S_2 and S_3 shown in Figure 25. The calculation of the principal stresses for a given time makes it possible to map the areas where purely compressive forces act. Also, the areas where tensile stresses reign are found. The principal stresses also help to determine the maximum and minimum stress for a given time. In the above cases, the orientation of the principal axes is of secondary importance. Naturally, when the maximum or minimum stresses are found, the orientation of these stresses can be calculated in order to determine for example crack creation, crack growth, or crack closure.

The principal stress that is perpendicular to the plane in question is denoted $\sigma_\perp$. The two principal stresses parallel to the plane are denoted σ_1 and σ_2. The principal stress σ_1 is smaller than σ_2 i.e., $\sigma_1 \leq \sigma_2$ at all points in the plane.

We consider first the principal stresses for the plane S_1. The normal principal stress $\sigma_\perp$ is σ_{yy}. We have:

$$S_1\text{: } (x,0,z) \qquad 0 \leq x \leq 1000,\ -500 \leq z \leq 500 \qquad \sigma_{xy} = \sigma_{yz} = 0,\ \sigma_\perp = \sigma_{yy}$$

Figure 37 shows the direction and magnitude of the two principal stresses σ_1 and σ_2 parallel to the plane S_1, and Figure 38 shows the perpendicular principal stress $\sigma_\perp = \sigma_{yy}$. The area around the edge of the repository, $400 \leq x$, $y \leq 600$, in Figures 37 and 38 are shown in greater detail in Figures 39 and 40.

In Figure 37 the two principal stresses σ_1 and σ_2 are calculated at a point in the plane S_1 marked by a cross. The cross is made up of two pairs of counter-pointing arrows. The two pairs of arrows are orthogonal to each other since they represent the direction of principal stresses σ_1 and σ_2. The counter-pointing arrows point outwards for tension ($\leftarrow\rightarrow$) and inwards for compression ($\rightarrow\leftarrow$). The magnitude of the principal stresses is indicated by the length of the arrows. The dotted line in Figure 37 is the 0-level curve for the principal stress $\sigma_\perp = \sigma_{yy}$ perpendicular to the plane S_1. The stress σ_{yy} changes sign, from compression around the repository to tension outside the repository. The dashed line is the 0-level curve of the largest principal stress σ_2 parallel to the plane S_1. Around the repository both parallel principal stresses σ_1 and σ_2 are negative but at the dashed line σ_2 changes sign and becomes tensile as can be seen by the outward direction of the 'tangential' component just outside the dashed line in Figure 37. There is also a small region at the ground surface ($z = 500$, $700 \leq x \leq 900$) where σ_2 is tensile. The principal stress σ_1 is compressive in the whole of the plane S_1.

The largest compressive stresses in Figure 37 are found close to the plane of the repository $z = 0$. The magnitude of these stresses is constant near the repository plane. The largest compressive stresses are parallel to the repository plane but nearing the edge of the repository ($x = 0$, $z = 0$) the compressive stresses change direction. At a distance of 200 metres or more from the repository the principal stress orientation has the character of a radial-tangential stress field.

At the ground surface $z = 500$ the principal stress σ_1 is orthogonal to the ground surface and it is zero because $\sigma_1 = \sigma_{zz}|_{z=500} = 0$. An enlargement of the area around the repository edge of Figure 37, $400 \leq x \leq 600$ and $-100 \leq z \leq 100$, is shown in Figure 39. The radial-tangential nature of the principal stresses σ_1 and σ_2 can clearly be seen here. The level curves of the principal stress $\sigma_\perp = \sigma_{yy}$ are shown in Figure 38. The stress is compressive around the repository ($0 \leq x \leq 600$, $-130 \leq z \leq 130$). The largest compressive stress is over -16 MPa. Tensile stresses exist from 130 above the repository to the ground surface. The tensile stresses are less than 2 MPa. An enlargement of the level curves of $\sigma_\perp$ around the repository edge of Figure 38, $400 \leq x \leq 600$ and $-100 \leq z \leq 100$, is shown in Figure 40.

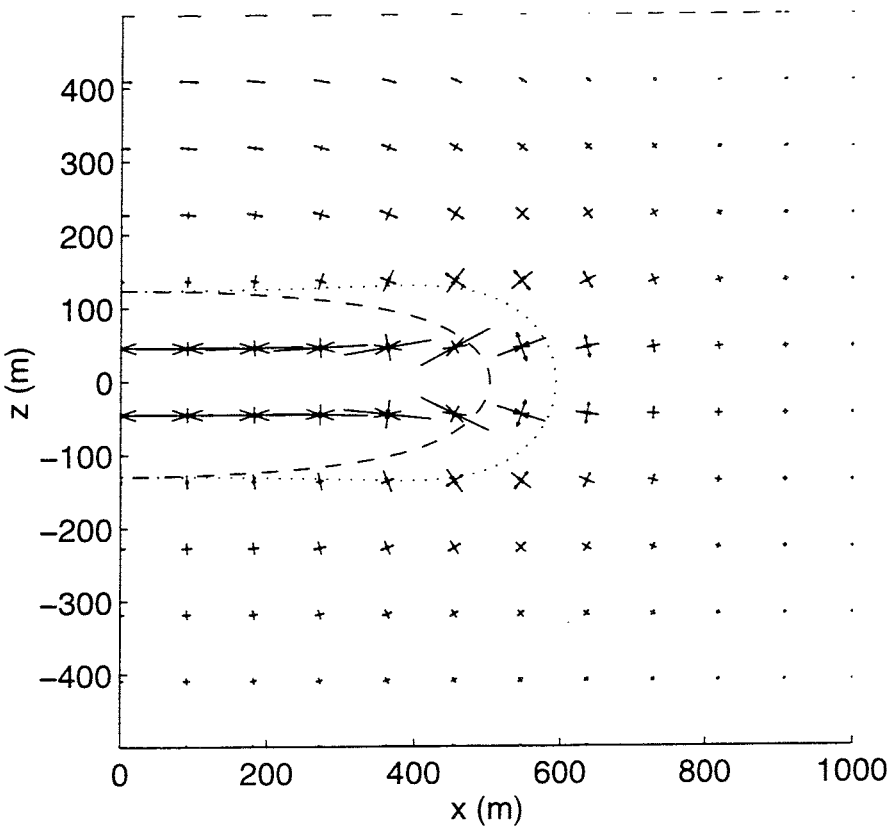

Figure 37. The orientation and magnitude of the two principal stresses parallel to the plane S_1 after 50 years. The dashed curve marks when σ_2 changes sign and the dotted curve marks where $\sigma_\perp = \sigma_{yy}$ changes sign. This figure is also shown in colour (Figure A5.9 in Appendix 5).

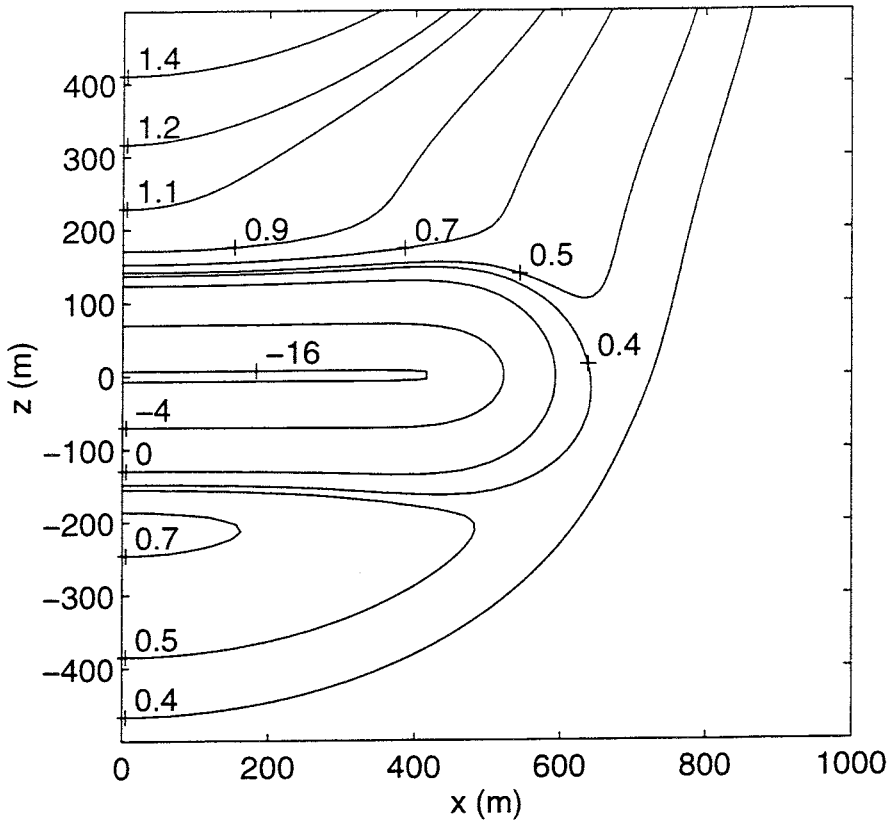

Figure 38. Level curves of the principal stress $\sigma_\perp = \sigma_{yy}$ perpendicular to the plane S_1 after 50 years. This figure is also shown in colour (Figure A5.10 in Appendix 5).

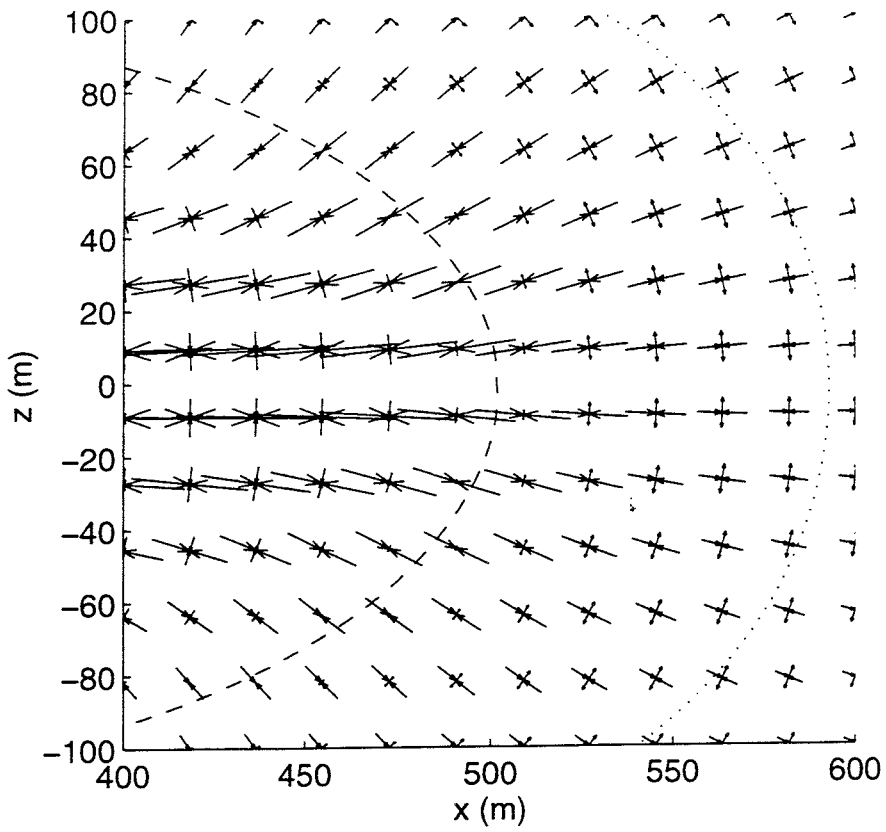

Figure 39. The orientation and magnitude of the two principal stresses parallel to the plane S_1 after 50 years. An enlargement of Figure 37.

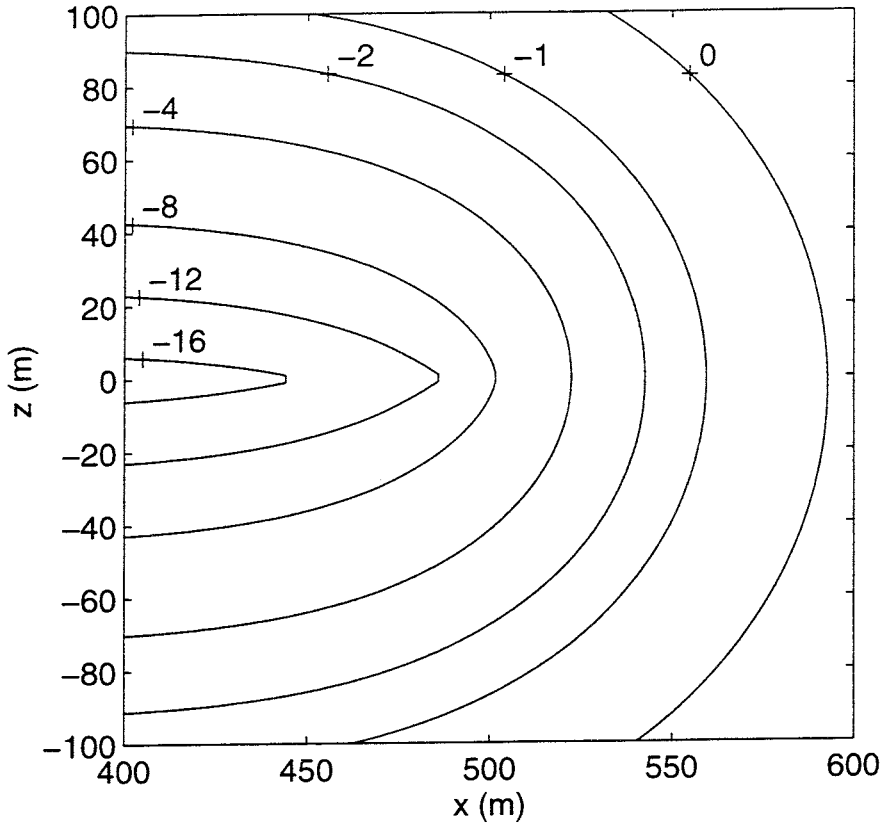

Figure 40. Level curves of the principal stress $\sigma_\perp = \sigma_{yy}$ perpendicular to the plane S_1 after 50 years. An enlargement of Figure 38.

The plane S_2 is approximately a symmetry plane for small times. One of the principal stresses is normal to the plane S_2 due to symmetry for small times. In this case $\sigma_\perp = \sigma_{zz}$ for small times. We have:

S_2: (x,y,0) $\quad 0 \leq x \leq 1000, 0 \leq y \leq 1000 \quad$ $\sigma_{yy}(x,y,0,t) = \sigma_{xx}(y,x,0,t)$
$\sigma_{yz}(x,y,0,t) = \sigma_{xz}(y,x,0,t)$
$\sigma_\perp = \sigma_{zz}$

The orientation of the principal stresses σ_1 and σ_2 is shown in Figure 41 and the level curves of $\sigma_\perp$ are shown in Figure 42.

The principal stresses in Figure 41 are only valid for small times because of the approximation mentioned in the beginning of this section. For $t = 10$ the error is undetectable, and the two principal stresses σ_1 and σ_2 in the plane S_2 are orthogonal. The magnitude of the stresses in the repository area is roughly constant. One of the principal stresses along the x-axis is parallel to the x-axis because the axis lies in the symmetry plane S_1. This is also true for stresses along the y-axis and diagonal $x = y$. At the centre $x = z = 0$ the two principal stresses σ_1 and σ_2 are equal, $\sigma_1 = \sigma_2$, and are thus degenerate. The level curves of $\sigma_\perp$ are shown in Figure 42.

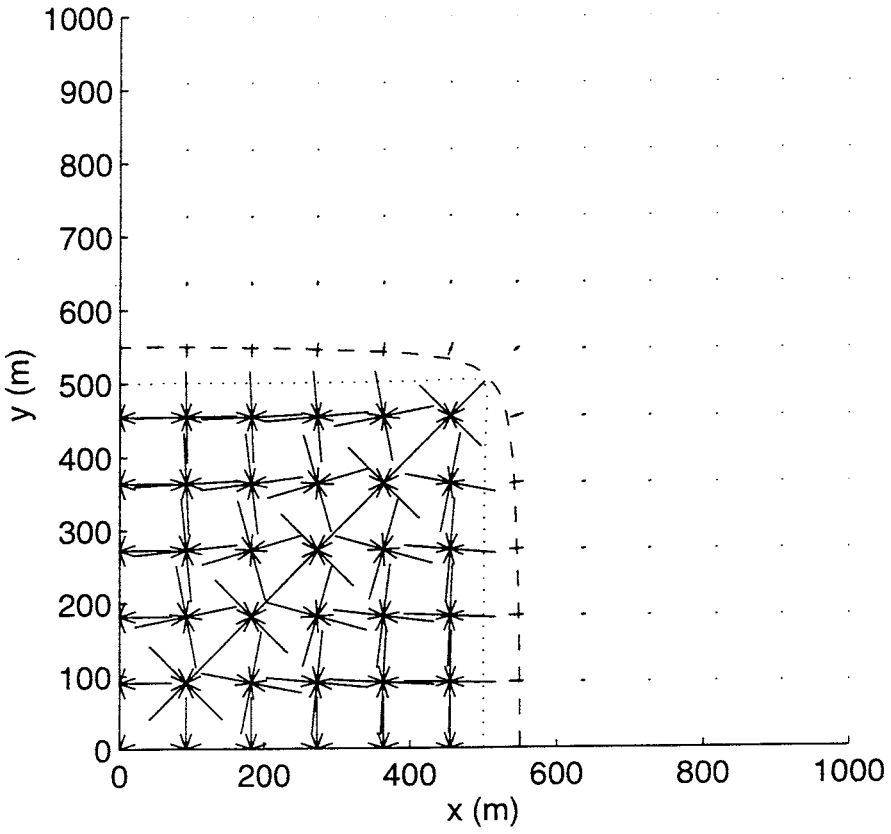

Figure 41. The orientation and magnitude of the two principal stresses parallel to the plane S_2 after 10 years.

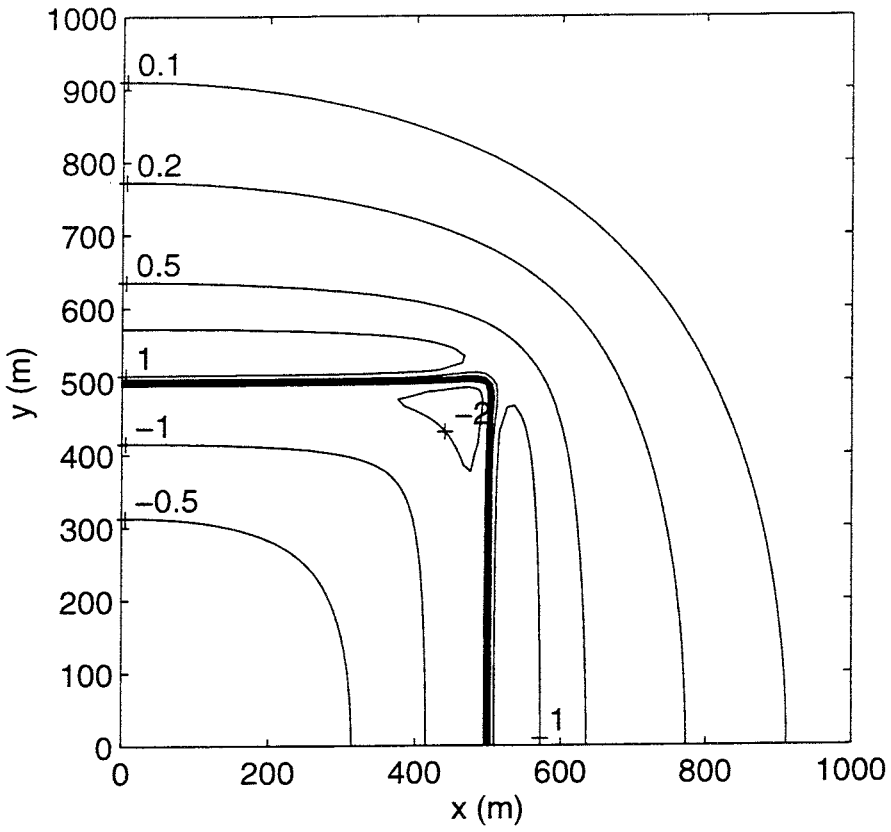

Figure 42. Level curves of the principal stress $\sigma_\perp = \sigma_{zz}$ perpendicular to the plane S_2 after 10 years.

The plane S_3 is also a symmetry plane. One of the principal stresses is normal to the plane S_3 due to symmetry. In this case $\sigma_\perp = \sigma_{xx} - \sigma_{xy}$. We have:

S_3: (x,x,z) $\quad 0 \leq x \leq 707, -500 \leq z \leq 500 \quad$ $\sigma_{yy} = \sigma_{xx}, \sigma_{yz} = \sigma_{xz}$
$\sigma_\perp = \sigma_{xx} - \sigma_{xy}$

The principal stresses σ_1 and σ_2 in the plane S_3 are shown in Figure 43 and the perpendicular stress $\sigma_\perp = \sigma_{xx} - \sigma_{xy}$ is shown in Figure 44.

The stresses in Figure 43 resemble those in Figure 37, and there is some resemblance between the level curves of $\sigma_\perp$ in Figure 44 and Figure 38. There is, however, a small island of tensile stress under the repository at $200 \leq x \leq 600$, $z = -250$ in Figure 44, but the stresses are less than 2 MPa. The unlabelled level curve in the upper left-hand corner of Figure 44 is the 2.5 MPa contour.

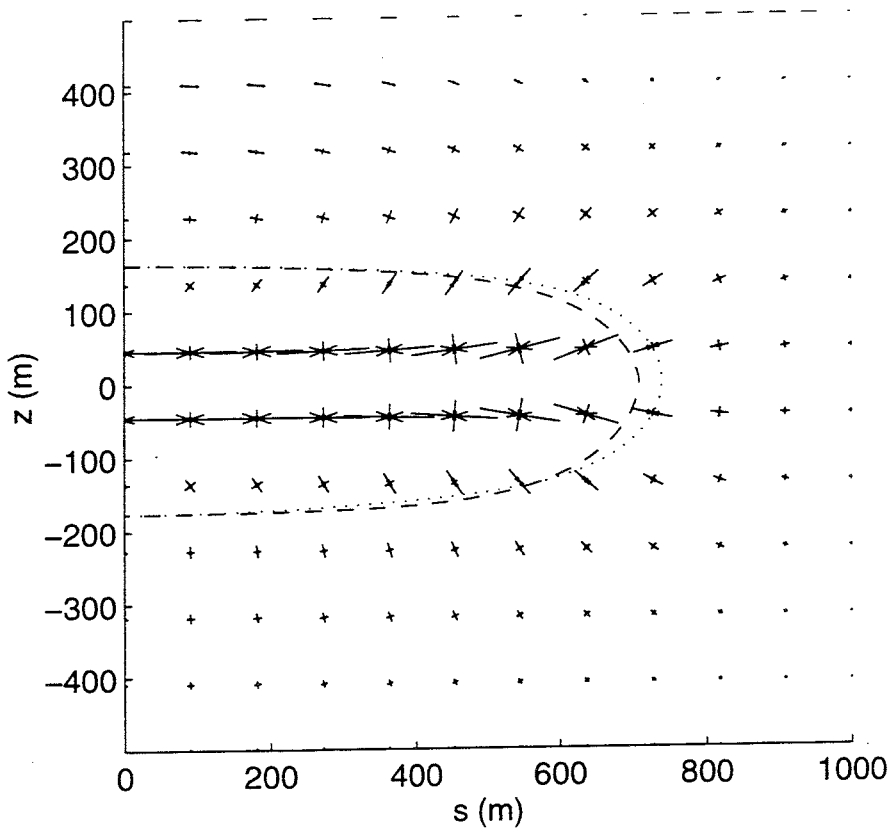

Figure 43. The orientation and magnitude of the two principal stresses parallel to the plane S_3 after 100 years.

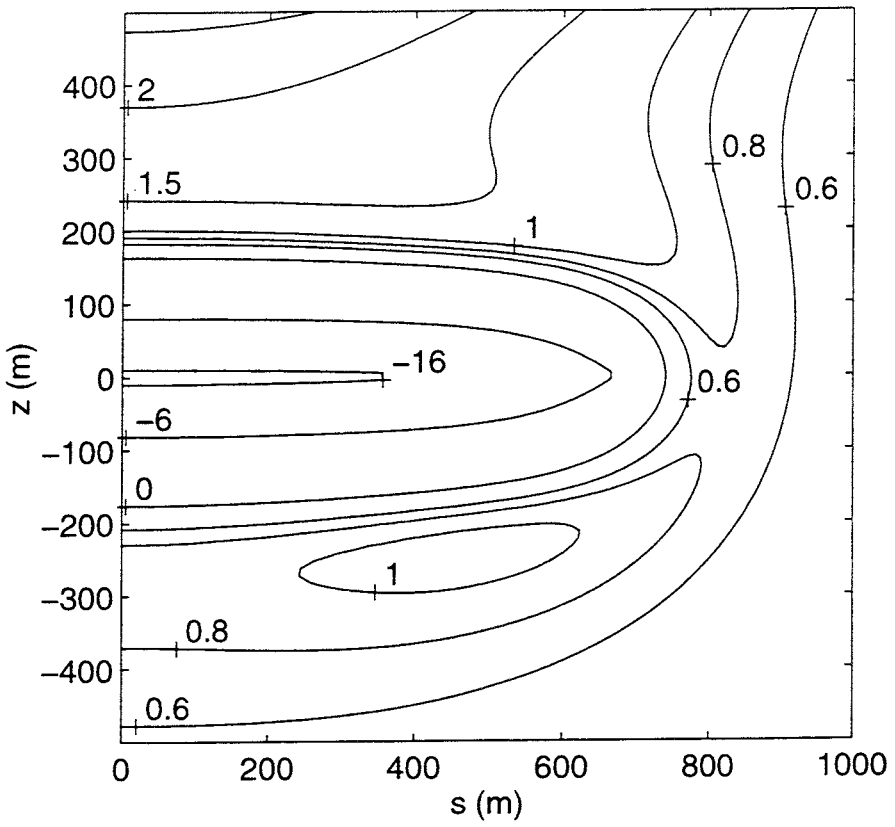

Figure 44. Level curves of the principal stress $\sigma_\perp = \sigma_{xx} - \sigma_{xy}$ perpendicular to the plane S_2 after 10 years.

11 Regions of compression and tension

From the above results in Sections 5 and 7-10, we get the following general picture of the tensile and compressive stresses. We will look at the horizontal and vertical stresses in a vertical and a horizontal cross-section.

In the *vertical* planes S_1 and S_3 the horizontal stresses are compressive in the repository area. Above and below the repository the horizontal stresses are tensile (See Figures 26 and 27). The distance to the tensile stresses above and the repository is roughly 50, 100 and 300 m for $t = 5$, 50 and 500 years, respectively, while the distance to the tensile stresses below the repository is somewhat larger. The tensile region above the repository extends all the way up to the ground surface. The stresses in this region are 2-3 times larger than the stresses in the tensile region below the repository. The vertical stresses are compressive above, below and in the repository area. The vertical stresses are tensile outside this region (See Figure 30). The distance to the tensile region to the right of the repository in Figure 30 is 2 and 30 m for $t = 50$ and 500 years, respectively.

In a *horizontal* cross-section (plane S_2) the vertical stresses are compressive inside the repository area and tensile outside in bands parallel to the repository edges (See Figure 32). The distance to these bands is roughly 2 and 30 m for $t = 50$ and 500 years, respectively. The horizontal stresses are compressive in the repository area and tensile outside (See Figure 31). The distance to these tensile regions from an edge of the repository is roughly 40, 90 and 220 m for $t = 5$, 50 and 500 years, respectively, and somewhat shorter at the corners of the repository.

12 Parameter sensitivity

The input data of the reference case is given by (29). Some of the parameters and their values are repeated here:

$$L = 500 \text{ m} \quad B = 500 \text{ m} \quad H = 500 \text{ m}$$

$$Q_0(0) = 1000 \text{ W}$$

$$\rho = 2700 \text{ kg/m}^3 \quad E = 50 \cdot 10^9 \text{ Pa} \quad \nu = 0.25$$

$$c = 800 \text{ J/(kg} \cdot \text{K)} \quad \lambda = 3.5 \text{ W/(m} \cdot \text{K)} \quad \alpha = 8.3 \cdot 10^{-6} \text{ 1/K} \tag{33}$$

The above parameters or certain combinations of them will be varied to determine their effects on the stresses.

All the stresses are directly proportional to the parameter p_0 and the total initial effect $Q_0(0)$ (for constant ratio q_1/q_2). We have:

$$\sigma \sim \frac{E\alpha}{1-\nu} \cdot \frac{Q_0(0)}{\rho c} \tag{34}$$

The change in the stresses is directly proportional to changes in E, α and $Q_0(0)$. Furthermore, these parameters do not change the time scale. A maximum or minimum will not be moved in time just because one of these parameters is altered. Doubling E, α or $Q_0(0)$ doubles all the stresses but does not affect the time scale. The parameters ν, ρ and c occur elsewhere in the solution formula so their influence on the stresses is not fully explained by their presence in (34).

All the remaining parameters affect the time scale as well as the magnitude of the stresses. These parameters are Poisson's number ν, the heat conductivity λ, the volumetric heat capacity ρc and the three lengths that define the geometry of the repository L, B and H. The thermal diffusivity $a = \lambda/(\rho c)$ is varied by varying λ since a is directly proportional to λ. The parameters

ρ and c always appear together in formulas as the volumetric heat capacity ρc. This is the reason why ρc is varied instead of the separate factors.

Naturally, changing the ratio q_1/q_2 and the decay times t_1 and t_2, or changing the number of exponentials will affect the magnitude and the time scale of the stresses but these changes are not studied here. Changes made to the tunnel spacings D' and canister spacings D have the same effect as changes to the total initial effect $Q_0(0)$ per canister. The total initial effect $Q_0(0)$ per canister is the only change to the heat source considered here.

The parameters or parameter combinations that are varied along with their reference values from (29) are:

$$L = 500 \text{ m} \quad H = 500 \text{ m} \quad \rho c = 2700 \cdot 800 = 2.16 \cdot 10^6 \text{ J/m}^3$$

$$\nu = 0.25 \quad \lambda = 3.5 \text{ W/(m} \cdot \text{K)} \tag{35}$$

Each of these parameters is varied by $\pm 10\%$ from the reference case (35) or (29) to find out how sensitive the stresses are to parameter variations. The effect on the stresses is not that large. To illustrate this insensitivity we also vary the parameters by $\pm 50\%$. These variations are much larger than the uncertainties encountered in parameter values under normal circumstances in the studied application.

The stresses that are followed are the minimum stress (maximum compressive stress) component at the centre of the repository (0,0,0) and the largest tensile stress component at the ground surface after 500 years. Usually, $\sigma_{xx}(0,0,0,t)$ is the minimum stress component at the centre and $\sigma_{xx}(0,0,500,500)$ is the largest stress component at the ground surface. The exception is when L is varied. When varying L the largest stress component at the centre (−50%) and at the ground surface (+50%) is σ_{yy} instead of σ_{xx}. The minimum stress at the centre is one of the largest compressive stresses encountered in this study. The stress at the ground surface for $t = 500$ years is the largest tensile stress found in this study for which the solution is valid. The time of the minimum stress at the repository centre is also determined.

The results of parameter variation by $\pm 10\%$ and $\pm 50\%$ are shown in Tables 5 and 6. The first row of Table 5 and 6 is the reference case corresponding to the input (29). In the following rows one parameter at a time is varied and the specified stresses and time are determined. The percentage within brackets is the percentage change from the reference stress.

Parameter	Variation	t (yrs.)	σ_{xx}(0,0,0,t)	(MPa)	σ_{xx}(0,0,500,500)	(MPa)
-	0%	66.6	−17.92		5.81	
L	−10%	[1]67.3	[1]−17.99	(−1%)	5.86	(−0.9%)
L	+10%	67.8	−18.04	(0.7%)	[2]6.07	(5%)
H	−10%	65.9	−17.85	(−0.4%)	7.73	(33%)
H	+10%	67.1	−17.97	(0.3%)	4.37	(−25%)
ρc	−10%	66.0	−18.82	(5%)	6.32	(9%)
ρc	+10%	67.2	−17.14	(−4%)	5.37	(−8%)
ν	−10%	66.7	−17.36	(−3%)	5.50	(−5%)
ν	+10%	66.5	−18.53	(3%)	6.14	(5%)
λ	−10%	67.2	−18.96	(6%)	5.92	(2%)
λ	+10%	66.0	−17.03	(−5%)	5.70	(−2%)

Table 5. Table showing how the value and position of the largest compressive stress component at the centre of the repository (0,0,0) is affected by parameter variation by $\pm 10\%$. The variation of the largest stress component at the ground surface (0,0,500) after 500 years is also shown.
[1] The minimum component is $\sigma_{yy}(0,0,0,67.3) = -17.99$. The minimum of σ_{xx} is $\sigma_{xx}(0,0,0,65.2) = -17.77$ MPa.
[2] The largest component is $\sigma_{yy}(0,0,500,500) = 6.07$ ($\sigma_{xx}(0,0,500,500) = 5.70$).

Parameter	Variation	t (yrs.)	σ_{xx}(0,0,0,t) (MPa)	σ_{xx}(0,0,500,500) (MPa)
-	0%	66.6	-17.92	5.81
L	-50%	[1]70.8	[1]-18.39 (-8%)	4.97 (-14%)
L	+50%	70.6	-18.31 (2%)	[2]6.82 (17%)
H	-50%	58.8	-17.05 (-5%)	13.09 (125%)
H	+50%	68.1	-18.07 (1%)	1.80 (-69%)
ρc	-50%	62.0	-24.64 (38%)	9.83 (69%)
ρc	+50%	68.9	-14.82 (-17%)	4.09 (-30%)
ν	-50%	67.2	-15.41 (-14%)	4.44 (-24%)
ν	+50%	66.0	-21.44 (19%)	7.72 (33%)
λ	-50%	70.4	-25.87 (44%)	6.24 (7%)
λ	+50%	64.0	-14.41 (-20%)	5.29 (-9%)

Table 6. Table showing how the value and position of the largest compressive stress component at the centre of the repository (0,0,0) is affected by parameter variation by ±50%. The variation of the largest stress component at the ground surface (0,0,500) after 500 years is also shown.
[1] The minimum component is $\sigma_{yy}(0,0,0,70.8) = -18.39$. The minimum of σ_{xx} is $\sigma_{xx}(0,0,0,55.0) = -16.56$ MPa.
[2] The largest component is $\sigma_{yy}(0,0,500,500) = 6.82$ ($\sigma_{xx}(0,0,500,500) = 5.00$).

The study shows that the stresses are relatively insensitive to parameter variations with the exception of H and ρc. Uncertainties in the parameter values thus become a non-critical aspect in the analysis.

13 Several repositories

Two repositories may be stacked one on top of the other or placed side by side. A repository is not filled all at once. The filling is gradual. The first canisters to be stored have already lost heat to the surroundings when new canisters are deposited. The mathematical problems of stacking two repositories (double-decker), placing repositories side by side and partially filling repositories are related. All three problems are solved by using the superposition technique.

The solution for one repository is given by Eq. (9). The length and width of the repository is $2L$ and $2B$, and the centre of the repository is located at (0,0,0). The repository is at a depth of H under the ground surface ($z = H$) and the repository is loaded at $t = 0$.

The addition of a new repository a with the dimensions $2L_a$ and $2B_a$, the centre at (x_a,y_a,z_a), at a depth of $H - z_a$ under the ground surface and loaded at $t = t_a$ is done by substitution or translation followed by superposition. The variables x, y, z, t and H in Eq. (9) are translated:

$$\begin{aligned} x &\rightarrow x - x_a \\ y &\rightarrow y - y_a \\ z &\rightarrow z - z_a \\ t &\rightarrow t - t_a \\ H &\rightarrow H - z_a \end{aligned} \tag{36}$$

Let us in arguments of the function f of Eq. (9) include the parameters H, L and B so that:

$$f(x,y,z,t) \rightarrow f(x,y,z,t;H,L,B) \tag{37}$$

Then the translated solution becomes:

$$f(x-x_a, y-y_a, z-z_a, t-t_a; H-z_a, L_a, B_a) \tag{38}$$

The total solution for the two repositories is obtained by adding the two solutions:

$$f(x,y,z,t;H,L,B) + f(x-x_a, y-y_a, z-z_a, t-t_a; H-z_a, L_a, B_a) \tag{39}$$

The upper limit of the time integral in the translated solution is $t - t_a$. If $t - t_a < 0$ then the time integral in Eq. (9) is set to zero because the new repository has not been loaded before $t = t_a$.

If the heat release of the canisters or the tunnel spacings are altered in the new repository then the decay times t_j and initial heat release $Q_0(0)$ and q_j of the input (29) have to be changed.

If several additional repositories a, b, c, ... are used then the total solution is obtained by superposition:

$$f(x,y,z,t;H,L,B) + \sum_{i=a,b,c,\ldots} f(x-x_i, y-y_i, z-z_i, t-t_i; H-z_i, L_i, B_i) \tag{40}$$

13.1 Stresses around two stacked repositories

The stresses around two stacked repositories are determined here. The input is the same as for the KBS-3 case in (29) with the following exceptions. The canisters are stored in two identical repositories, one on top of the other. The first (upper) repository is 500 metres below the ground surface ($H = 500$) at $z = 0$. The second (lower) repository is 100 metres below the upper repository at $z = -100$ (See Figure 45). The two identical repositories are dimensioned so that the total heat release is the same as in the reference case (29). Both repositories are loaded at the same time ($t_a = 0$). The data that has been changed in the reference case (29) is:

$$L = L_a = 500/\sqrt{2} \approx 354 \text{ m} \quad B = B_a = 500/\sqrt{2} \text{ m} \quad H = 500 \text{ m} \quad z_a = -100 \text{ m}$$

$$x_a = 0 \quad y_a = 0 \quad z_a = -100 \text{ m} \quad t_a = 0$$

The total area of the two repositories is 1 km^2 as in the reference case (29).

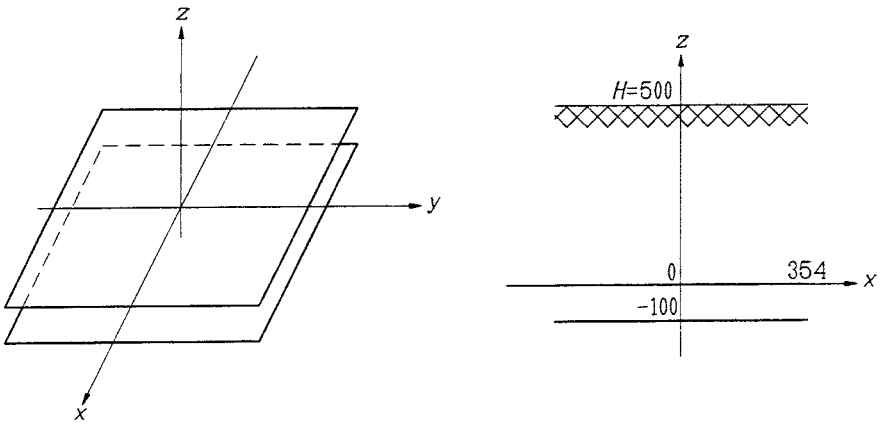

Figure 45. Left: Thermoelastic problem with two time-dependent rectangular heat source planes. Right: A vertical cross-section of the two repositories.

The solution for a stacked repository is obtained by superposition according to the formulas in the preceding section.

The horizontal stress σ_{xx} in the vertical plane S_1 is shown in Figure 46 for the above modified KBS-3 data with $t = 50$ years.

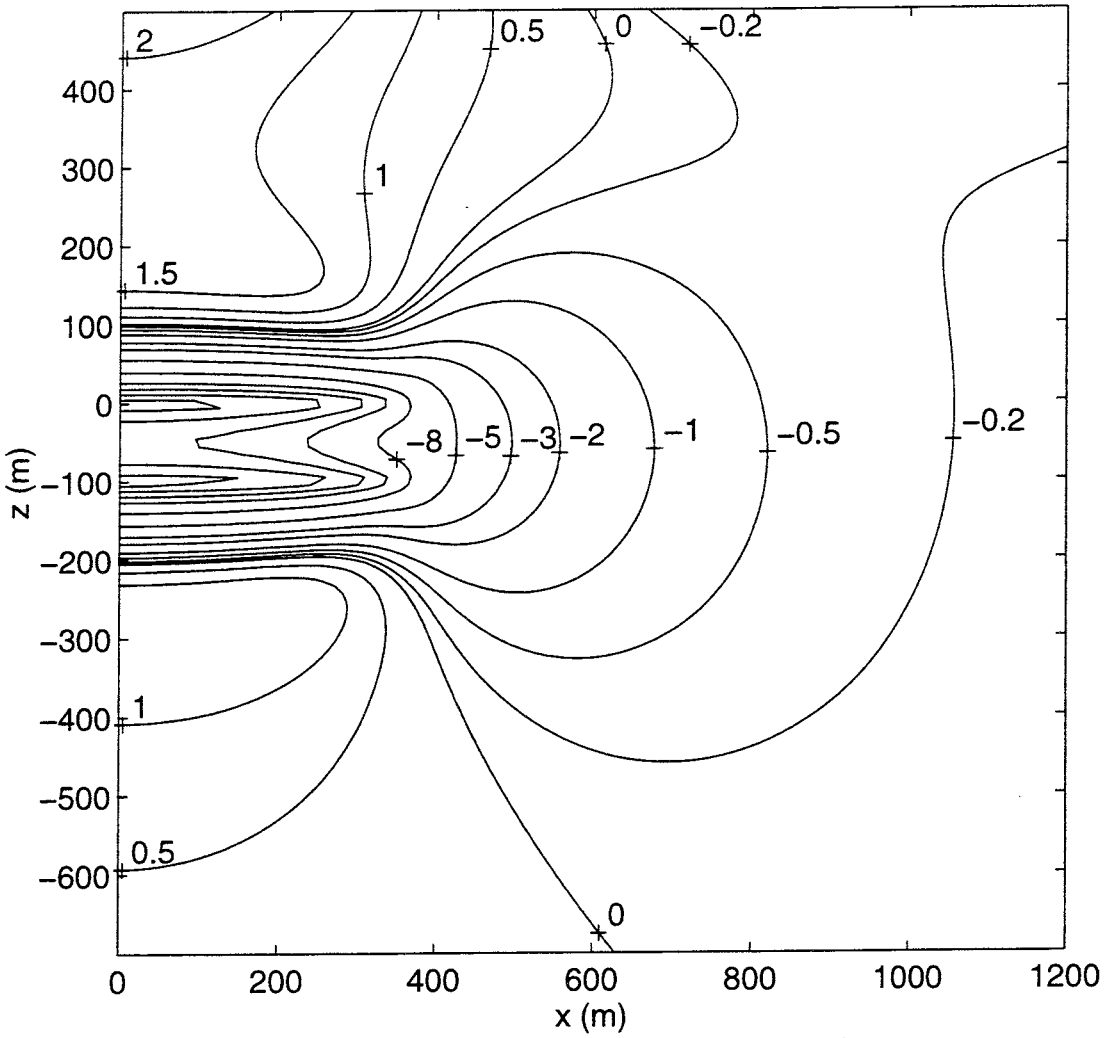

Figure 46. The horizontal stress σ_{xx} in the plane S_1 around two stacked repositories after 50 years. This figure is also shown in colour (Figure A5.11 in Appendix 5).

The two horizontal repositories are at $z = 0$ and $z = -100$, and they extend from $x = 0$ to $x = 354$. The stresses around and between the two repositories are compressive. Above and below these compressive regions are regions of tension. The largest tensile stresses are found at the ground surface. The stresses at the centres of the repositories are over -17 MPa. The innermost, unlabelled level curves at the central region of the repositories, from $x = 0$ to $x = 125$-150, correspond to -17 MPa. The -17 MPa level curve is followed by the -15, -13 and -11 MPa level curves, in that order (all unlabelled). Figure 46 can be compared with Figure 26. The only apparent differences are that the stresses are absolutely larger, and the compressive region somewhat larger in the stacked repositories case. This applies to all the Figures in this section.

Reducing the size of the repository does not reduce the size of the maximum stresses due to insensitivity to variations in the length L (See Section 12).

In Figure 47 the vertical stress σ_{zz} in the vertical plane S_1 is shown for $t = 50$ years. This figure can in some extent be compared with Figure 30 where $t = 100$ years.

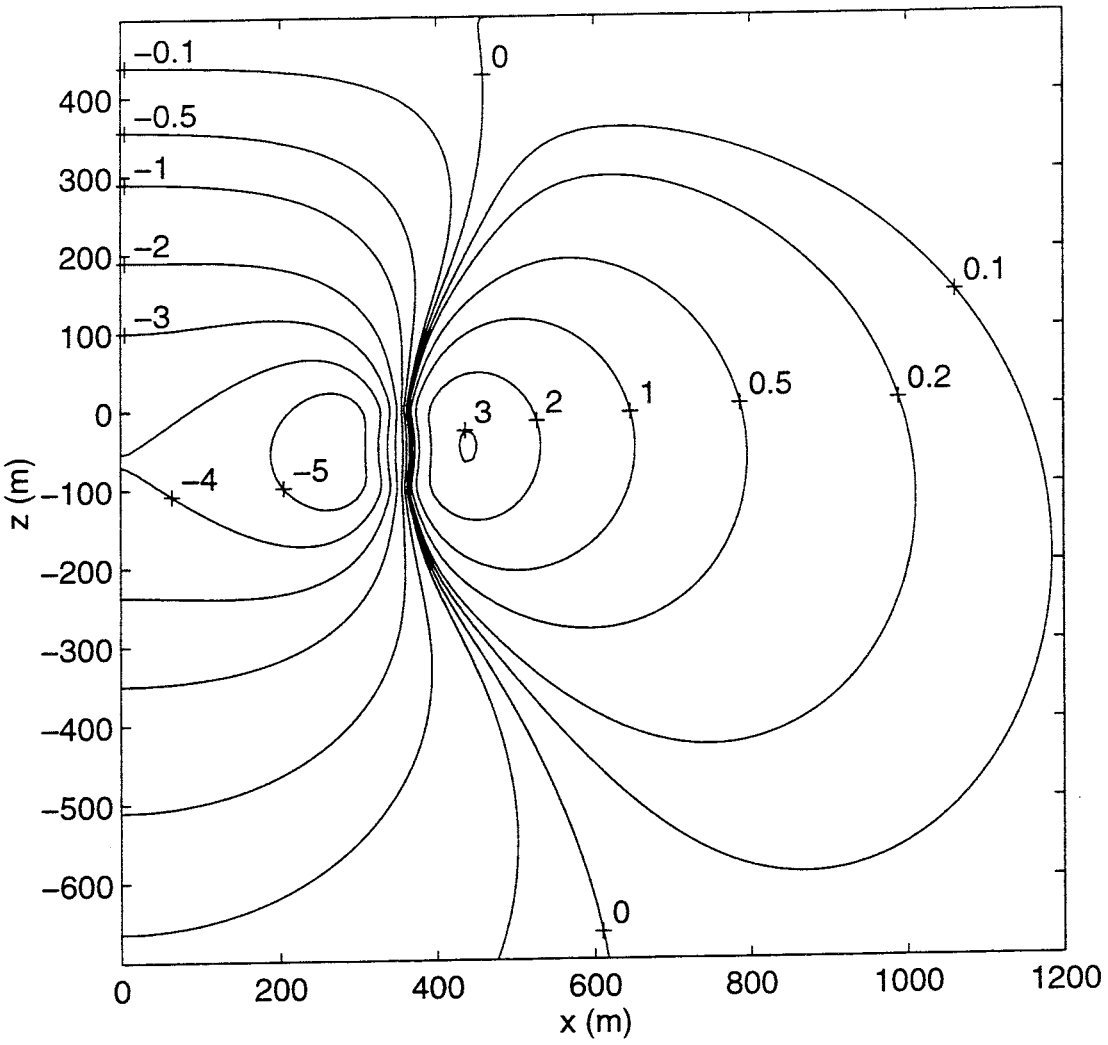

Figure 47. The vertical stress σ_{zz} in the plane S_1 around two stacked repositories after 50 years.

The horizontal stress σ_{xx} in the vertical plane S_1 is shown in Figure 48 for $t = 500$ years. This figure can be compared with Figure 4.

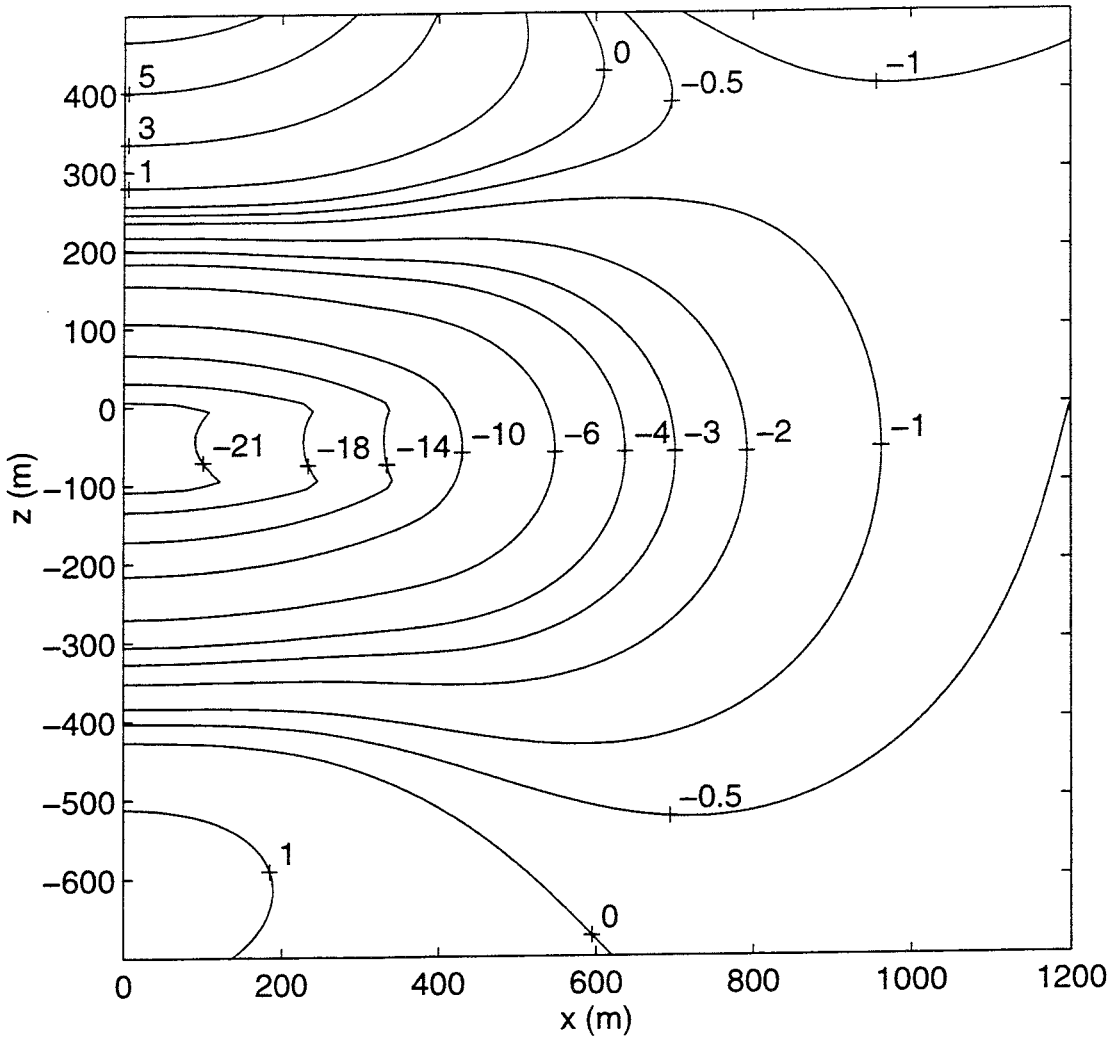

Figure 48. The horizontal stress σ_{xx} in the plane S_2 around two stacked repositories after 500 years.

In Figure 49 the vertical stress σ_{zz} in the vertical plane S_1 is shown for $t = 500$ years.

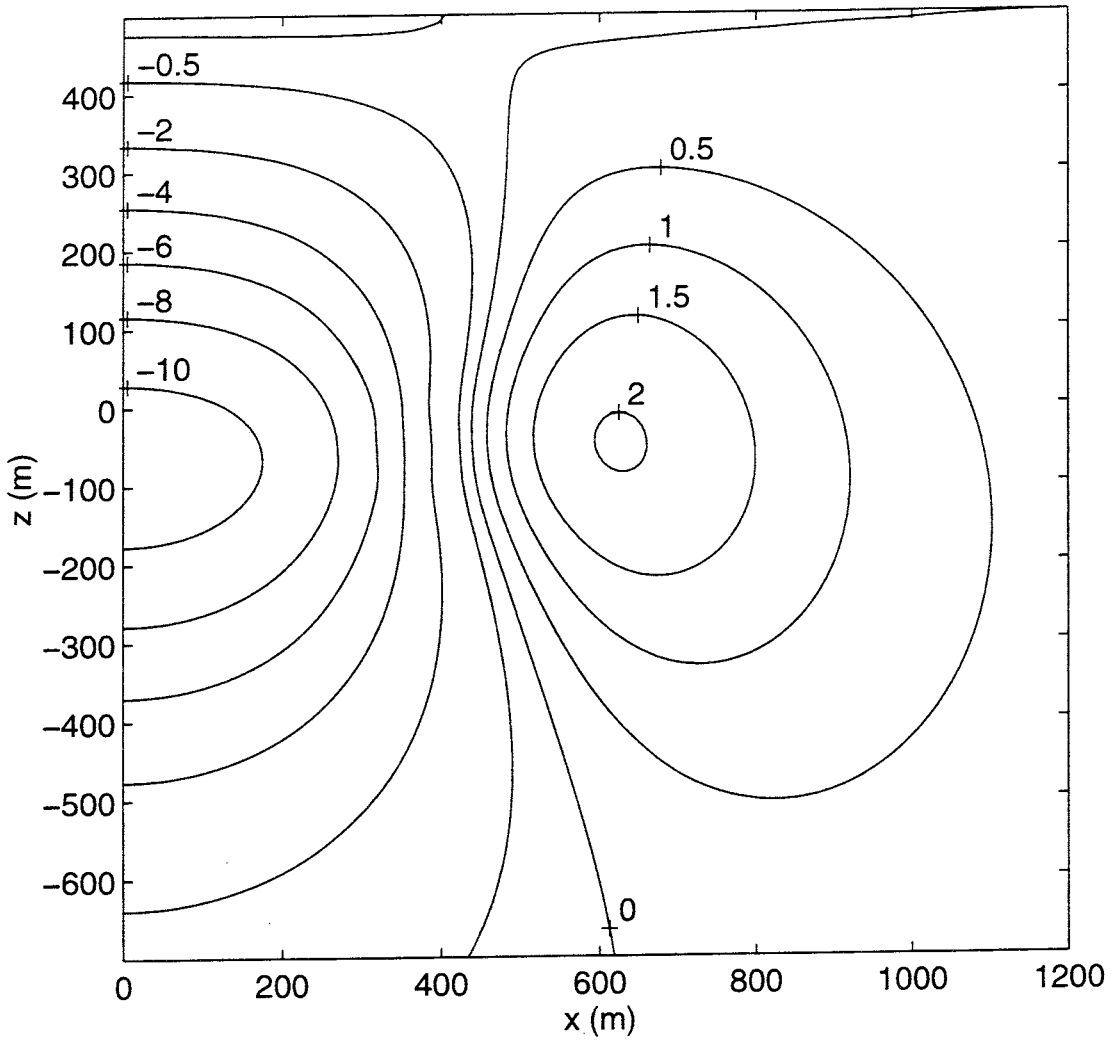

Figure 49. The vertical stress σ_{zz} in the plane S_2 around two stacked repositories after 500 years.

The general picture of the stresses in the stacked repositories case is similar to that of the single repository case (if the total heat release is the same).

References

Claesson J, Hellström G, 1995. Thermoelastic Stress Due to an Instantaneous Finite Line Heat Source in an Infinite Medium. Dept. of Mathematical Physics, Lund University, Sweden. SKB Technical Report TR 96-11.

Claesson J, Probert T, Jan. 1996. Temperature Field due to Time-Dependent Heat Sources in a Large Rectangular Grid. I. Derivation of an analytical solution. Dept. of Mathematical Physics, Lund University, Sweden. SKB Technical Report TR 96-12.

Claesson J, Probert T, May 1996. Thermoelastic Stress due to a Rectangular Heat Source in a Semi-infinite Medium. I. Derivation of an analytical solution. Dept. of Mathematical Physics, Lund University, Sweden. SKB Technical Report TR 96-13.

Hökmark H, 1996. Canister Positioning - Stage 1 Thermomechanical Nearfield Rock Analysis. SKB Report AR D-96-014.

Israelsson J, June 1995. Global Thermo-Mechanical Effects from a KBS-3 Type Repository, Phase 1; Elastic Analyses. Itasca Geomekanik AB, Borlänge, Sweden.

Probert T, Claesson J, Apr. 1997. Temperature Field due to Time-Dependent Heat Sources in a Large Rectangular Grid. II. Application for the KBS-3 repository.. Dept. of Mathematical Physics, Lund University, Sweden. (To be published as a SKB Technical Report.)

Itasca, 1993. Itasca-1993 3DEC, 3-D Distinct Element Code. Version 1.5 User's Manual. Itasca Consulting Group, Inc., Minneapolis, USA.

SKB 91, 1992. SKB 91 Final Disposal of Spent Nuclear Fuel. Importance of the Bedrock for Safety. SKB Technical Report TR-92-20.

Appendix 1. Quadrantal infinite solution

Only the two functions T_{qi} (K) and C (1/m^2), Eqs. (17-18), are needed to describe the stress and strain fields of the basic quadrantal infinite solution (index qi). The number of variables is reduced by using dimensionless coordinates.

The two functions T_{qi} and C can be rewritten as a time factor times a dimensionless function of dimensionless coordinates:

$$x' = \frac{x}{\sqrt{4at}} \quad y' = \frac{y}{\sqrt{4at}} \quad z' = \frac{z}{\sqrt{4at}} \quad r' = \frac{r}{\sqrt{4at}} \tag{41}$$

$$T_{qi}(x,y,z,t) = \frac{e_0}{\pi\rho c} \cdot \frac{1}{\sqrt{4at}} \cdot T_q\,(x',y',z')$$

$$T_q(x',y',z') = \sqrt{\pi} \cdot \mathrm{erf}(x') \cdot \mathrm{erf}(y') \cdot \mathrm{e}^{-(z')} \tag{42}$$

$$C(p,r,t) = \frac{1}{4at} \cdot C'(p',r')$$

$$C'(p',r') = \frac{1}{r'} \cdot \frac{p'}{(r')^2-(p')^2} \cdot \left[\mathrm{erf}\,(r') - r' \cdot \mathrm{e}^{-\left((r')^2-(p')^2\right)} \cdot \frac{\mathrm{erf}(p')}{p'}\right] \quad p' = x',\ y' \tag{43}$$

Both functions T_q and C' are dimensionless.

The behaviour of the strain and stress fields of the quadrantal solution can be studied by examining the functions $T_q(x',y',z')$ and $C'(p',r')$.

Appendix 2. Displacements without double integrals

The calculation of the displacement components according to Eqs. (9) and (23) involves a double integral. This integral may be reduced to a single integral by integration by parts. The (quadrantal) displacement components for the jth exponential become:

$$u^{qe}(x,y,z,t;j) = I_e(t;j) \cdot \left[-\frac{u_0}{2}\ln\left(\frac{r+y}{r-y}\right) + u^{mb}(x,y,z)\right] +$$

$$+ u_0 \int_{1/\sqrt{4at}}^{\infty} I_e[t - 1/(4as^2);j] \cdot \frac{\mathrm{erf}(ys)}{s} \cdot \mathrm{e}^{-(r^2-y^2)s^2}\,ds \tag{44}$$

$$v^{qe}(x,y,z,t;j) = I_e(t;j) \cdot \left[-\frac{u_0}{2}\ln\left(\frac{r+x}{r-x}\right) + v^{mb}(x,y,z)\right] +$$

$$+ u_0 \int_{1/\sqrt{4at}}^{\infty} I_e[t - 1/(4as^2);j] \cdot \frac{\mathrm{erf}(xs)}{s} \cdot \mathrm{e}^{-(r^2-x^2)s^2}\,ds \tag{45}$$

$$w^{qe}(x,y,z,t;j) = I_e(t;j) \cdot \left[u_0 \arctan\left(\frac{xy}{zr}\right) + w^{mb}(x,y,z)\right] -$$

$$u_0 z\sqrt{\pi} \int_{1/\sqrt{4at}}^{\infty} I_e[t - 1/(4as^2);j] \cdot \mathrm{erf}(xs) \cdot \mathrm{erf}(ys) \cdot \mathrm{e}^{-z^2s^2}\,ds \tag{46}$$

The integral factor I_e in each term of the displacement components is:

$$I_e\,(t;j) = \frac{q_j t_j}{e_0} \cdot \left[1 - \exp\left(-\frac{t}{t_j}\right)\right] \tag{47}$$

Appendix 3. Comparison with other models

3DEC solution (Contribution by H. Hökmark)

The text about the 3DEC model and calculations has been written by H. Hökmark of Clay Technology in Lund, Sweden (See (Hökmark H, 1996)). The figures of Appendix 6 are discussed here. These figures were also provided by H.Hökmark.

General

A comparison between the analytical solution and a numerical solution obtained using the 3-dimensional distinct element code 3DEC (Itasca, 1993) is made in this section. All illustrations described here are found in Appendix 6.

Correspondence between the analytical and numerical solutions

All conditions regarding rock thermomechanical properties, initial power and fuel decay characteristics assumed in the 3DEC model are the same as those used in the KBS-3 application of the analytical solution, (29).

The 3DEC thermal logic does not allow for ideally smeared-out heat sources. Area heat sources must be represented as grids of point sources. In the model described here, 6680 individual fuel canister were explicitly modeled within a 1000×1000 m^2 quadratic region.

In 3DEC an external boundary is required to truncate the far-field. Even if the boundaries are located at large distances from the heated region some boundary effects will still be found, in particular at later times.

Model description

The 3DEC model is shown in Figure A6.1. Due to symmetry only one quarter of the semi-infinite rock mass needs to be modeled. Only thermal stresses are considered here, which means that the S_1 and S_3 planes are principal stress planes. This is approximately true also for the S_2 plane. The vertical boundaries and the bottom boundary were fixed in the normal direction, but free to displace in the shear directions. The boundary representing the ground surface was free in all directions.

Results

Figure A6.2 shows the horizontal stress σ_{xx} contours in the horizontal S2 plane after 50 years of heat generation. See Figure 31 for comparison with the analytical results. The agreement is obvious with regard to the general appearance as well as with regard to position of individual contours. The 1 MPa contour, for instance, intersects the x-axis at a little more than 700 m and the y-axis at a little more than 550 m in both solutions. The 8 MPa contour follows the edge of the repository very closely in both solutions, and a similar region of tension, starting at $y =$ 600 m is found in both cases. The disordered appearance of the contours within the repository region is due to stress variations that result from the point source distribution used to represent the rectangular heat source.

The upper part of Figure A6.3 shows vertical stress contours after 50 years of heat generation. See Figure 32 for comparison with the analytical results. Again the agreement is very satisfactory with both solutions giving a compressive stress maximum in the repository corner, and with almost identical ridges of tension outside the edge of the repository.

The lower part of Figure A6.3 shows principal stress tensor symbols in the portion of the S2 plane indicated with a dashed rectangle in the upper part. In 3DEC, displayed stress tensors

are projections onto the viewing plane. In this case the viewing plane is a also a principal stress plane, meaning that the projected symbols give a correct picture of orientation and relative magnitude of the in-plane principal stresses, while the out-of-plane principal stress is not visible. The color coding is made with respect to the major principal stress. The legend gives the maximum principal stress (21.9 MPa) found in the plot. This figure overestimates the effective value (mainly due to local stress variations caused by the point source representation of the rectangular heat source). A relevant value is obtained by calculating an average over a small but representative volume around the origin. This gives 17.8 MPa. The corresponding analytical result is 17.6 MPa.

The upper part of Figure A6.4 shows vertical stress contours after 1000 years of heat production. See Figure 34 for comparison with the analytical results. The agreement is very satisfactory: the tension/compression contour intersects the coordinate axes at about 570 m distance from the origin. Ridges of increased tension (>1 MPa) are found at about 800 m distance from the origin. The 1 MPa compressive stress contour follows the edge of the repository in the same way in both solutions. The compressive stress maximum, found in the repository corner after 50 years, has disappeared in both solutions and a larger, but less intense, compressive stress maximum has formed in the central region.

The lower part is a close-up of the region indicated with the dashed rectangle, and shows in-plane principal stresses in that region. The maximum stress is obtained by calculating the average over a small volume around the origin and is found to be 12.4 MPa. The corresponding analytical result is 12.1 MPa.

Figures A6.5 and A6.6 show stresses in the S_1 plane after 50 years and 1000 years, respectively. The upper parts show out-of-plane principal stress contours. Corresponding analytical results are found in Figures 38 and 29. After 50 years the agreement is satisfactory. After 1000 years some small differences are found:

1. The magnitude of the tensile stress at the ground surface just above the repository is somewhat larger in the analytical solution

2. The tensile region below the repository is closer to the repository in the analytical solution. The compression/tension contour intersects the -500 m level at about 300 m distance from the z-axis in the analytical solution, and at 500 m in the numerical solution. The 1 MPa compressive stress contour intersects the z-axis at about -420 m in the analytical solution, and at about -450 m in the numerical solution.

The first difference depends on the representation of the ground surface. The analytical expressions do not produce a completely traction-free boundary, while this is the case for the numerical solution. The second difference is a boundary effect in the numerical model, caused by the truncation of the far- field at 1000 m depth below the repository. Both differences are significant only at large distances from the repository. In the interior of the model the agreement is very convincing also after 1000 years.

The lower parts of Figures A6.5 and A6.6 show orientation and magnitude of in-plane principal stresses in a small portion of the plane near the edge of the repository.

Figure A6.7 shows stresses in the S_3 plane after 100 years. The upper part shows vertical stress contours. See Figure 36 for comparison with the analytical solution. The same pattern of tensile and compressive stress maxima outside and inside the edge of the repository, respectively, are found in the two solutions. The lower part shows in-plane principal stress orientations and magnitudes in the repository edge region.

Conclusions

The comparisons presented here have regarded the stress state after 50 years and 1000 years. Similar comparisons have been made for times 10 years, 100 years, 300 years and 500 years. The results regarding general shape and development of the stress field were found to agree closely. No differences in excess of about 0.75 MPa were found that could not be attributed to: 1) stress variations in the interior caused by different ways of representing the rectangular heat source, 2) boundary effects caused by truncation of the far-field in the numerical model or 3) inability of the analytical solution to produce a traction-free boundary at the ground surface. Although this does not mean that systematic sources of small errors may not exist, it clearly demonstrates the general reliability of the analytical solution.

STRES3D solution

The thermoelastic stress caused by a KBS-3 type repository has been investigated with a program called STRES3D in Israelsson (June 1995).

General

The three-dimensional, semi-analytical model approximates the canisters with point heat sources. The temperature and stress fields for each point source are given by analytical formulas. A mirror solution is used to satisfy temperature and normal stress boundary conditions at the ground surface, Eqs. (4). The boundary conditions of the shear stresses at the ground surface are imposed by replacing the shear stresses with equivalent point shear forces. This model is valid for longer times compared with our analytical model. A comparison with Israelsson's results will give us more insight of the validity of the our model. In Israelsson's study the stress field is calculated for six different cases. The six cases correspond to variations in the total initial effect $Q_0(0)$ (3 values) and in the heat conductivity λ (2 values). The following data are used in Israelsson's reference cases:

$$
\begin{aligned}
&L = 500 \text{ m} \quad B = 500 \text{ m} \quad H = 505 \text{ m} \\
&J = 2 \quad q_1 = 0.753 \cdot Q_0(0)/(DD') \text{ W/m}^2 \quad q_2 = 0.247 \cdot Q_0(0)/(DD') \text{ W/m}^2 \\
&t_1 = 46 \text{ y} \quad t_2 = 780 \text{ y} \\
&Q_0(0) = 1440, 1656 \text{ or } 2400 \text{ W} \quad DD' = 6 \cdot 40 \text{ m}^2 \\
&\rho = 2700 \text{ kg/m}^3 \quad E = 60 \cdot 10^9 \text{Pa} \quad \nu = 0.22 \\
&c = 740.74 \text{ J/(kg} \cdot \text{K)} \quad \lambda = 3.0 \text{ or } 3.7 \text{ W/(m} \cdot \text{K)} \quad \alpha = 8.5 \cdot 10^{-6} \text{ 1/K}
\end{aligned} \tag{48}
$$

The largest value of $Q_0(0)$ in combination with the smallest value of λ results in the largest maximum (compressive) principal stress at the repository centre (Case 1), and the smallest value of $Q_0(0)$ combined with the largest value of λ results in the smallest (Case 2).

Results

A comparison between the maximum compressive principal stresses at the centre of the repository according to Israelsson's model and our analytical solution are shown in Table 7. The differences between the two models are less than 1 MPa in both cases for $t = 100$ and 400 years. Note that the stresses in Table 7 are the excess thermoelastic stress plus the natural occurring stresses of Section 4.

t (yrs.)	Anal. σ_1 (MPa)	STRES3D σ_1 (MPa)
Case 1	$q_0(0) = 10.0$ W/m^2	$\lambda = 3.0$W/(mK)
100	-66.8	-66.1
400	-63.5	-64.5
1000	-56.4	-58.7
Case 2	$q_0(0) = 6.0$ W/m^2	$\lambda = 3.7$W/(mK)
100	-50.5	-50.3
400	-48.5	-49.2
1000	-44.3	-45.7

Table 7. A comparison between Israelsson's model and our analytical solution for two cases.

Appendix 4. Manual for the computer code

Introduction

This short manual describes how to use the computer model that calculates the stress field derived in (Claesson J, Probert T, Jan. 1996) and applied in (Probert T, Claesson J, Apr. 1997). The numerical model is implemented in MATLAB version 4.2c.1 in the Windows 3.11 milieu run on DOS 6.22. The numerical solution has the same structure as the general solution formula Eqs. (210) of (Claesson J, Probert T, May 1996), p. 34.

m-files

Six m-files are used. These m-files are:

- **stress.m**
- **eax.m**
- **eay.m**
- **ee.m**
- **et.m**
- **consts.m**

The first five are function files and the last is a script file. This function **stress** calls all the other m-files.

The function m-file **stress** calculates the stress components at the point (x,y,z) for the time t. The function **stress** returns a matrix containing the stress components. Each stress component is separated into three terms corresponding to the three different parts of the solution. These parts are the *quadrantal infinite* solution (index qi), the *mirror* solution (index m) and the *boundary* solution (index b). Each component is summed and integrated according to the general formula, Eq. (210) of (Claesson J, Probert T, May 1996), for an exponentially decaying, rectangular heat source. This is indicated by the prefix I in front of the indices qi, m and b.

$$\begin{bmatrix} \sigma_{xx}^{Iqi}(x,y,z,t) & \sigma_{xx}^{Im}(x,y,z) & \sigma_{xx}^{Ib}(x,y,z) \\ \sigma_{yy}^{Iqi}(x,y,z,t) & \sigma_{yy}^{Im}(x,y,z) & \sigma_{yy}^{Ib}(x,y,z) \\ \sigma_{zz}^{Iqi}(x,y,z,t) & \sigma_{zz}^{Im}(x,y,z) & \sigma_{zz}^{Ib}(x,y,z) \\ \sigma_{xy}^{Iqi}(x,y,z,t) & \sigma_{xy}^{Im}(x,y,z) & \sigma_{xy}^{Ib}(x,y,z) \\ \sigma_{xz}^{Iqi}(x,y,z,t) & \sigma_{xz}^{Im}(x,y,z) & \sigma_{xz}^{Ib}(x,y,z) \\ \sigma_{yz}^{Iqi}(x,y,z,t) & \sigma_{yz}^{Im}(x,y,z) & \sigma_{yz}^{Ib}(x,y,z) \end{bmatrix} = \text{stress}\,(x,y,z,t) \tag{49}$$

The four function m-files **eax**, **eay**, **ee** and **et** are the integrands of the time integrals in Eqs. (207-209) of (Claesson J, Probert T, May 1996), p. 34. These functions are called by **stress**.

The input is initiated by the script m-file **consts** that is called by **stress**. The input data consists of five parts:

- Geometry of the repository (L, B, H)
- Mechanical properties of the rock mass (ρ, E, ν)
- Thermal properties of the rock mass (c, α, λ, a)
- Heat source data (J, t_i, q_i)

- Numerical parameter (n)

Any item of data may be altered. If the number of exponentials is changed then the number of decay times t_i and initial heat releases q_i must be changed accordingly.

Integration

The only controllable numerical procedure is the time integration. The time integral is evaluated numerically. This is done with the simple Trapezoidal rule which has proven to be sufficient. The number of sampling points may be changed but a value around $n = 200$ is quite sufficient for the calculations presented in this paper. The error is less than 0.01% in comparison with $n = 10000$.

Execution times

All the calculations in MATLAB have been run on an Intel Pentium 90 MHz PC. One call of **stress** takes between 1.5 and 2 seconds depending on size of the arguments in the Error function calls. An Error function call takes between 5 and 8 milliseconds.

Doubling n from 200 to 400 increases the execution time by roughly 50% but this also depends on the size of the arguments in the Error function calls.

The resolution and execution times for stresses illustrated in the figures of Sections 4, 6, 7, 8 and 9 are the following. The stress field at a given point for 300 times or the stress field at 300 points along a line for a given time takes 7 to 10 minutes to calculate. The stress field for a given time in a plane consisting of 100×100 points takes 4 to 6 hours.

Appendix 5. Selected colour figures

The colour figures below have been shown earlier in black and white. The figure number within brackets is the earlier figure numbering. The colour bar scale in the first figure is used in all the other figures. The unit MPa is used in all the figures (level curves and colour scale). The level curve markings are hard to see in a few of the colour figures. In these few cases the original black and white figures are of some help.

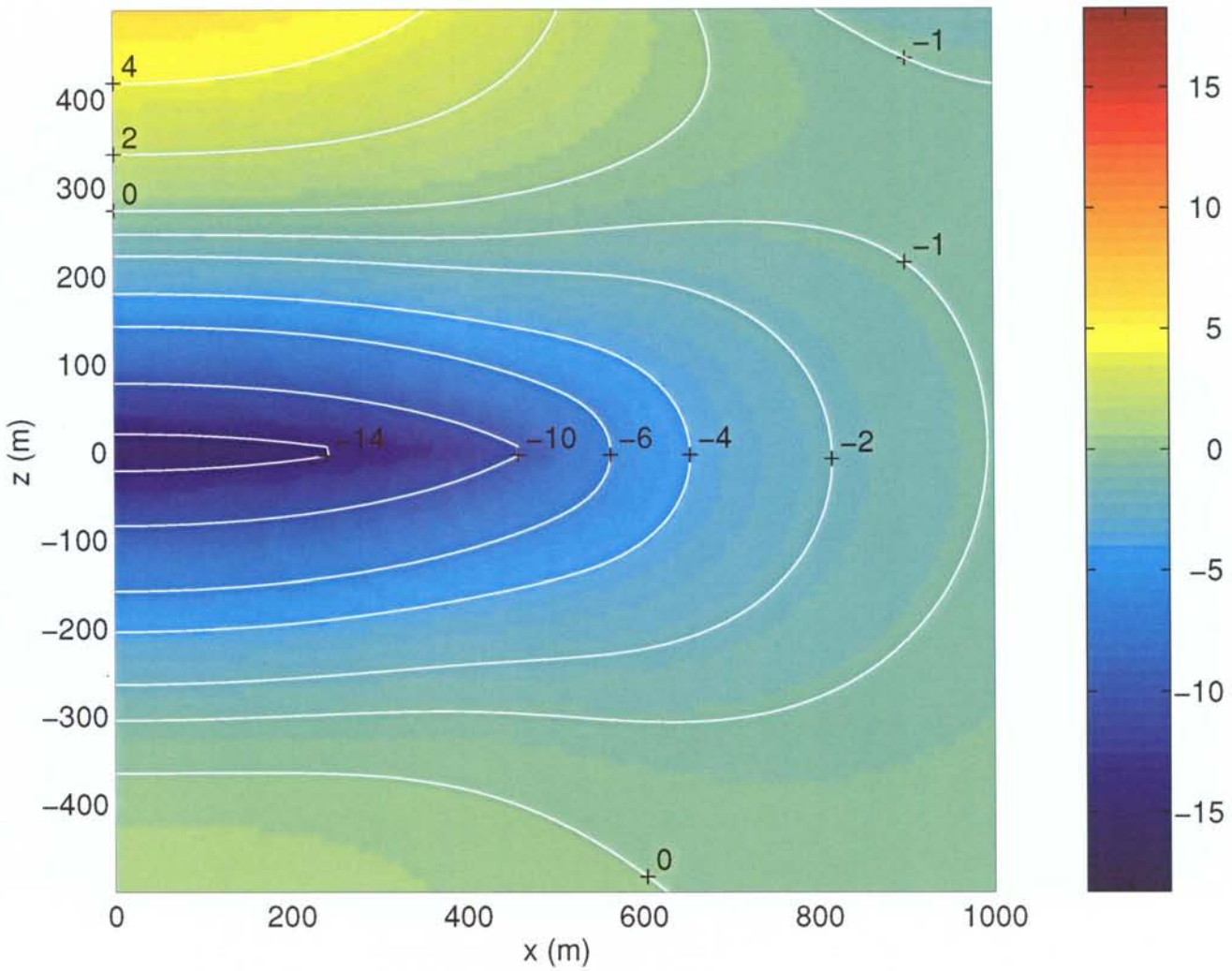

Figure A5.1. (Fig. 4) The stress σ_{xx} $(x, 0, z, 500)$ shown in a vertical cross-section of the repository after 500 years (xz-plane, $y = 0$).

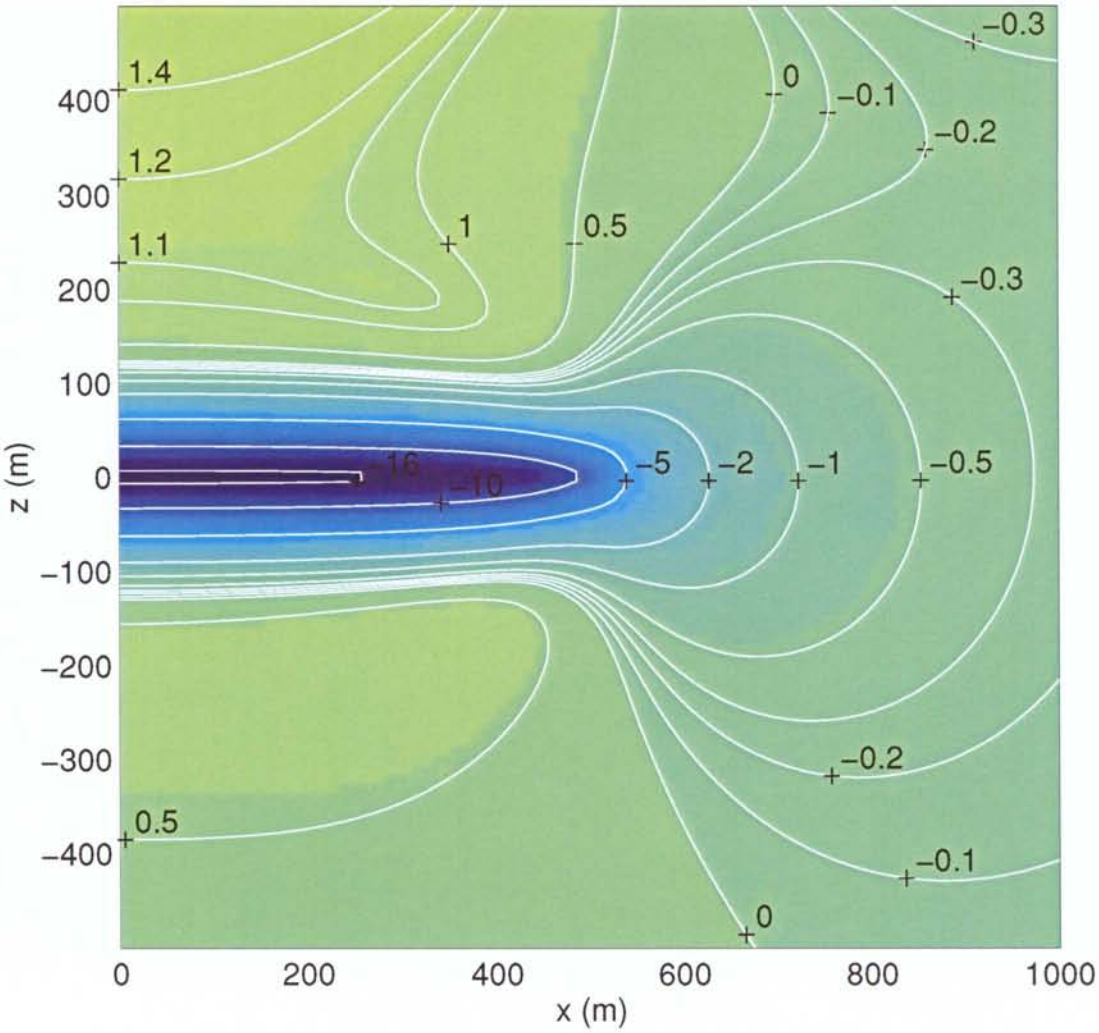

Figure A5.2. (Fig. 26) The horizontal stress σ_{xx} in the plane S_1 after 50 years.

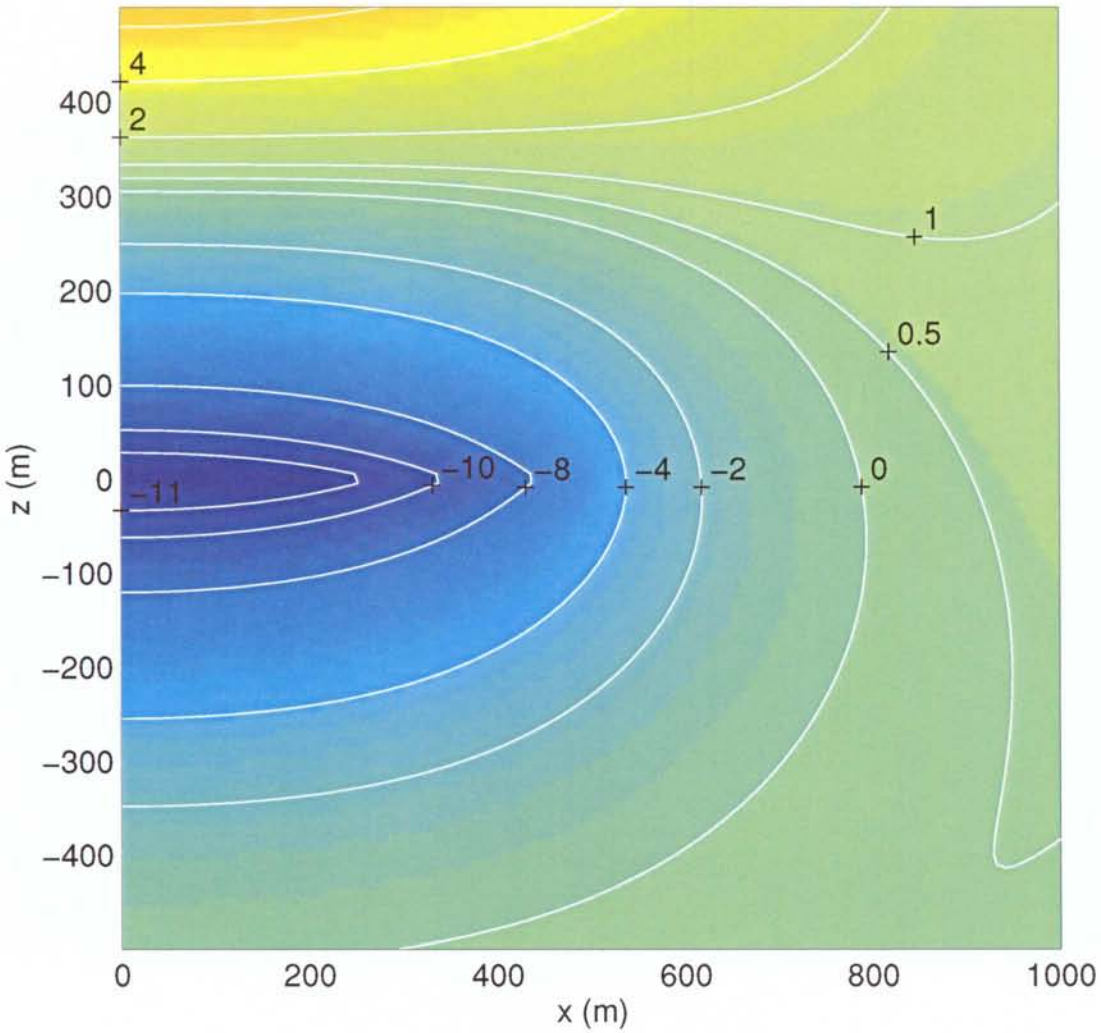

Figure A5.3. (Fig. 29) The horizontal stress σ_{yy} in the plane S_1 after 1000 years.

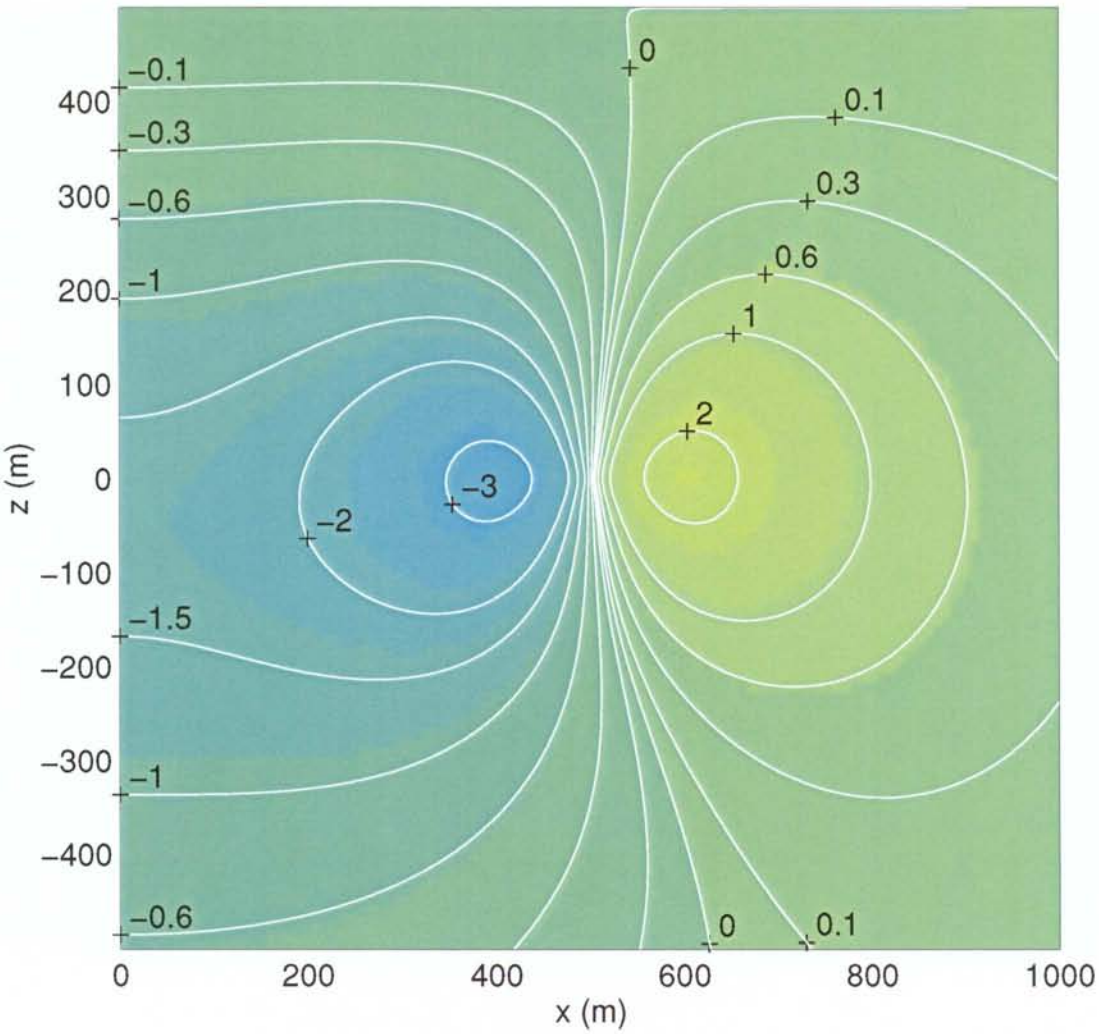

Figure A5.4. (Fig. 30) The vertical stress σ_{zz} in the plane S_1 after 100 years.

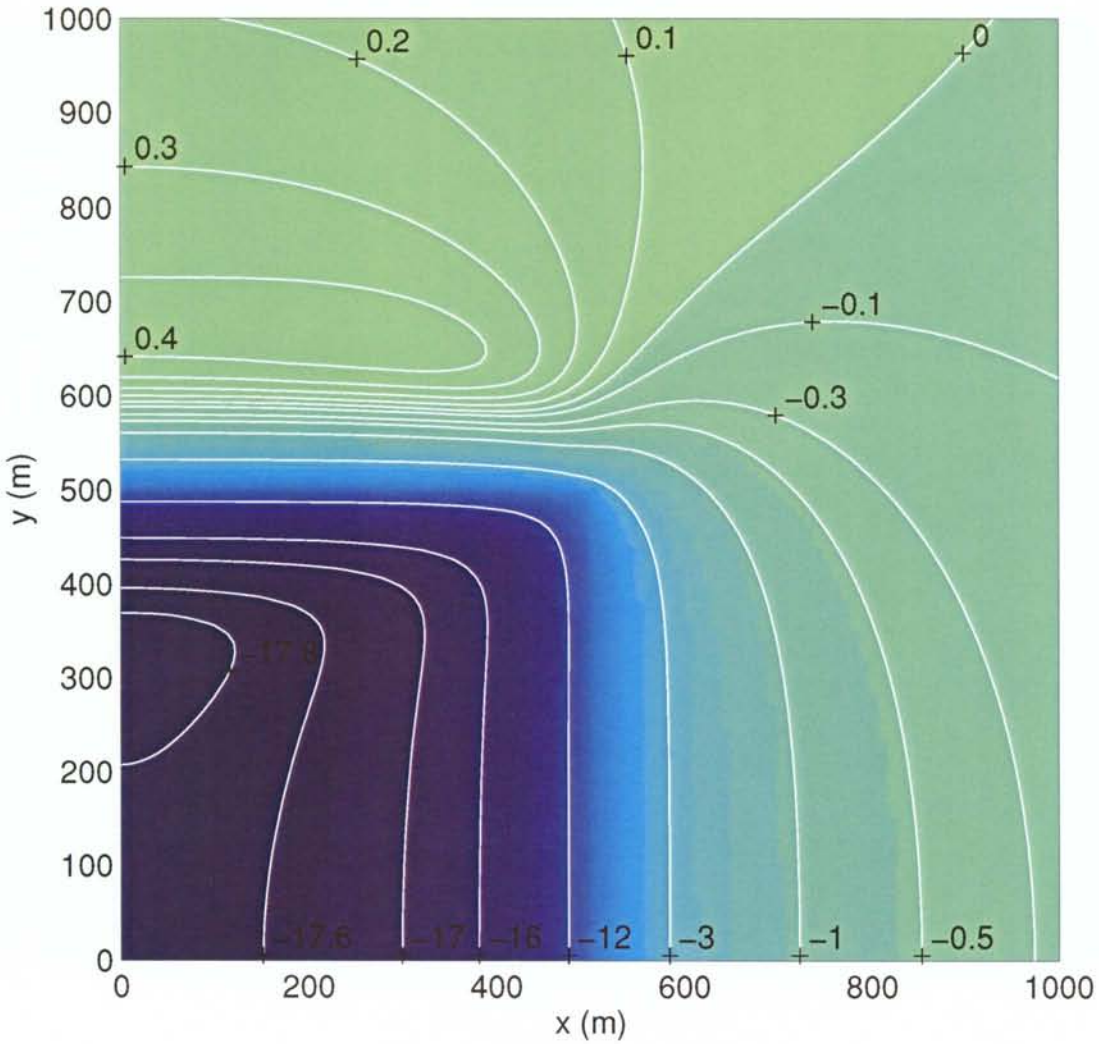

Figure A5.5. (Fig. 31) The stress σ_{xx} in the plane S_2 after 50 years.

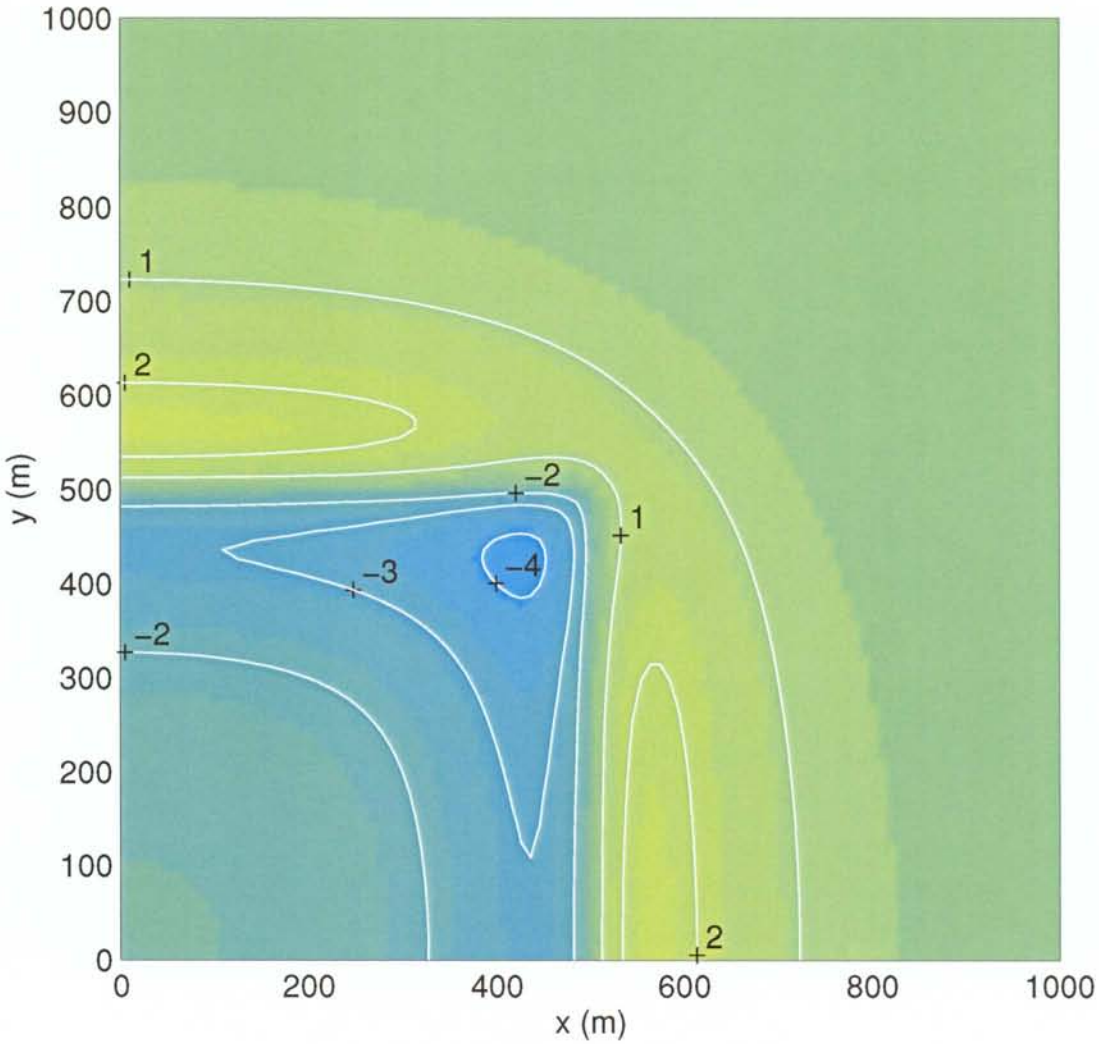

Figure A5.6. (Fig. 32) The vertical stress σ_{zz} in the horizontal plane S_2 after 50 years.

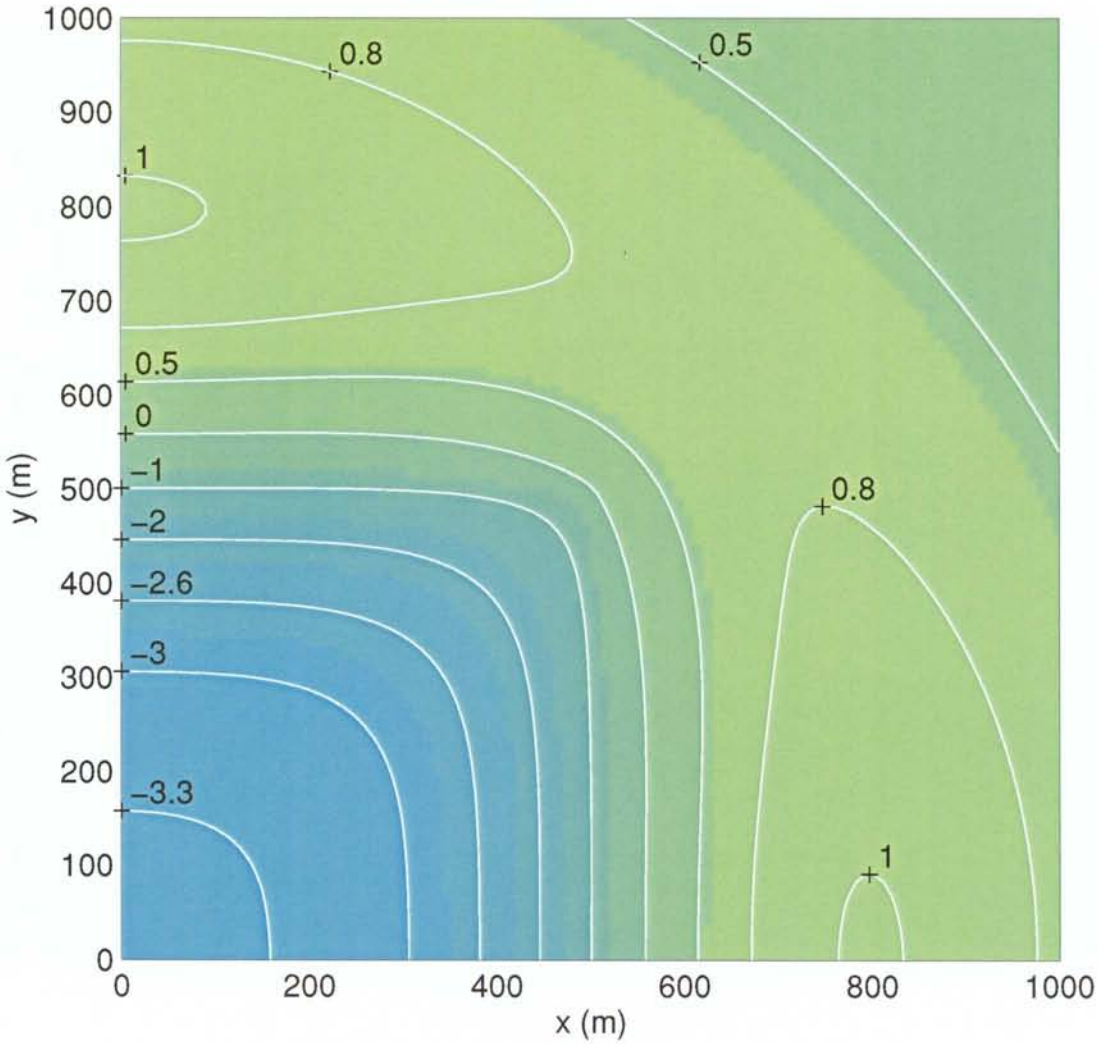

Figure A5.7. (Fig. 34) The vertical stress σ_{zz} in the plane S_2 after 1000 years.

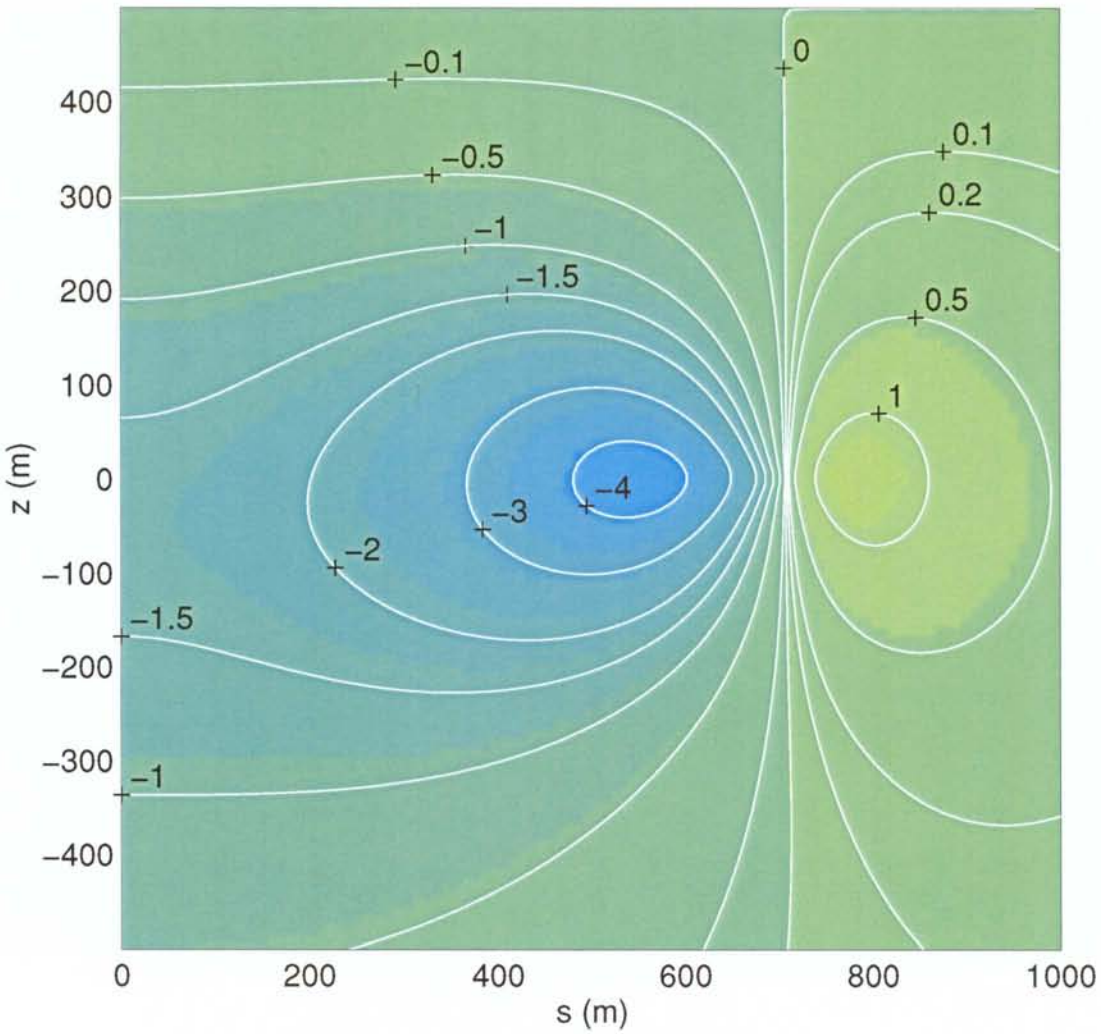

Figure A5.8. (Fig. 36) The stress σ_{zz} in the plane S_3 after 100 years.

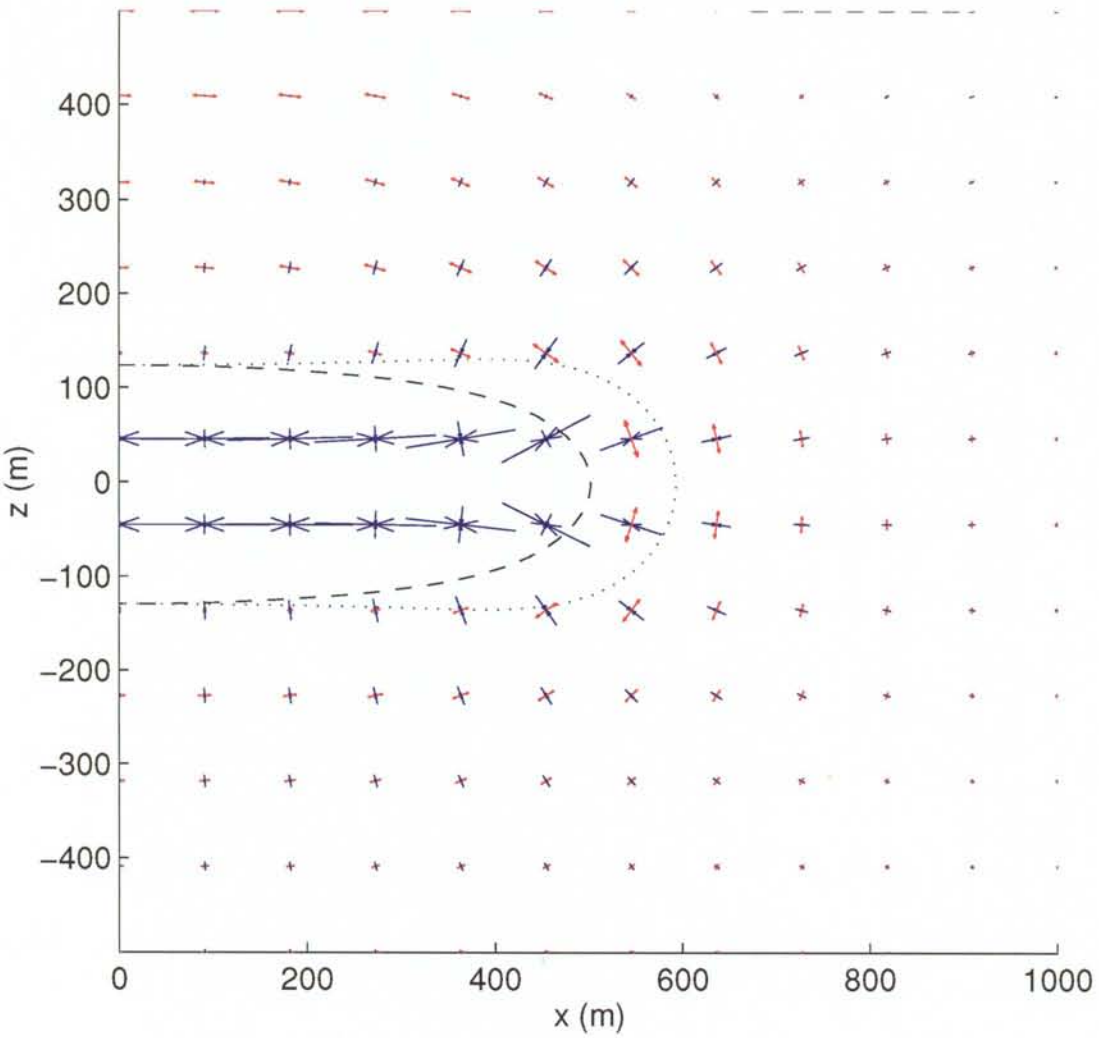

Figure A5.9. (Fig. 37) The orientation and magnitude of the two principal stresses parallel to the plane S_1 after 50 years. The dashed curve marks when σ_2 changes sign and the dotted curve marks where $\sigma_\perp = \sigma_{yy}$ changes sign.

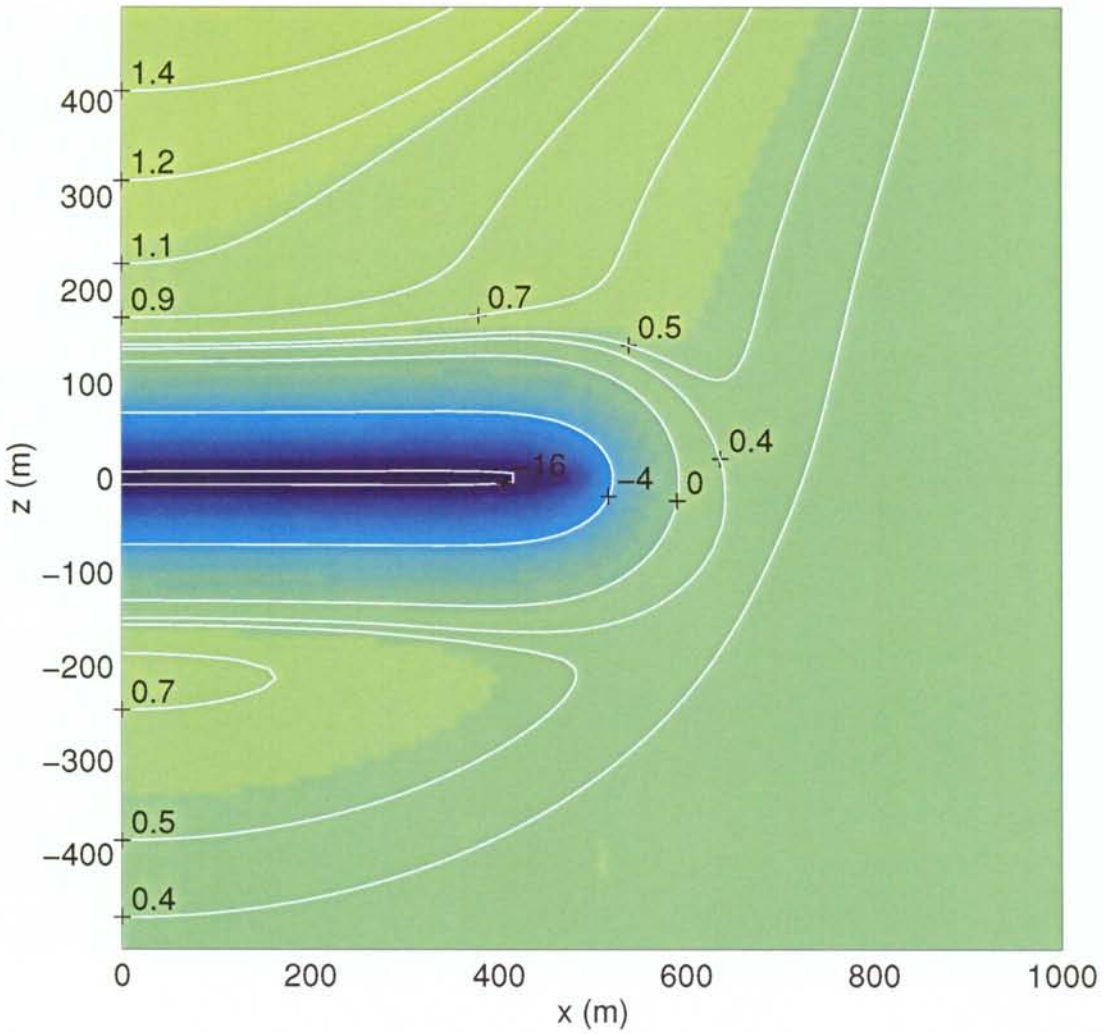

Figure A5.10. (Fig. 38) Level curves of the principal stress $\sigma_{\perp} = \sigma_{yy}$ perpendicular to the plane S_1 after 50 years.

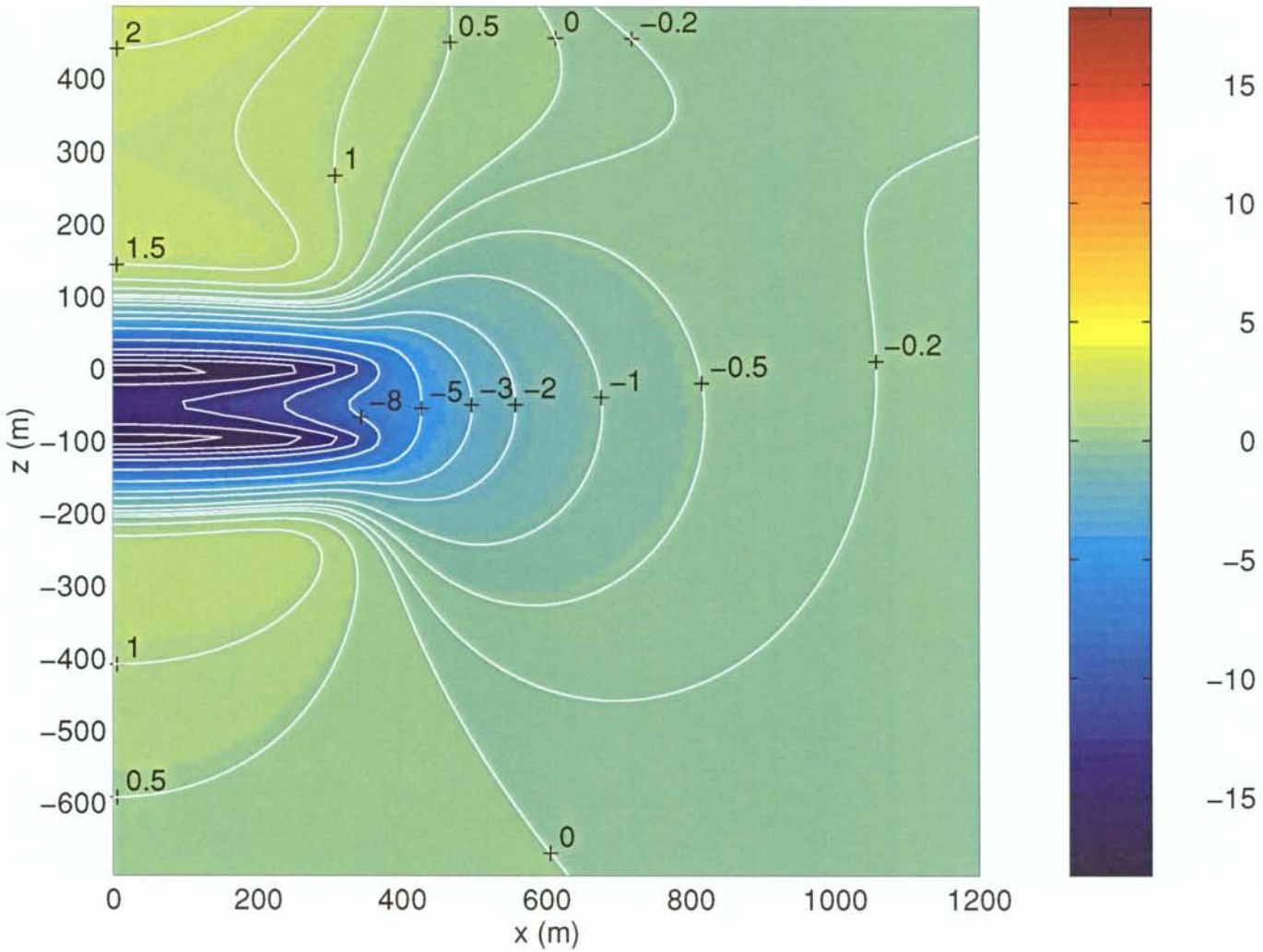

Figure A5.11. (Fig. 46) The horizontal stress σ_{xx} in the plane S_1 around two stacked repositories after 50 years.

Appendix 6. Stresses according to 3DEC (H. Hökmark)

The figures presented here are discussed in Appendix 3. The discussion in Appendix 3 and the figures in this section were provided by H. Hökmark.

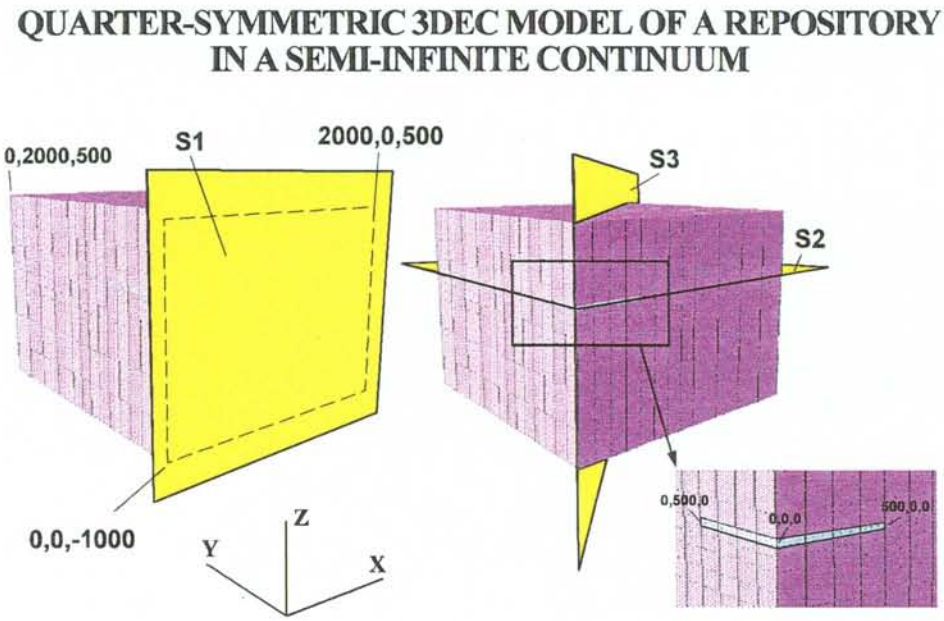

Figure A6.1. 3DEC model with planes S_1, S_2 and S_3 selected for plotting stresses. The lower right part is a close-up showing the repository position.

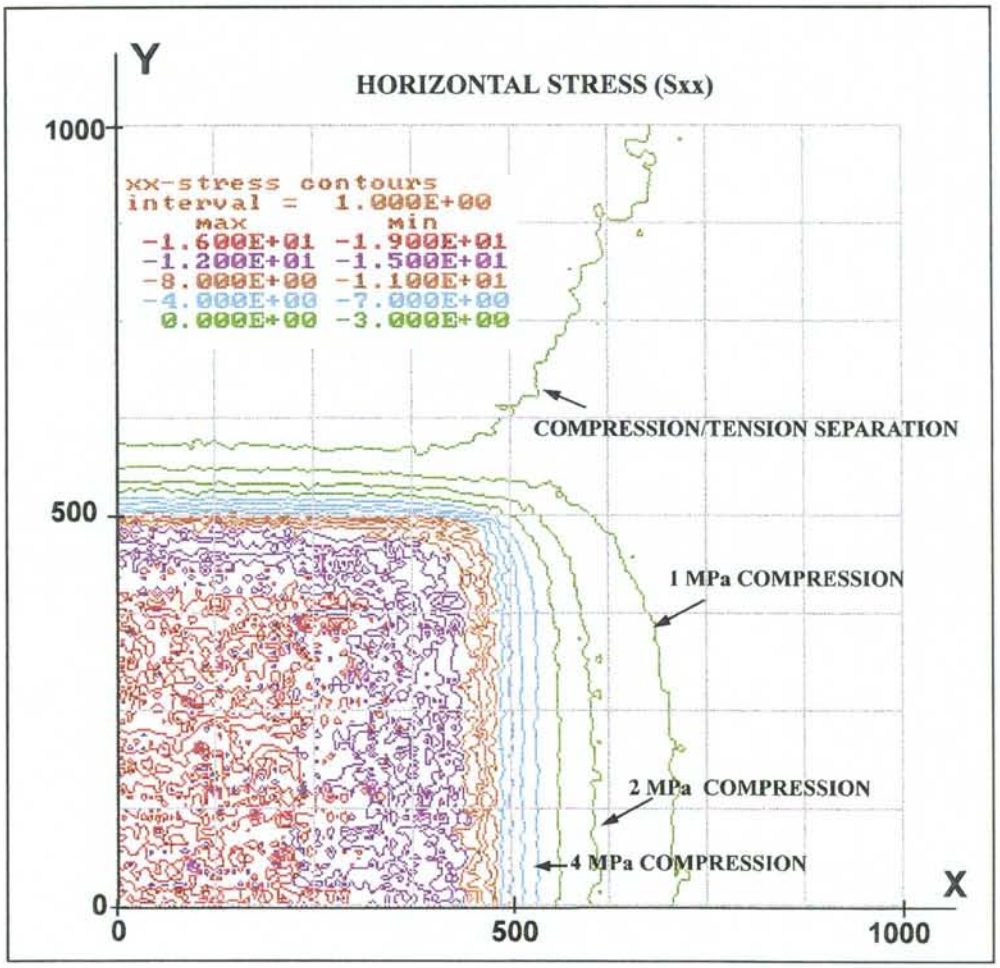

Figure A6.2. σ_{xx} stress contours. 1 MPa/contour and 4 contours/colour.

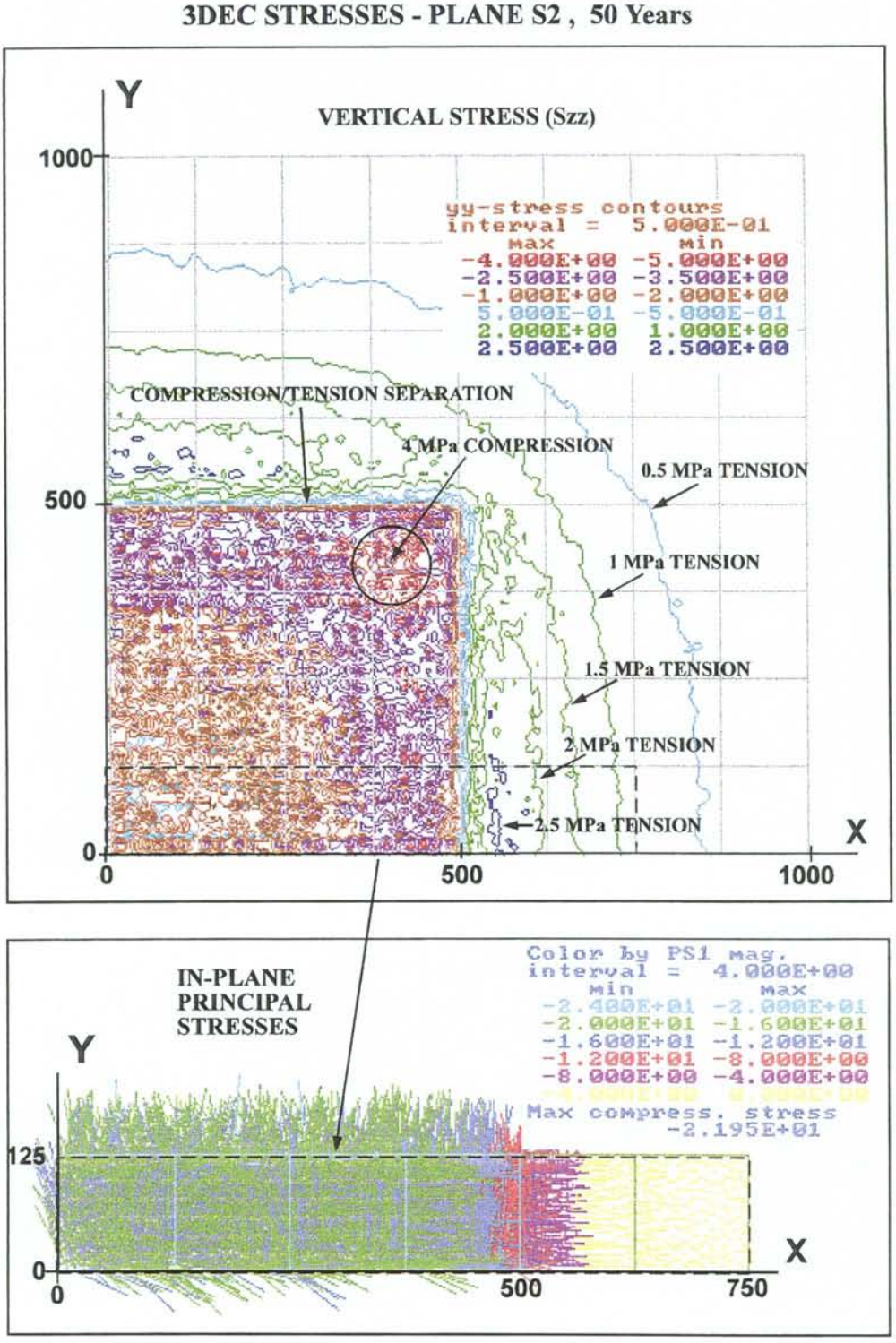

Figure A6.3. Upper: Vertical stress contours with 0.5 MPa/contour and 3 contours/colour. The stress component notation in the colour legend is due to the left-hand coordinate system used in 3DEC and is not valid here.
Lower: Close-up of indicated rectangular part of the S_2 plane.

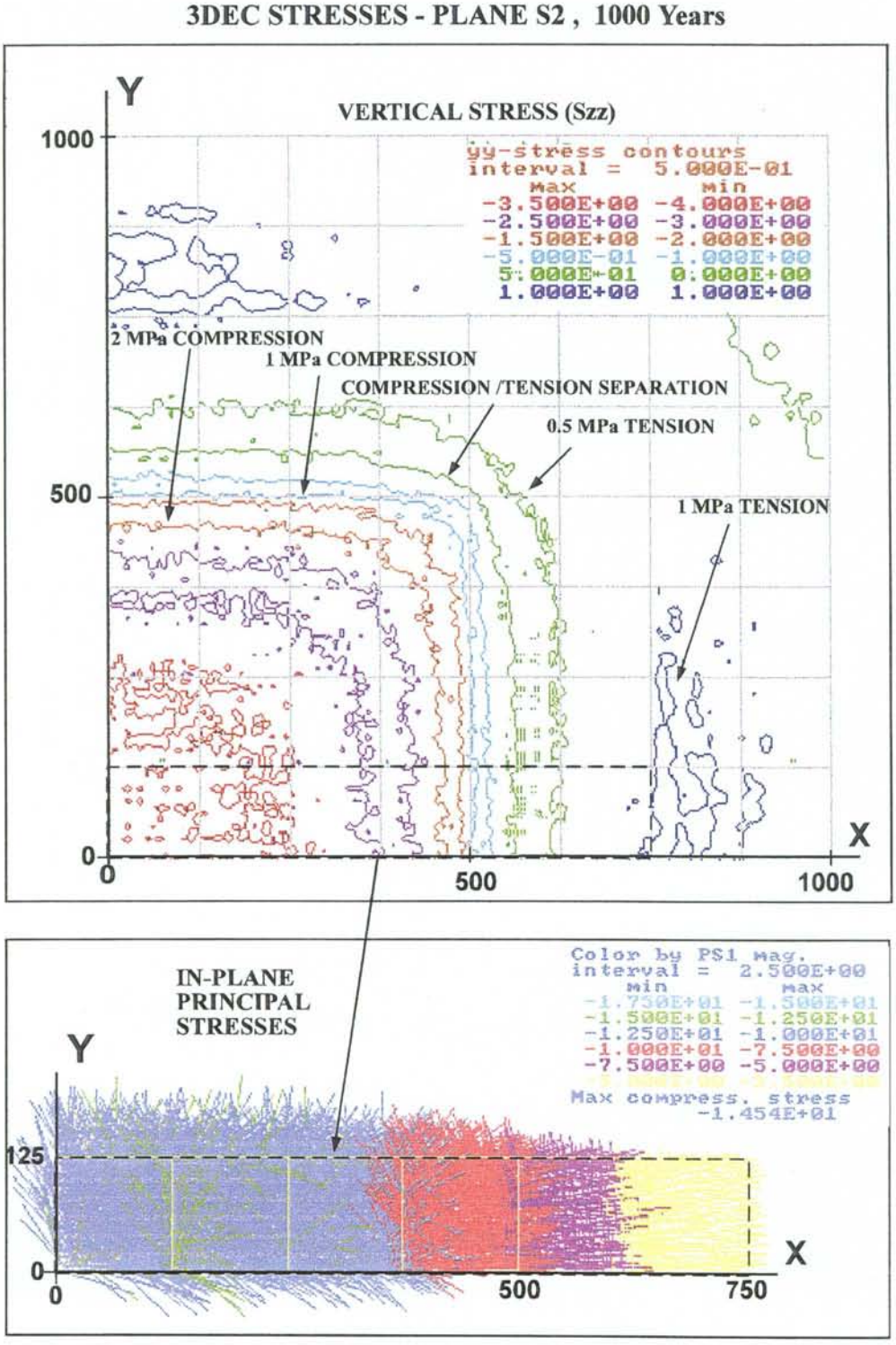

Figure A6.4. Upper: Vertical stress contours with 0.5 MPa/contour and 2 contours/colour. The stress component notation in the colour legend is due to the left-hand coordinate system used in 3DEC and is not valid here.
Lower: Close-up of indicated rectangular part of the S_2 plane.

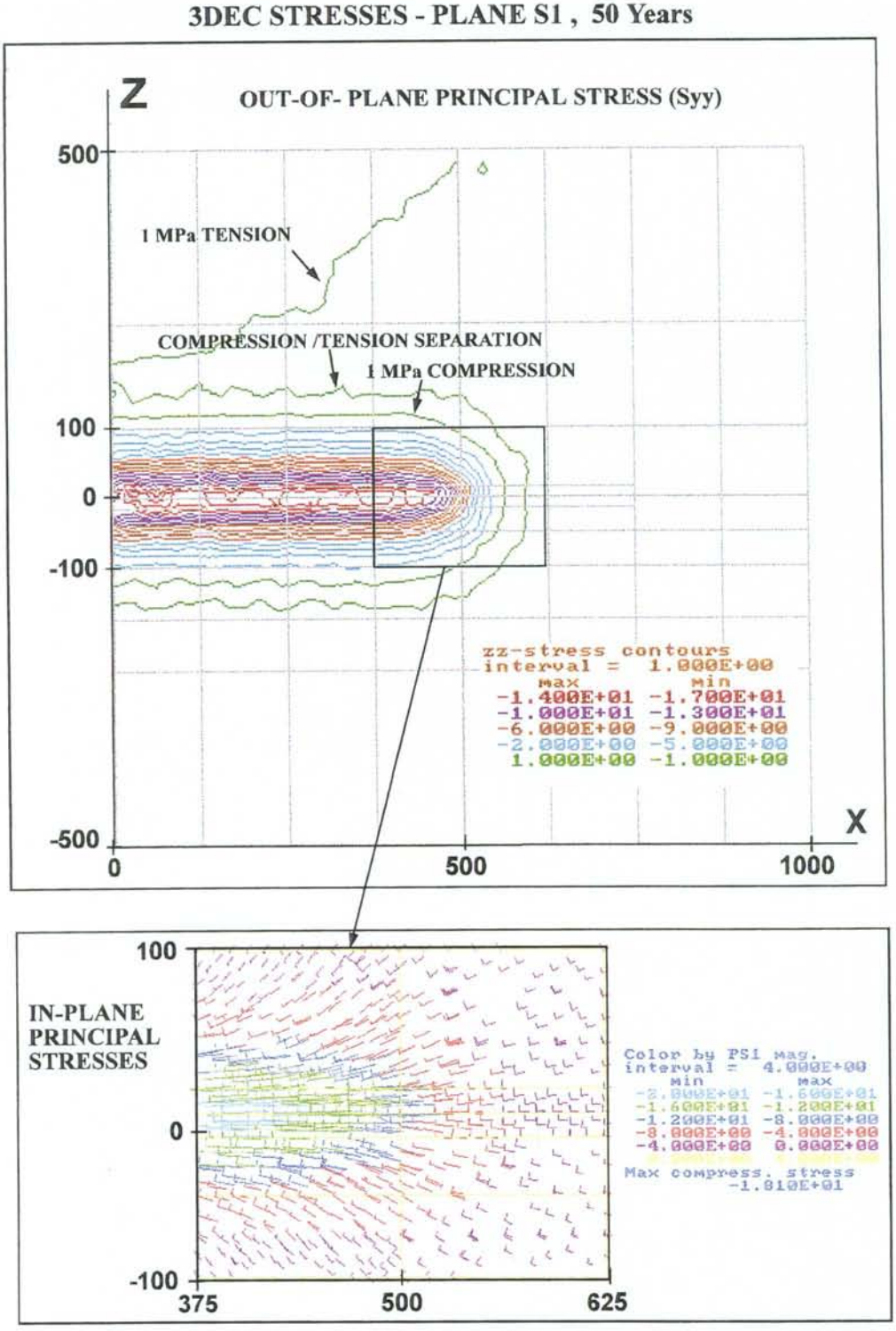

Figure A6.5. Upper: Out-of-plane stress contours with 1 MPa/contour and 4 contours/colour. The stress component notation in the colour legend is due to the left-hand coordinate system used in 3DEC and is not valid here.
Lower: Close-up of indicated rectangular part of the S_1 plane.

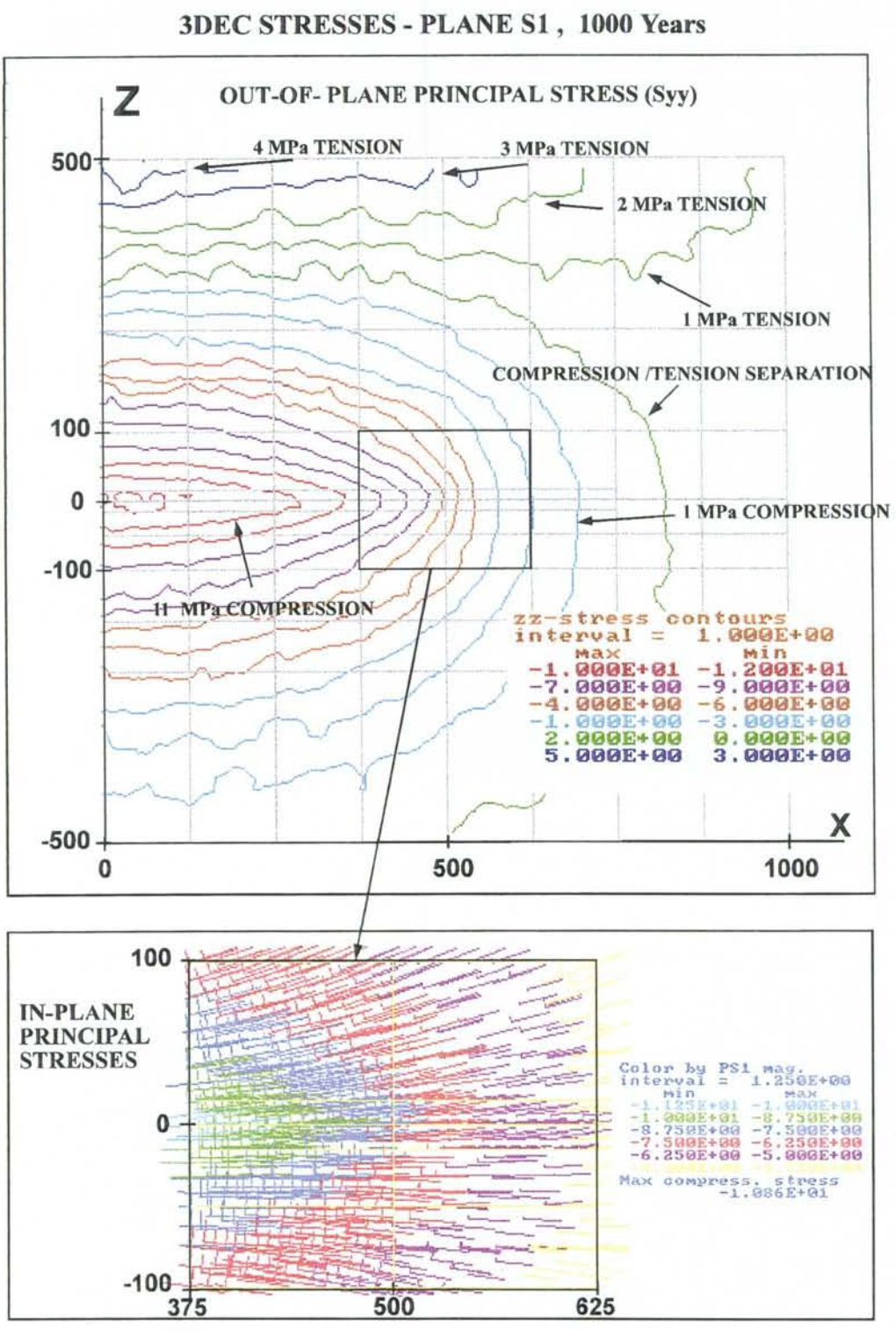

Figure A6.6. Upper: Out-of-plane stress contours with 1 MPa/contour and 3 contours/colour. The stress component notation in the colour legend is due to the left-hand coordinate system used in 3DEC and is not valid here.
Lower: Close-up of indicated rectangular part of the S_1 plane.

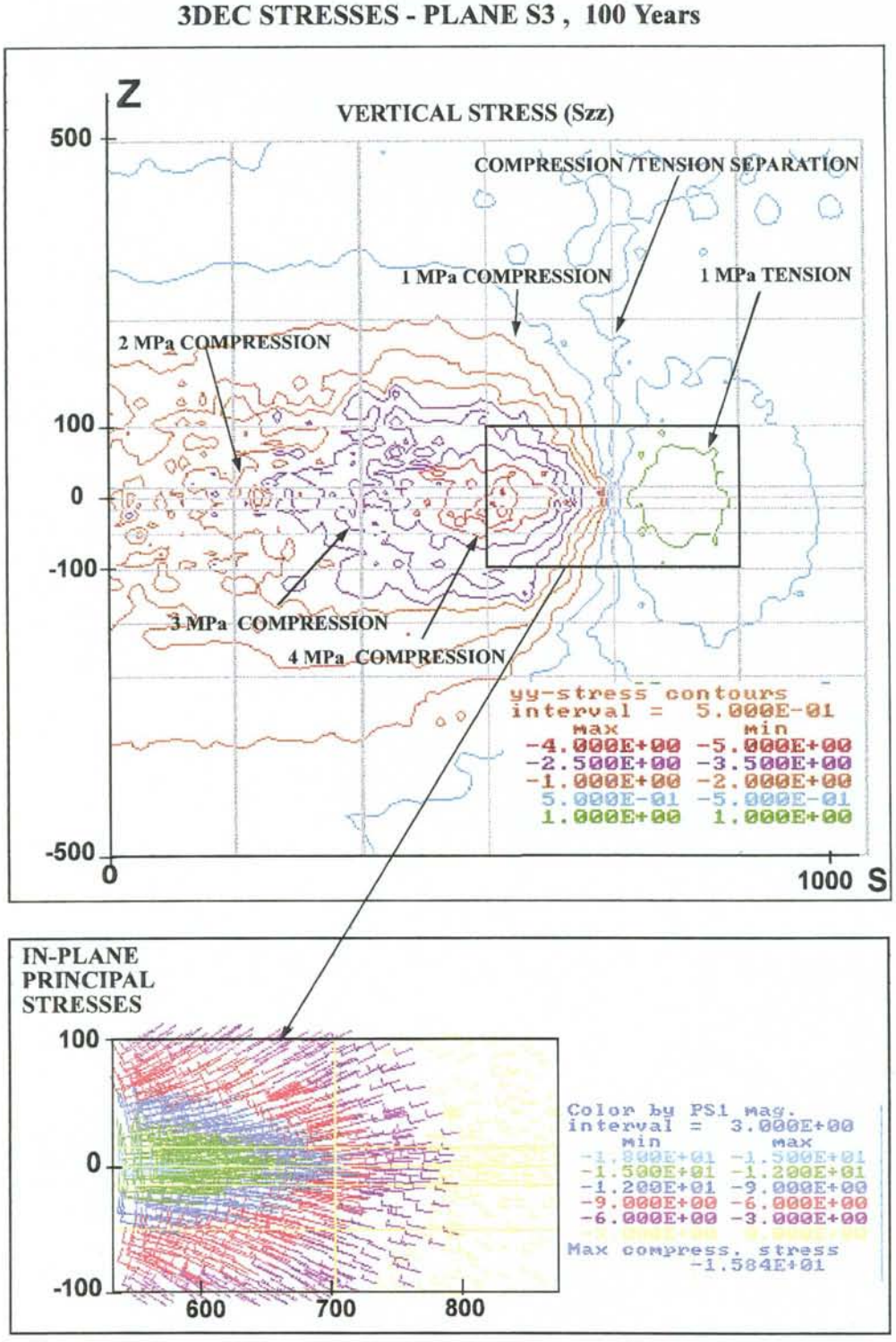

Figure A6.7. Upper: Vertical stress contours with 0.5 MPa/contour and 3 contours/colour. The stress component notation in the colour legend is due to the left-hand coordinate system used in 3DEC and is not valid here.
Lower: Close-up of indicated rectangular part of the S_3 plane.

List of SKB reports

Annual Reports

1977-78
TR 121
KBS Technical Reports 1 – 120
Summaries
Stockholm, May 1979

1979
TR 79-28
The KBS Annual Report 1979
KBS Technical Reports 79-01 – 79-27
Summaries
Stockholm, March 1980

1980
TR 80-26
The KBS Annual Report 1980
KBS Technical Reports 80-01 – 80-25
Summaries
Stockholm, March 1981

1981
TR 81-17
The KBS Annual Report 1981
KBS Technical Reports 81-01 – 81-16
Summaries
Stockholm, April 1982

1982
TR 82-28
The KBS Annual Report 1982
KBS Technical Reports 82-01 – 82-27
Summaries
Stockholm, July 1983

1983
TR 83-77
The KBS Annual Report 1983
KBS Technical Reports 83-01 – 83-76
Summaries
Stockholm, June 1984

1984
TR 85-01
Annual Research and Development Report 1984
Including Summaries of Technical Reports Issued during 1984. (Technical Reports 84-01 – 84-19)
Stockholm, June 1985

1985
TR 85-20
Annual Research and Development Report 1985
Including Summaries of Technical Reports Issued during 1985. (Technical Reports 85-01 – 85-19)
Stockholm, May 1986

1986
TR 86-31
SKB Annual Report 1986
Including Summaries of Technical Reports Issued during 1986
Stockholm, May 1987

1987
TR 87-33
SKB Annual Report 1987
Including Summaries of Technical Reports Issued during 1987
Stockholm, May 1988

1988
TR 88-32
SKB Annual Report 1988
Including Summaries of Technical Reports Issued during 1988
Stockholm, May 1989

1989
TR 89-40
SKB Annual Report 1989
Including Summaries of Technical Reports Issued during 1989
Stockholm, May 1990

1990
TR 90-46
SKB Annual Report 1990
Including Summaries of Technical Reports Issued during 1990
Stockholm, May 1991

1991
TR 91-64
SKB Annual Report 1991
Including Summaries of Technical Reports Issued during 1991
Stockholm, April 1992

1992
TR 92-46
SKB Annual Report 1992
Including Summaries of Technical Reports Issued during 1992
Stockholm, May 1993

1993
TR 93-34
SKB Annual Report 1993
Including Summaries of Technical Reports Issued during 1993
Stockholm, May 1994

1994

TR 94-33

SKB Annual Report 1994

Including Summaries of Technical Reports Issued during 1994

Stockholm, May 1995

1995

TR 95-37

SKB Annual Report 1995

Including Summaries of Technical Reports Issued during 1995

Stockholm, May 1996

1996

TR 96-25

SKB Annual Report 1996

Including Summaries of Technical Reports Issued during 1996

Stockholm, May 1997

List of SKB Technical Reports 1997

TR 97-01

Retention mechanisms and the flow wetted surface – implications for safety analysis

Mark Elert

Kemakta Konsult AB

February 1997

TR 97-02

Äspö HRL – Geoscientific evaluation 1997/1. Overview of site characterization 1986–1995

Roy Stanfors[1], Mikael Erlström[2], Ingemar Markström[3]

[1] RS Consulting, Lund

[2] SGU, Lund

[3] Sydkraft Konsult, Malmö

March 1997

TR 97-03

Äspö HRL – Geoscientific evaluation 1997/2. Results from pre-investigations and detailed site characterization. Summary report

Ingvar Rhén (ed.)[1], Göran Bäckblom (ed.)[2], Gunnar Gustafson[3], Roy Stanfors[4], Peter Wikberg[2]

[1] VBB Viak, Göteborg

[2] SKB, Stockholm

[3] VBB Viak/CTH, Göteborg

[4] RS Consulting, Lund

May 1997

TR 97-04

Äspö HRL – Geoscientific evaluation 1997/3. Results from pre-investigations and detailed site characterization. Comparison of predictions and observations. Geology and mechanical stability

Roy Stanfors[1], Pär Olsson[2], Håkan Stille[3]

[1] RS Consulting, Lund

[2] Skanska, Stockholm

[3] KTH, Stockholm

May 1997

TR 97-05

Äspö HRL – Geoscientific evaluation 1997/4. Results from pre-investigations and detailed site characterization. Comparison of predictions and observations. Hydrogeology, groundwater chemistry and transport of solutes

Ingvar Rhén[1], Gunnar Gustafson[2], Peter Wikberg[3]

[1] VBB Viak, Göteborg

[2] VBB Viak/CTH, Göteborg

[3] SKB, Stockholm

June 1997

TR 97-06

Äspö HRL – Geoscientific evaluation 1997/5. Models based on site characterization 1986–1995

Ingvar Rhén (ed.)[1], Gunnar Gustafson[2], Roy Stanfors[3], Peter Wikberg[4]

[1] VBB Viak, Göteborg

[2] VBB Viak/CTH, Göteborg

[3] RS Consulting, Lund

[4] SKB, Stockholm

October 1997

TR 97-07

A methodology to estimate earthquake effects on fractures intersecting canister holes

Paul La Pointe, Peter Wallmann, Andrew Thomas, Sven Follin

Golder Associates Inc.

March 1997

TR 97-08

Äspö Hard Rock Laboratory Annual Report 1996

SKB

April 1997

TR 97-09

A regional analysis of groundwater flow and salinity distribution in the Äspö area

Urban Svensson

Computer-aided Fluid Engineering AB

May 1997

TR 97-10
On the flow of groundwater in closed tunnels. Generic hydrogeological modelling of nuclear waste repository, SFL 3–5
Johan G Holmén
Uppsala University/Golder Associates AB
June 1997

TR 97-11
Analysis of radioactive corrosion test specimens by means of ICP-MS. Comparison with earlier methods
R S Forsyth
Forsyth Consulting
July 1997

TR 97-12
Diffusion and sorption properties of radionuclides in compacted bentonite
Ji-Wei Yu, Ivars Neretnieks
Dept. of Chemical Engineering and Technology, Chemical Engineering, Royal Institute of Technology, Stockholm, Sweden
July 1997

TR 97-13
Spent nuclear fuel – how dangerous is it? A report from the project "Description of risk"
Allan Hedin
Swedish Nuclear Fuel and Waste Management Co,
Stockholm, Sweden
March 1997

TR 97-14
Water exchange estimates derived from forcing for the hydraulically coupled basins surrounding Äspö island and adjacent coastal water
Anders Engqvist
A & I Engqvist Konsult HB, Vaxholm, Sweden
August 1997

TR 97-15
Dissolution studies of synthetic soddyite and uranophane
Ignasi Casas[1], Isabel Pérez[1], Elena Torrero[1], Jordi Bruno[2], Esther Cera[2], Lara Duro[2]
[1] Dept. of Chemical Engineering, UPC
[2] QuantiSci SL
September 1997

TR 97-16
Groundwater flow through a natural fracture. Flow experiments and numerical modelling
Erik Larsson
Dept. of Geology, Chalmers University of Technology, Göteborg, Sweden
September 1997

TR 97-17
A site scale analysis of groundwater flow and salinity distribution in the Äspö area
Urban Svensson
Computer-aided Fluid Engineering AB
October 1997

TR 97-18
Release of segregated nuclides from spent fuel
L H Johnson, J C Tait
AECL, Whiteshell Laboratories, Pinawa, Manitoba, Canada
October 1997

TR 97-19
Assessment of a spent fuel disposal canister. Assessment studies for a copper canister with cast steel inner component
Alex E Bond, Andrew R Hoch, Gareth D Jones, Aleks J Tomczyk, Richard M Wiggin, William J Worraker
AEA Technology, Harwell, UK
May 1997

TR 97-20
Diffusion data in granite Recommended values
Yvonne Ohlsson, Ivars Neretnieks
Department of Chemical Engineering and Technology, Chemical Engineering, Royal Institute of Technology, Stockholm, Sweden
October 1997

TR 97-21
Investigation of the large scale regional hydrogeological situation at Ceberg
Anders Boghammar[1], Bertil Grundfelt[1], Lee Hartley[2]
[1] Kemakta Konsult AB, Sweden
[2] AEA Technology, UK
November 1997

TR 97-22

Investigations of subterranean microorganisms and their importance for performance assessment of radioactive waste disposal. Results and conclusions achieved during the period 1995 to 1997

Karsten Pedersen
Göteborg University, Institute of Cell and Molecular Biology, Dept. of General and Marine Microbiology, Göteborg, Sweden
November 1997

TR 97-23

Summary of hydrogeologic conditions at Aberg, Beberg and Ceberg

Douglas Walker[1], Ingvar Rhén[2], Ioana Gurban[1]
[1] INTERA KB
[2] VBB Viak
October 1997

TR 97-24

Characterization of the excavation disturbance caused by boring of the experimental full scale deposition holes in the Research Tunnel at Olkiluoto

Jorma Autio
Saanio & Riekkola Oy, Helsinki, Finland
September 1997

TR 97-25

The SKB Spent Fuel Corrosion Programme.
An evaluation of results from the experimental programme performed in the Studsvik Hot Cell Laboratory

Roy Forsyth
Forsyth Consulting
December 1997

ISSN 0284-3757
CM Gruppen AB, Bromma, 1998